Final Scientific Report

Federal Agency to which Report is submitted: DOE EERE – Wind & Water Power Program

Recipient: Atargis Energy Corporation, DUNS #962384686

Award Number: DE-EE0003635

Project Title: Cycloidal Wave Energy Converter

Project Period: Oct 10, 2010 to March 31, 2012. Extended to August 31st, 2012

Principle Investigator: Stefan Siegel, President and CTO, stefan.siegel@atargis.com, 719-214-8815 x 201

Report Submitted by: Stefan Siegel

Date of Report: November 30th, 2012

Executive Summary

This program allowed further advancing the development of a novel type of wave energy converter, a Cycloidal Wave Energy Converter or CycWEC. A CycWEC consists of one or more hydrofoils rotating around a central shaft, and operates fully submerged beneath the water surface. It operates under feedback control sensing the incoming waves, and converts wave power to shaft power directly without any intermediate power take off system. Previous research consisting of numerical simulations and two dimensional small 1:300 scale wave flume experiments had indicated wave cancellation efficiencies beyond 95%.

The present work was centered on construction and testing of a 1:10 scale model and conducting two testing campaigns in a three dimensional wave basin. These experiments allowed for the first time for direct measurement of electrical power generated as well as the interaction of the CycWEC in a three dimensional environment. The Atargis team successfully conducted two testing campaigns at the Texas A&M Offshore Technology Research Center and was able to demonstrate electricity generation. In addition, three dimensional wave diffraction results show the ability to achieve wave focusing, thus increasing the amount of wave power that can be extracted beyond what was expected from earlier two dimensional investigations. Numerical results showed wave cancellation efficiencies for irregular waves to be on par with results for regular waves over a wide range of wave lengths. Using the results from previous simulations and experiments a full scale prototype was designed and its performance in a North Atlantic wave climate of average 30kW/m of wave crest was estimated. A full scale WEC with a blade span of 150m will deliver a design power of 5MW at an estimated levelized cost of energy (LCOE) in the range of 10-17 US cents per kWh. Based on the new results achieved in the 1:10 scale experiments these estimates appear conservative and the likely performance at full scale will exceed this initial performance estimates.

In advancing the Technology Readiness Level (TRL) of this type of wave energy converter from 3 to 4, we find the CycWEC to exceed our initial estimates in terms of hydrodynamic performance. Once fully developed and optimized, it has the potential to not just outperform all other WEC technologies, but to also deliver power at a lower LCOE than competing conventional renewables like wind and solar. Given the large wave power resource both domestically and internationally, this technology has the potential to lead to a large improvement in our ability to produce clean electricity at affordable cost.

Accomplishments

The actual accomplishments are matching the original goals and objectives of the project as outlined in the proposal. In this section, we itemize the achievement in bullet form. Details on each of the achievements can be found in the following section (Project Activities and Results) as well as its respective subsections.

- Advanced the TRL of the CycWEC from 3 to 4

- Designed and built a 1:10 scale CycWEC model
- Conducted two testing campaigns at the Texas A&M Offshore Technology Research Center
- Performed direct shaft power measurements and produced electricity from wave energy for the first time using a CycWEC
- Developed and validated a 2D inviscid panel code
- Developed feedback control algorithms for irregular wave cancellation.
- Achieved >99% irregular wave cancellation in numerical simulations, showing irregular wave cancellation efficiency to be on par with earlier harmonic wave cancellation results.
- Developed viscous estimate software code
- Developed 3D wave diffraction code
- Designed a full scale CycWEC for a North Atlantic wave climate
- Established performance and cost estimates for a full scale CycWEC: 5MW power output and lower device and LCOE costs than Solar, Wind or any competing WEC technology.

Project Activities and Results

The project consisted of three main activities which are detailed in the following subsections. These are experimental investigations testing a 1:10 scale CycWEC prototype, numerical simulations based on a in house developed panel code investigating irregular wave cancellation under feedback control, and conceptual design and performance estimate of a full scale CycWEC prototype. While this section provides a synopsis of the scientific results and findings, more detail can be found in related peer reviewed scientific papers as well as patent applications where all of these results have been published. The respective references are detailed in the following section.

Experiments

The experimental investigations form the corner stone of the TRL advancement work performed within this project. Initially, two measurement campaigns had been planned to be conducted at the Texas A&M Offshore Technology Research center, with tentative scheduled dates of August 2011 and January 2012. OTRC operates under a queued scheduling system that lines up all projects but will not guarantee the exact testing dates until one week prior to testing. These constraints, beyond the control of the customer, resulted in problems planning and maintaining the schedule as proposed. While the first testing campaign took place as scheduled, equipment failures along with the necessary unscheduled maintenance at OTRC delayed our second campaign until July of 2012. This was a contributing factor that caused Atargis to seek a 6 Month extension of this program beyond what was originally scheduled

in order to be able to conduct the second measurement campaign. Despite all scheduling woes, both measurement campaigns were conducted successfully. The following subsections detail model design and construction, as well as the results achieved during each of the two measurement campaigns.

Model Design and Construction

The design and construction of a 1:10 scale model of a double blade CycWEC dominated the first year of the program. The basic dimensions of the model were chosen for efficient interaction with the waves that the testing facility, the Texas A&M Offshore Technology Research Center wave basin, was able to support. The design wave of that facility is a wave with a period of 2.5s, wave length of 9.75m and wave height of up to 0.9m. As previous research results have conclusively shown, the radius of the CycWEC scales with the wave length of the design wave; while the chord length scales with the wave height. Optimization based on viscous estimates for a chosen design wave height of 0.55m led to a WEC radius of R=1m, and hydrofoil chord length of c=0.75m. The chord length in turn determines a minimum hydrofoil span, since hydrofoil performance for small aspect ratios is reduced due to end effects. On the other hand, the span needs to be small compared to the wave basin width to avoid wall interaction effects. These considerations led to a design choice of S=4.5m for the 1:10 scale prototype model. Figure 1 shows the CAD design of the wave energy converter including the struts supporting the model, the hydrofoils and the generator enclosures. All components shown in white are manufactured from epoxy resin/fiberglass which provides the required surface finish and allows for cost efficient construction of the complex geometry. These components were built in female CNC machined molds to achieve the required precision.

Figure 1: CAD design of CycWEC 1:10 scale model

While the model appears straightforward in terms of the externally visible components, there is a significant amount of electromechanical systems installed inside of the model in order to achieve successful operation. Both blades are free to pivot around the quarter chord location, and feature an independent linear electromechanical actuator at each end installed inside the support strut. The struts also featured instrumentation for fluid dynamic measurements, in particular a 5 hole probe was

installed in the leading edge of each strut at the radial location of the blade shaft. This probe provided measurement of the incoming flow velocity and direction, allowing for determination of the angle of attack of the blade. As both actuator electronics and data acquisition systems were not water proof, the struts were sealed to provide a dry operating environment for the electronic components inside. To provide both power and data connection to the rotating strut environments, a slip ring at the end of each motor shaft connected the strut electronics to the generator enclosures. Each generator enclosure had an independent 3 phase AC gear motor with an 80:1 gear ratio. Encoders at the main shaft as well as at the motor shaft allowed for four quadrant motor control as well as feedback control of the shaft position. In addition, each generator enclosure featured additional data acquisition equipment used to measure shaft torque directly by means of a load cell, as well as motor temperature measurement and leak detection. While the data acquisition relied entirely on distributed networked DAQ modules operating over a CAN bus system, the motor controllers were located in an electronics rack on the tunnel bridge that also provided housing for the main control computer. The main computer provided both feedback control of the WEC during operation by means of wave gauge signals, as well as all data acquisition and logging functions. It also operated the winch motors to position the model in the vertical direction by means of set of gear motors.

In order to install the model in the wave tank, a mounting frame was designed that attaches the generator enclosures to the bridge spanning the OTRC wave tank. Figure 2 shows the WEC model and mounting frame (gray) attached to the existing tunnel bridge (green). The mounting frame consists of two main beams of rectangular cross section extending vertically into the water. The WEC is attached to these beams by means of two wheeled dollies, which allow the position of the WEC to be adjusted in the vertical direction. The model can also be moved above the water for service access using this system. Two gear motors located on top of the beams along with a wire rope pulley system achieve positioning in the vertical direction. The mounting frame itself is attached to the bridge by a total of eight pushrods. The pushrods are laid out such that independent measurement of the vertical, horizontal and lateral forces transmitted to the bridge is possible by means of load cells installed in the pushrods. By measuring these forces along with the rotational position of the WEC shaft, the lift and drag forces created by the hydrofoils can be calculated.

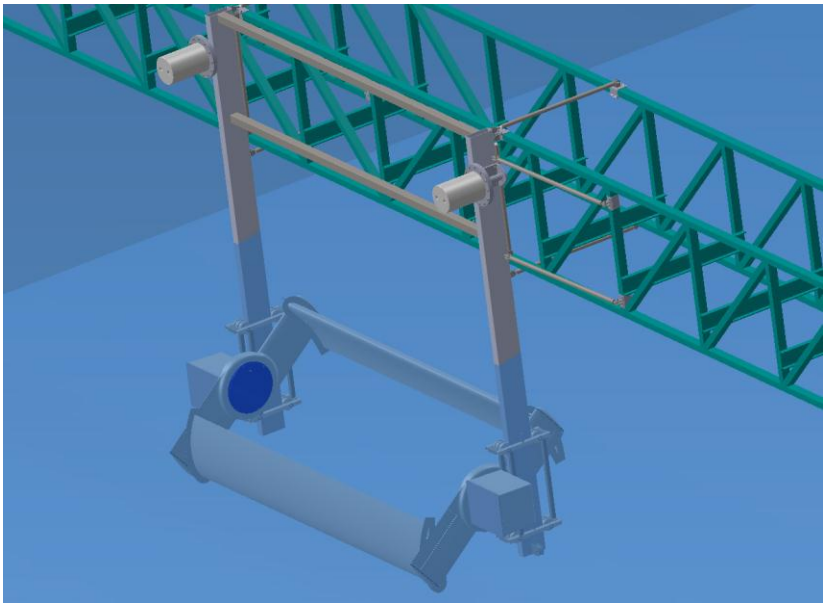

Figure 2: CAD designs of CycWEC 1:10 scale model attached to OTRC bridge

Corresponding to the CAD sketch of Figure 2, Figure 3 shows the actual model being installed in the OTRC wave tank. Beyond the components shown in the simplified CAD sketch, PVC pipes used both as conduits for electrical cables and cooling air supply / exhaust for the generators can be seen. The model is suspended from a crane and in the process of being attached to the tunnel bridge by means of the connecting pushrods. The model was successfully installed for the first measurement campaign and operated in wave generation mode; for a detailed discussion of the experimental results see the following section.

However, the first measurement campaign also unveiled deficiencies in the original model design, or more specifically, the mounting system. While the loads generated by the model in operation had been estimated in the design process leading up to OTRC-1 and communicated to and approved as safe by the director of the OTRC facility, the observations during the first testing campaign showed that the bridge was unable to support the loads generated by the model in operation safely. In particular, due to the lack of torsional stiffness of the open cross section, the bridge structure was twisting to a degree that was deemed unsafe for loads beyond about 25% of the design load. In response to these problems, the mounting system was entirely redesigned for the OTRC-2 testing campaign.

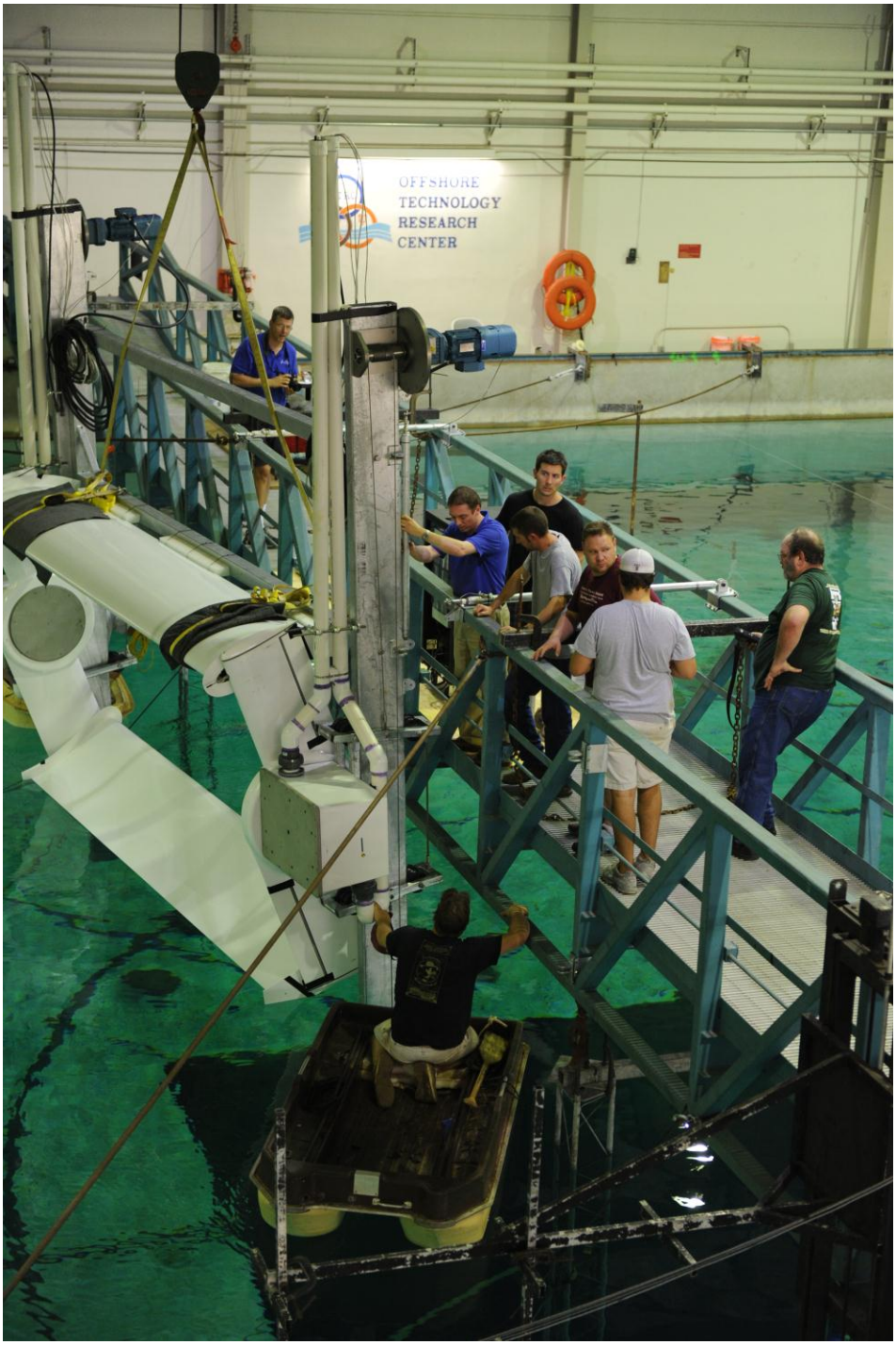

Figure 3: CycWEC 1:10 scale model being attached to the OTRC bridge using an overhead crane

A CAD model of the WEC attached to the redesigned mounting frame is show in Figure 4. The new design was made independent from the tunnel bridge and instead used a total of six attachment points in the tunnel floor to transmit the loads generated by the WEC. The main beams from the first testing campaign were recycled and extended in length, and attached to two newly constructed A-frame footers that in turn connected the entire mounting frame to the tunnel floor. While more complex than the original mounting system, the redesigned structure provided the structural integrity that the bridge could not provide. In addition to the structural redesign, the positioning system to lift the WEC into and out of the water was also improved by replacing the wire rope system with an ACME nut and spindle drive. This increased the stiffness of the positioning system and in turn prevented unintended vertical travel of the WEC during operation.

Figure 4: CAD model of redesigned CycWEC mount for OTRC-2 testing campaign

While the redesign addressed all issues encountered during the OTRC-1 testing campaign, the installation now required under water attachment of the frame to the tunnel floor using divers. Figure 5 shows divers in the process of attaching the WEC mounting frame to the tunnel floor during the OTRC-2 model commissioning process.

Figure 5: Divers attaching mounting frame to tunnel floor hard points

While the need to attach the redesigned mounting frame to the tunnel floor added complexity to the installation process, other model improvements reduced installation effort so that the time required for model installation was actually reduced from the first testing campaign. One major improvement was the addition of brakes to both the main shaft generators as well as the linear actuators providing blade pitch control. Adding brakes made the model a rigid unit, simplifying handling in the staging area by means of cranes and thus speeding up the installation process.

OTRC-1

The OTRC Measurement Campaign 1 was conducted from August 19th through September 2nd 2011 at the Texas A&M Offshore Technology research center wave basin. In preparation, the OTRC Staff under the direction of Dr. Richard Mercier started calibrating the wave generation facilities in accordance with a previously agreed test plan on August 19th. Setup of the bridge and data acquisition system, and calibration and installation of the wave probes was completed by Monday August 22nd. Calibration of the wave maker drive signals occurred on Tuesday and Wednesday, August 23-24. Delivery and assembly of the CycWEC model took place on Wednesday August 24th while the waves were being calibrated. The CycWEC was installed in the basin on Thursday August 25th. Testing of the CycWEC took

place from Friday August 26th through Friday morning, September 2, a total of 5.5 days. The afternoon of Friday September 2 was allocated for removal of the CycWEC from the basin and decommissioning.

A combination of measurement equipment from both OTRC and Atargis was used to acquire data in order to evaluate the performance of the CycWEC during these tests. As outlined in the model design and construction section, the CycWEC model was equipped with load cells to measure shaft torque on each side of the model as well as vertical force, horizontal force and lateral force. In addition, shaft position information from the main shaft motor controllers was logged, along with motor shaft power and current. The four linear actuators used to adjust the pitch angle of the CycWEC blades provided updates on their position in real time which was logged as well.

OTRC contributed measurement equipment consisted of a total of 12 capacitive wave gauges, which were arranged in an equidistant fashion around the CycWEC model. The locations are shown in Figure 6, and capture the radiated waves in all directions. Gauges 4-6 were located down-wave of the CycWEC, gauges 7-10 on the side and gauges 1-3 up-wave of the WEC. The objective of this setup was to be able to compare the performance of the CycWEC in an environment where waves are free to travel in all directions. The earlier two dimensional wave generation capabilities were fully understood from simulations as well as the 1:300 wave flume experiments. These had shown waves to be mainly generated down-wave of the CycWEC, with little or no harmonic waves of shorter wavelength present. The wave gauge measurements in this test campaign were used to fully quantify the three dimensional wave generation performance of the CycWEC.

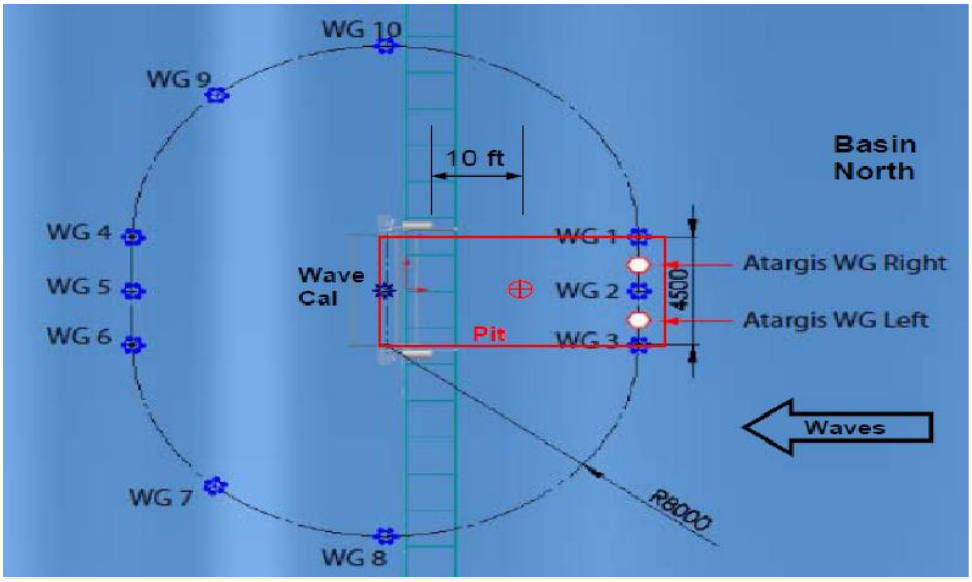

Figure 6: Wave gauge locations relative to CycWEC position for OTRC basin

A typical view of the wave tank with the CycWEC rotating is shown in Figure 7. The CycWEC is rotating in the counter-clockwise direction in this picture, and waves radiating right to left can be seen on the left side of the CycWEC. While difficult to distinguish in this picture, much smaller, if any, waves were seen on the right side of the CycWEC. It can also be observed that the waves feature an almost straight crest directly down-wave of the CycWEC blades, but a semicircular pattern on the sides of the CycWEC. The latter effect was a new observation that was made for the first time during the OTRC-1 testing campaign, where for the first time the width of the wave basin was larger than the span of the CycWEC blades. In earlier 1:300 scale experiments the blades of the WEC spanned the width of the wave channel, thus preventing sideways propagation of any waves by design.

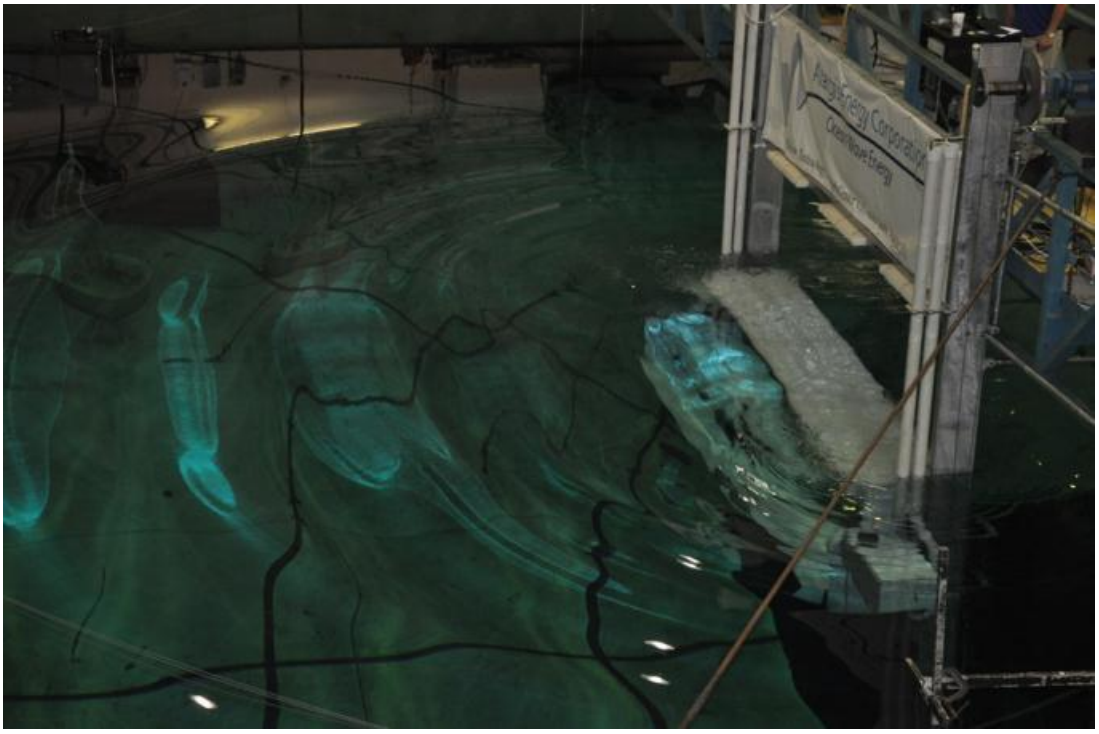

Figure 7: Picture of surface elevation for a wave generation experimental run.

Figure 8 shows data from a wave generation measurement experiment where the main shaft of the CycWEC was submerged to a submergence depth of 1.25 meters, and rotated at a period of 2.5s with blades 1 and 2 pitched to an angle of attack of +5 and - 5 degrees, respectively. The height of the generated waves was analyzed using a Direct Fourier transform based on the entire length of the measurement run which lasted 120s in time and thus is a time average of the wave heights encountered during that period. It was compared to results from a numerical three dimensional diffraction model, further described in the 3D Diffraction section of this document. It is evident that large wave heights were encountered down-wave of the CycWEC at wave gauge locations 4,5 and 6, while up-wave only small waves were present (wave gauges 1, 2 and 3). These results agree well with the earlier two-

dimensional wave flume experiments at 1:300 scale, where the CycWEC was also able to generate waves traveling predominantly in the down-wave direction. An effect not present in these earlier experiments by design is the generation of waves traveling in the lateral direction, which is evident in the measurements of the down-wave located wave gauges 7 and 9 as well as (to a lesser degree) 8 and 10. The observation that waves propagate in a 3D fashion both from wave gauge data as well as direct visual observations initiated the development of the 3D diffraction numerical model in order to understand these effects as well as their impact on CycWEC performance both quantitatively and qualitatively. While more detailed results from the numerical diffraction simulations are included in the 3D diffraction section of this document, in Figure 8 the results from these simulations are shown for comparison with the wave gauge measurements. There is both quantitative and qualitative good agreement between experiment and simulation. However, some differences are also evident. In particular, the up-wave wave heights in the experiment are larger than the zero wave height predicted by the numerical model by design. This effect is most likely due to waves reflected from both the wave basin sides as well as the far end of the basin. While the latter is equipped with a large number of screens to prevent reflections, the suppression is less than complete for any of these systems, with typical reflections on the order of 10% or more of the incoming wave height. The OTRC screen system at the testing time was also in poor maintenance with portions of the screens missing due to corrosion caused by extended exposure to tunnel water, further increasing the reflected wave heights. With respect to the reflections from the side walls, the OTRC facility features no wave damping system – active or passive - at all, resulting in near perfect reflection of the waves impacting the basin side walls. These effects combined caused higher amplitudes at locations where there were no waves predicted by the numerical model. Detailed analysis of the wave heights encountered during the first cycles of rotation, where no waves were re-reflected and impacting the wave gauges yet, added further evidence that is supporting this theory.

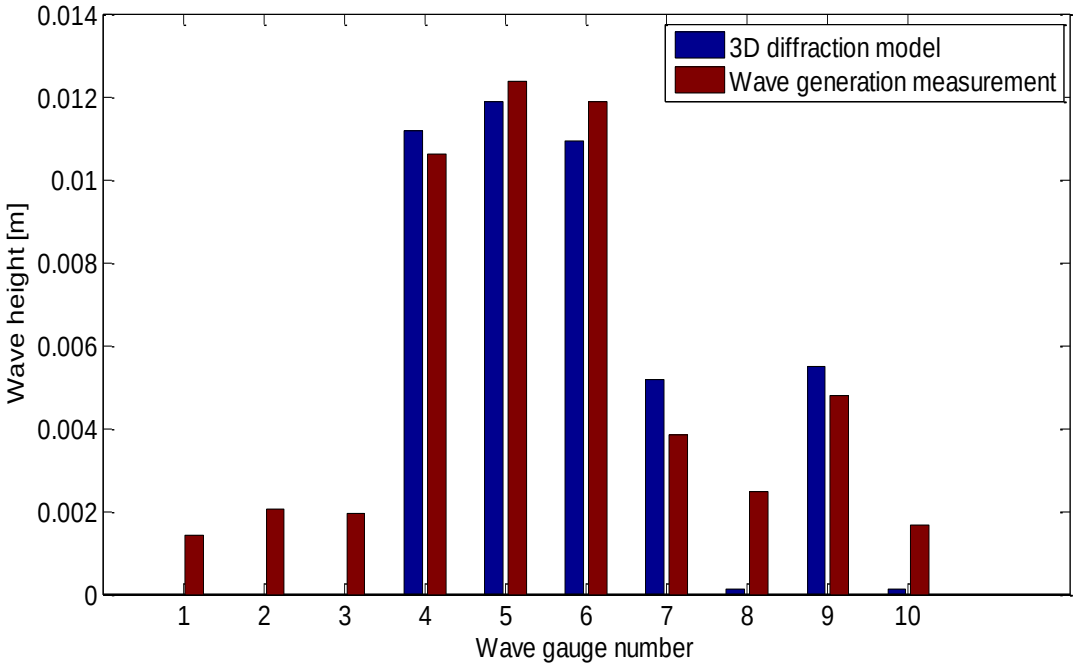

Figure 8: Comparison of fundamental wave height for a submergence depth of 1.25 meters, angle of attack of 5 degrees and rotational speed of 2.5 seconds. Experimental data (red) is compared to 3D diffraction numerical results (blue).

During a parameter study investigating the main parameters of submergence depth, rotational period and blade pitch angles, a set of measurements were performed very close to the surface. Based on numerical simulations (see Siegel 2012), close to the surface higher harmonic waves become dominant over the fundamental wave that has the same period as the rotation of the CycWEC. Also, the numerical parameter study showed that the optimal ratio between the CycWEC diameter 2R and the wavelength λ is a ratio of $2R/\lambda = 1/\pi$. This effect can be seen in the data presented in Figure 9, which shows the height of the fundamental wave H1 along with the heights of the first and second harmonic waves, H2 and H3. For higher rotational periods, the harmonic waves are dominant compared to the fundamental wave. The second harmonic exhibits a distinct maximum amplitude at a rotational period of T=3.5s. The wave length of this wave is λ=18.84m with $2R/\lambda = 0.106$, and thus almost exactly matches the optimal ratio of $2R/\lambda = 1/3\pi$ for a second harmonic wave. Similarly, theory predicts an optimal period of T=2.0s for the first harmonic wave, which is just outside of the data range shown in Figure 9. However, a steep increase in the H2 wave height for smaller wave periods points to the existence of this maximum. The data shown in Figure 9 is thus consistent with earlier numerical and experimental findings about harmonic wave generation as a function of CycWEC diameter, and supports the theory about optimal wave generation being achieved when the rotational velocity of the hydrofoils match the celerity of the

generated wave. It should be noted though that the results shown in Figure 9 were achieved at a far shallower submergence than what will be encountered in typical operation of the CycWEC, where harmonic waves are minimized by deeper submergence and symmetric pitching of the hydrofoils, thus maximizing the fundamental wave over harmonic waves.

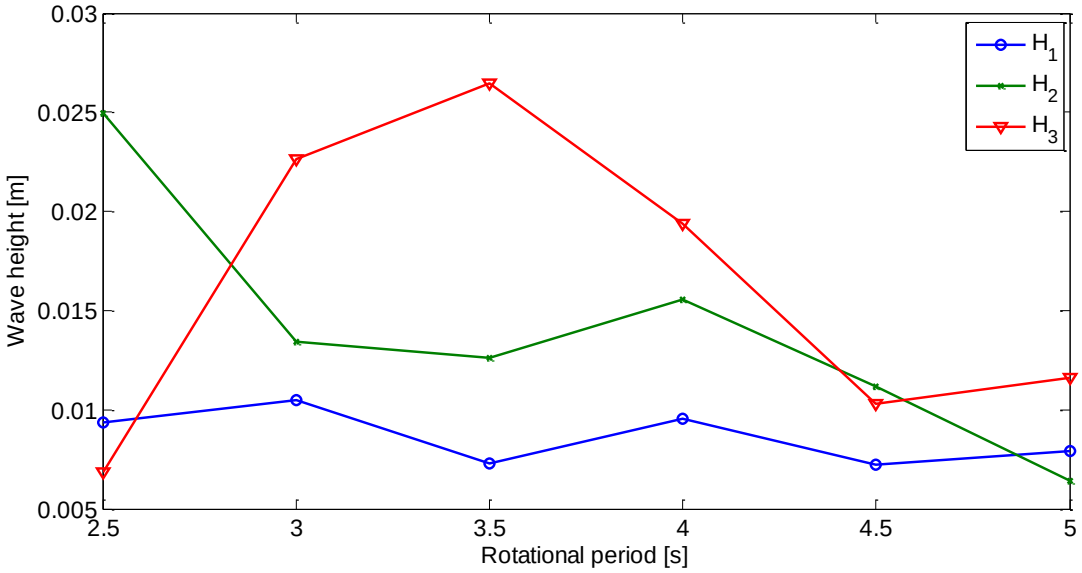

Figure 9: Wave heights measured at wave gauge 5 for shallow submergence yc and asymmetric blade pitch. Shown are wave heights of the fundamental wave (blue), first harmonic (green) and second harmonic (red).

The impact of submergence in reducing harmonic wave height is show in Figure 10, where the height of the third harmonic wave can be seen to decrease steeply with increasing submergence. Blade pitch was asymmetric for these measurements, thus the first harmonic wave height is also large and only expected to decrease at depths beyond the range that could be investigated in the present experiments.

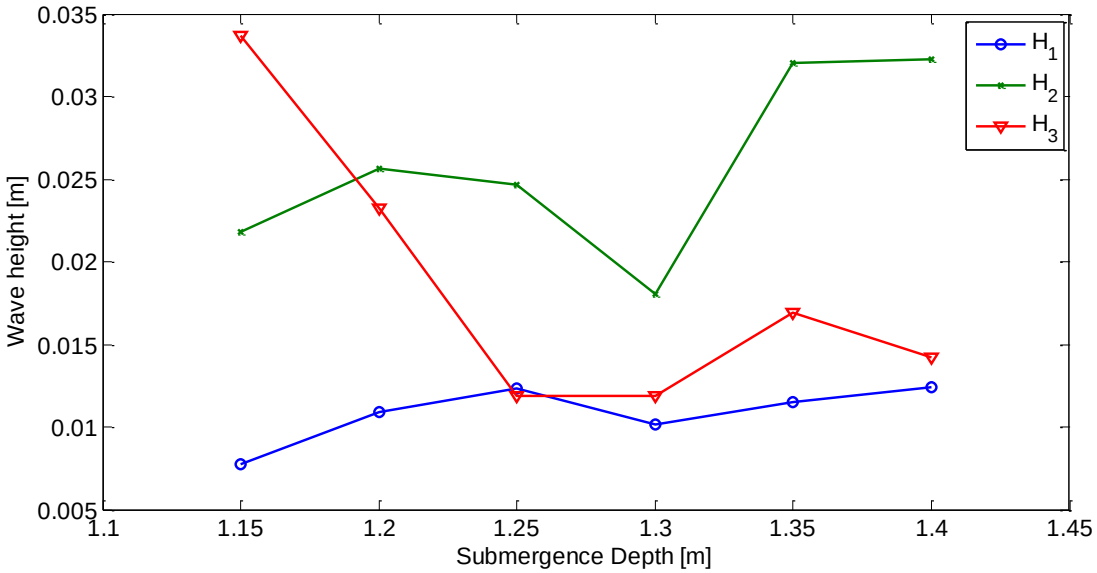

Figure 10: Wave heights measured at wave gauge 5 for varying submergence depths for fundamental frequency (blue), first harmonic (green) and second harmonic (red) with asymmetric pitch of the blades.

Wave height is expected to be a linear function of blade pitch angle and thus blade circulation. This is well supported by the fundamental wave height data shown in Figure 11, which is symmetric around zero blade pitch and increases for both positive and negative pitch angles equally. The second harmonic shows similar behavior, while the first harmonic wave height is asymmetric, most likely due to nonlinear effects which will require further investigation.

Another result from wave height measurements was that the wave heights measured at the wave gauge locations which were located at a distance of 8m or about ¾ of a design wave length from the CycWEC yielded much smaller wave heights than what was expected based on the two dimensional numerical simulations and wave channel experiments. It was discovered that this effect is due to the three dimensional diffraction of the generated waves. While a wave in a two dimensional wave channel conserves wave power by maintaining its wave height as it progresses, a cylindrical wave spreading in a circular fashion maintains wave height by a reduction in wave height as it travels outward, i.e. H~1/R with R being the distance from the wave source. Once this effect was accounted for, the wave heights observed in the OTRC-1 experiment at the wave gauge locations were found to be consistent with the two dimensional wave height results from earlier investigations.

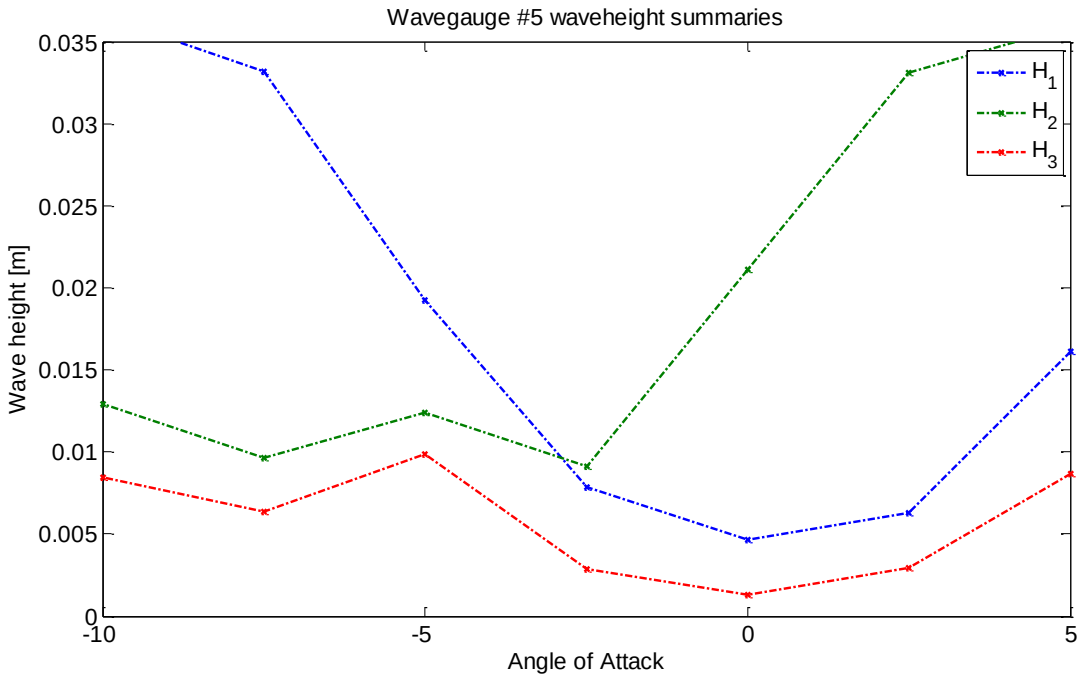

Figure 11: Measured wave heights of down wave wave gauge versus angle of attack. Fundamental wave (H1), first harmonic (H2) and second harmonic (H3) are shown.

Similar to the wave heights, the overall force measurements also vary linearly with angle of attack, as shown in Figure 12. The main shaft torque is almost flat for the pitch angles investigated, indicating that a large portion of the shaft torque is due to skin friction rather than lift induced drag. This again agrees with expectations based on airfoil theory. It also can be seen that a small offset in minimum lift force exists. While minimum lift was expected at a zero degree pitch angle, this point is shifted to an angle of about 1 degree at which still a small amount of lift is being produced. This effect is most likely produced by the finite thickness of the hydrofoil and the respective displacement effect at zero pitch angle.

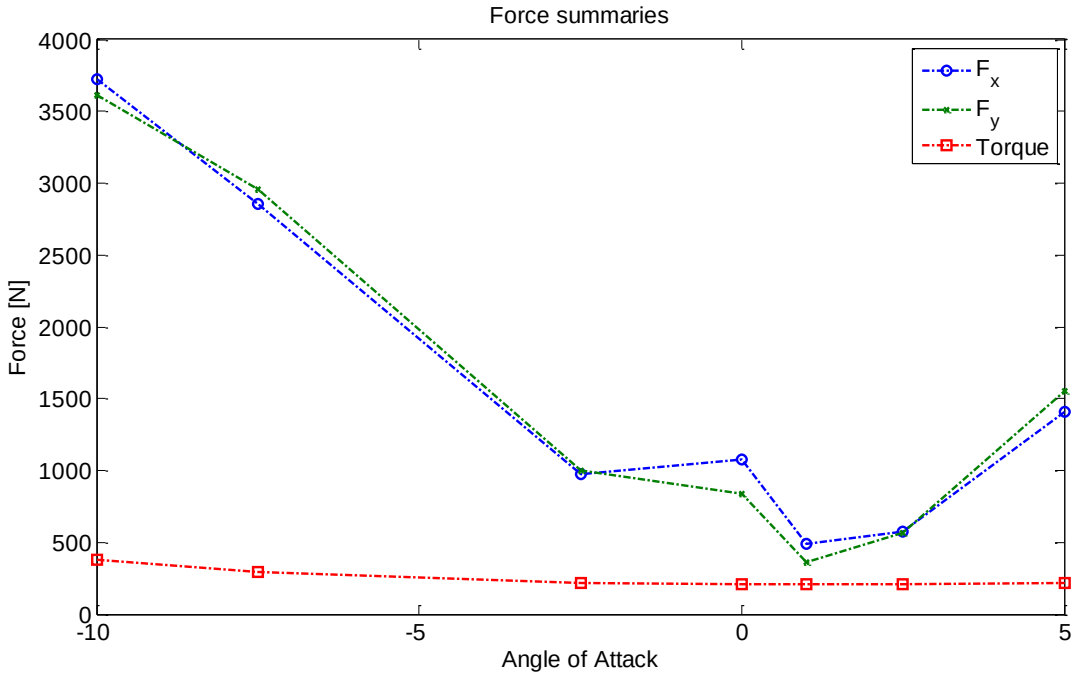

Figure 12 Hydrofoil average lift force versus angle of attack.

The hydrofoils employed in the 1:10 scale model are expected to develop lift forces up to 23kN at maximum blade velocity/minimum rotational period, and maximum blade pitch. As the blade pitch was increased, two problems emerged, one of which can be seen in the data presented in Figure 13. As the peak force in this measurement run approaches 10 kN (2.2 metric tons), the motor controllers operating both sides of the main shaft were not able to keep in sync with each other due to the commensurate increase in shaft torque. The large shaft torque loading caused issues with the synchronization between left and right motors and subsequently led to an emergency stop of the CycWEC at about 35s into the measurement run.

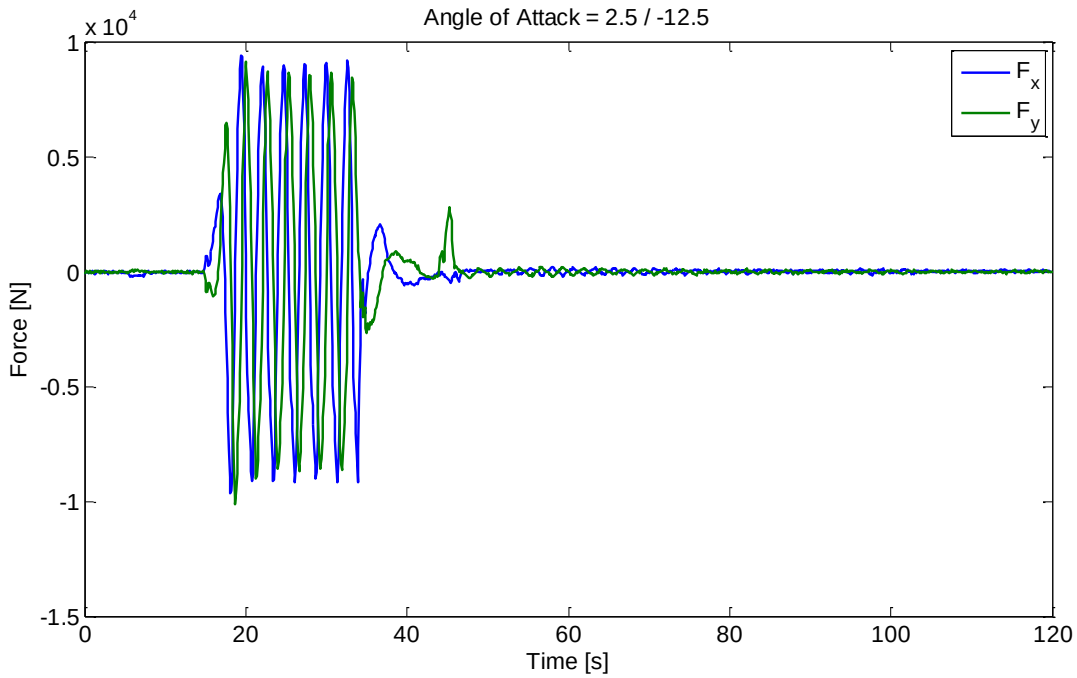

Figure 13: Horizontal (Fx) and vertical (Fy) force components for large angle pitch angles of 2.5 degrees for blade 1, and -12.5 degrees for blade 2.

A second problem associated with the larger lift forces was a twisting of the OTRC tunnel bridge, to which the model was structurally attached during the OTRC-1 measurement campaign. This twisting was severe enough that on request of the facility director no measurements with larger pitch angles were conducted during the OTRC-1 campaign. These had to be postponed pending redesign of the structural attachment of the model mount to the wave basin facility.

In summary, parameter studies varying angle of attack, rotational speed, and submergence depth were completed. Very good quantitative and qualitative agreement was achieved in comparison with earlier 2D simulations and wave channel experiments at small scale. Wave heights of the fundamental (H1), first harmonic (H2), and second harmonic (H3) waves are in agreement with these earlier investigations. The fundamental wave height varies linearly with angle of attack just as earlier experimental and numerical findings predicted. As a scientifically new discovery, the three dimensional wave generation patterns of the CycWEC could be observed for the first time. This observation led to the development of the numerical 3D diffraction model which was found to be in excellent agreement with the wave gauge data measured during the OTRC-1 testing campaign.

The first tests with the newly built and commissioned model also revealed a number of improvements needed in terms of model hardware, which were detailed in the model design and construction section of this report. One particular concern was that the following error induced shutdown of the main shaft

motors caused a twist in the overall CycWEC model, since very little stiffness exists in the torsional direction between left and right side. This subsequently caused loads on the blade attach fittings for which these fittings were never designed. A solution to this problem was found in retrofitting the main shaft motors with brakes to prevent twist in the model during emergency shutdown situations.

The lack of brakes on the pitch actuators also caused issues, mainly during model installation. As the blades were not held fixed in place when the pitch actuators were powered down, they would tend to pitch on their own during hoisting operations under the influence of gravity, with risk of damage to the actuators when hitting the end stops. Preventing this made the model commissioning process unnecessarily time consuming and difficult, which is why the pitch actuators were retrofitted with brakes between testing campaigns. The cost of retrofitting brakes was found to be far less than the cost of lost testing time.

The time between the first and second testing campaign was thus used both for data analysis, as well as to implement these improvements in both hard and software.

OTRC-2

The OTRC-2 testing campaign, which was severely delayed from the originally scheduled testing date of January 2012, finally commenced from June 22nd (delivery of model) to July 19th, 2012. In preparation, the model mount had been entirely redesigned so that the CycWEC loads were directly transmitted to hard points in the tunnel floor. In addition, all motors and actuators were equipped with brakes in order to improve installation and commissioning. As a result, model installation and commissioning was reduced from almost a week at OTRC-1 to a couple of days at OTRC-2.

Significant additional effort was spent to improve the synchronization of both main shaft sides by improving both the position measurement using directly coupled main shaft encoders in addition to the motor shaft encoders, as well as by improving the main shaft drive control software. These improvements were tested and evaluated in dry runs to address the problems encountered during OTRC-2, and even emergency stop operations artificially induced during testing would keep both sides of the main shaft within a couple of degrees of misalignment thus minimizing the risk of any structural damage due to main shaft twist.

The feedback control software had also undergone improvements and further dry run testing. The wave height estimation algorithm that had been employed for feedback controlled irregular wave cancellation studies (see Irregular Wave Cancellation section for results), was implemented in the Labview based control software of the 1:10 scale CycWEC. It was subsequently tested with all hardware in the loop, where a wave gauge was attached to a linear computer controlled slide to simulate the waves passing the wave gage by dipping the gage in a stationary water reservoir. These hardware-in-the-loop dry runs would include all hardware and software employed in the actual experiment and thus allow for testing of the estimation and control algorithm under realistic test conditions including electrical noise, data

transfer delays and software processing time. These dry runs enabled the successful wave cancellation runs performed at OTRC-2.

The output of the estimation algorithm for an actual (NOT simulated) measurement run is shown in Figure 14. The input signal to the wave estimation algorithm is the wave gauge signal shown in blue, while the outputs of the algorithm are the wave height shown in green, along with the phase of the wave shown in radians in red. The latter is used to synchronize the rotation of the CycWEC during wave cancellation and is thus the most important feedback quantity. While there is a lag in estimated wave height during the start of the experimental run, the wave phase and wave height signals represent the measured wave gage signals properties extremely well, in particular for the periodic portion of the measurement run.

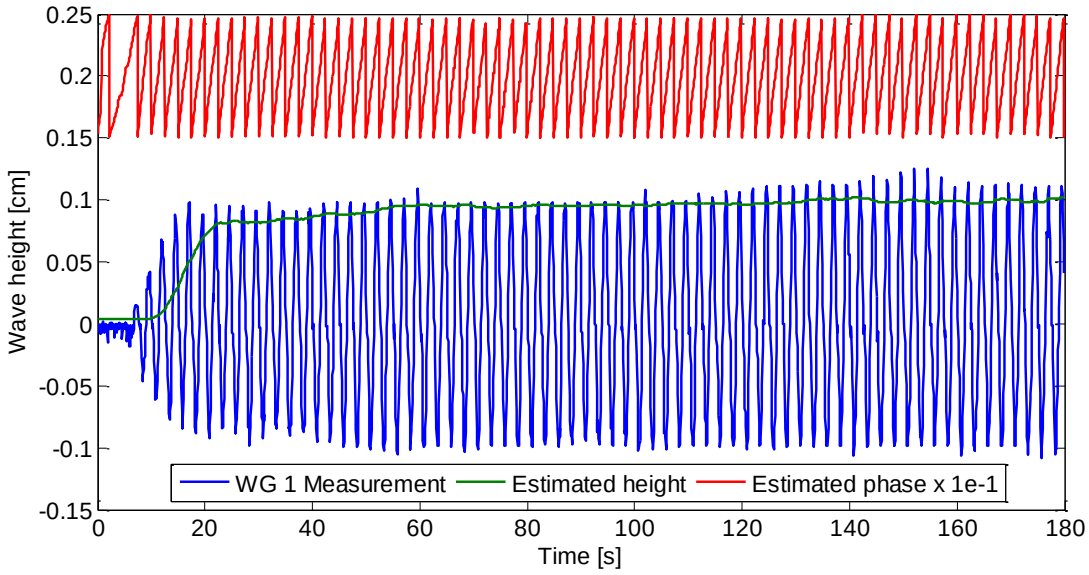

Figure 14: Wave estimator performance. Upwave wave gauge measurement (blue) used for control of CycWEC. Estimated wave height (green) and estimated phase (red) at CycWEC location

The proper blade pitch is important for wave energy conversion efficiency as well, since a mismatch in wave height produced by the CycWEC with the incoming wave height will cause shaft power losses: If the wave height produced by the CycWEC is less than the incoming wave, only partial wave cancellation will be achieved with the remainder of the wave height not being extracted. If the CycWEC generates a wave height that is larger than the incoming wave, the power for the additional wave height produced will need to be provided by the CycWEC. Figure 15 shows the relationship between shaft power and angle of attack, which is expected to be quadratic as the wave power increases quadratically with angle of attack and thus wave height which are linearly related. This trend is evident in the data shown in

Figure 15 where much larger shaft power increases are shown for larger blade pitch angles than for smaller blade pitch angles.

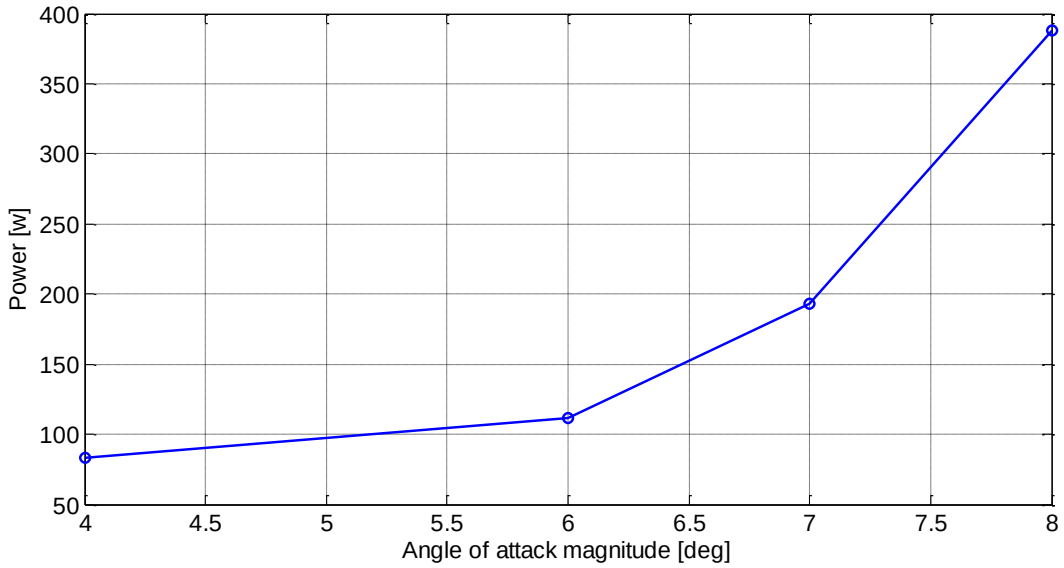

Figure 15: Measured shaft power versus angle of attack magnitude at constant submergence depth yc = 1.5 m and constant rotational period T = 2.5s

The synchronization between incoming wave and rotation of the CycWEC is essential, which has been confirmed by both numerical simulations and wave channel experiments. The shaft power data shown in Figure 16 demonstrates that this is just as crucial at the 1:10 scale level as in the previous investigations. In the runs shown in Figure 16, the phase between the estimated phase of the incoming wave and the angle of the main shaft was systematically varied. This was done using a comparatively small fixed blade pitch, which prevented net shaft power from being produced. As a result, the shaft power required to rotate the CycWEC was reduced by the amount of wave power extracted, however at no time was the extracted power larger than losses due to skin friction, gear box losses etc. The minimum shaft power was achieved for a phase between the wave and the main shaft angle of 245 degrees. At this point, the shaft power was about 30 percent less than in situations where the phase was mismatched. The investigation shown in Figure 16 was performed to find the optimal feedback phase delay, which was subsequently used for wave cancellation runs at larger wave heights and blade pitch angles.

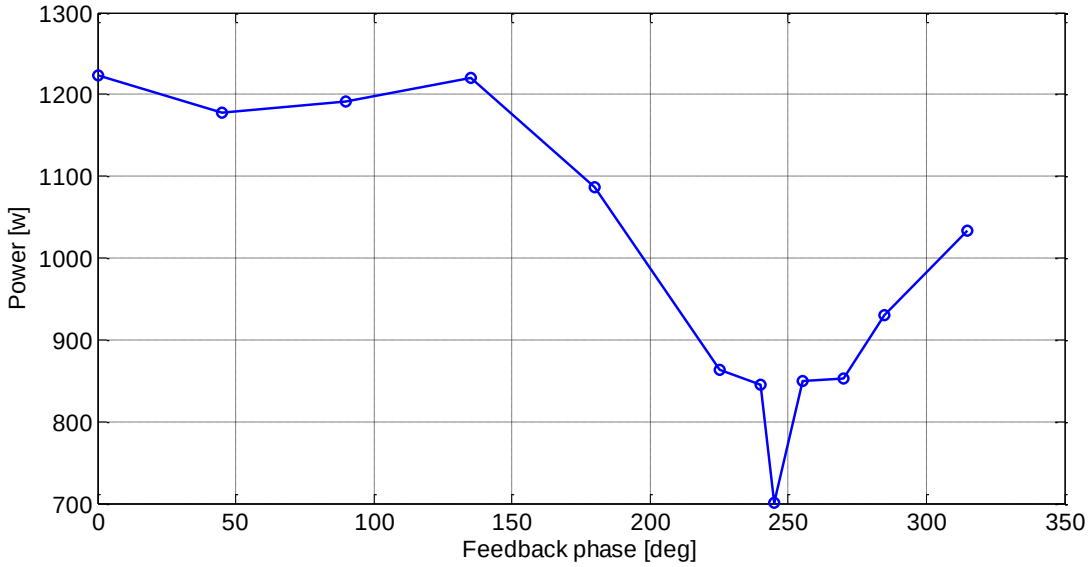

Figure 16: Power versus phase between incoming wave and rotation of CycWEC.

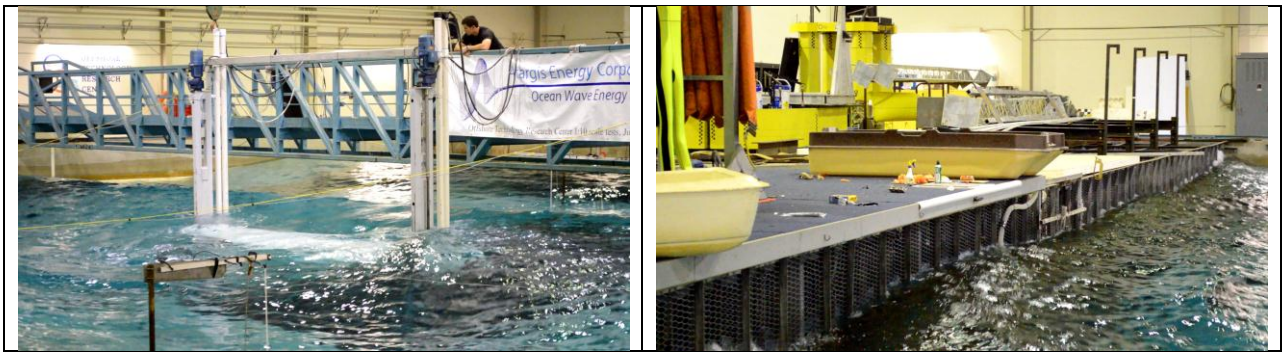

Figure 17: Wave Cancellation water surface pictures. Left, view of submerged CycWEC in operation. Right, remaining waves impinging on wave tank screen system

Pictures of the wave tank in operation during a wave cancellation run are shown in Figure 17. The CycWEC is barely visible beneath the surface in the center of the left picture, and it is difficult to gage the impact of the CycWEC on the incoming wave as it is obscured by smaller short wavelength surface ripples. In the picture on the right, the waves entering the screen system can be seen. The interaction between the CycWEC and the incoming wave is evident there, as the wave crests are not a straight line any more but rather modulated in the spanwise direction by the almost circular wave generated by the CycWEC. This picture thus provides indirect evidence of wave power extraction achieved by the CycWEC.

Direct evidence, or rather the measurement results from a successful wave cancellation run are shown in Figure 18. The data has been phase averaged over all measured cycles, with a sign convention of positive power being power delivered from the motor controller to the motor, while negative power indicating the motor operating as generator and delivering power back to the controller. While there are brief periods of positive power delivery throughout the entire revolution (T=2.5s), the average power extracted is just under 500W of electric power. The data shown in Figure 18 is based on the motor controller information, but consistent results were achieved with direct shaft torque measurements.

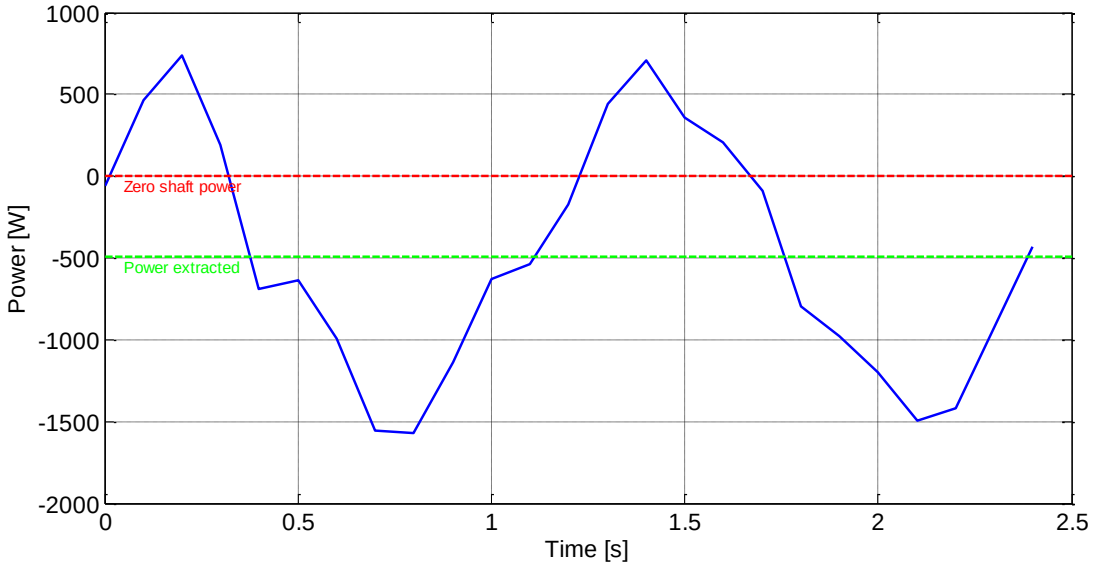

Figure 18: Phase averaged power measurement of both left/right motors throughout one period. The time average or mean value shows -491 Watts of extracted power

An important operational consideration is the ability of the CycWEC to self-start the rotation in the presence of a wave. Self-starting greatly simplifies the control electronics of the CycWEC, since instead of a four quadrant capable motor/generator controller only a two quadrant capable generator controller can be employed. To investigate the self-start capabilities, the CycWEC was exposed to incoming waves with the main shaft brakes applied. The torque at the main shaft was then measured using load cells. In a deep water wave, the wave induced flow direction changes through 360 degrees with each wave passage. If the flow direction is such that the hydrofoil produces lift, and the direction of the resulting lift force is partially aligned with the direction of rotation, shaft torque is produced. Figure 19 shows that this is indeed the case for a large portion of the revolution, enabling the CycWEC to self-start.

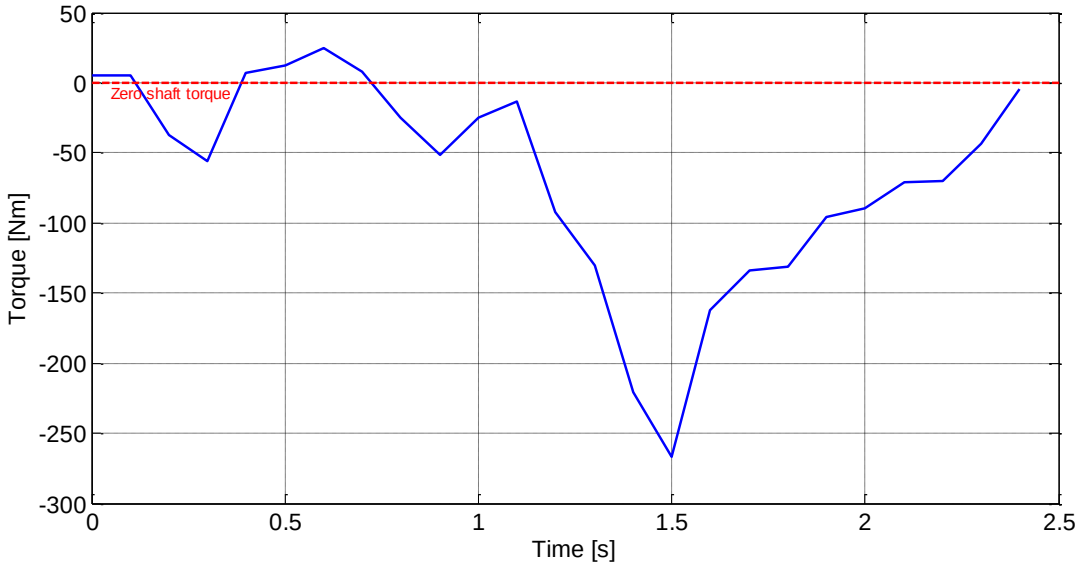

Figure 19: Phase averaged torque of a stationary CycWEC at a fixed angle of attack (+/-5 deg) with incoming wave with a period of 2.5 seconds. Negative torque values indicate self-start up capability

During OTRC-2, additional tests were run to evaluate the wave generation capabilities at larger pitch angles, which could not be performed during OTRC-1 due to structural issues of the support bridge. A parameter study showing the shaft power as a function of submergence depth is shown in Figure 20. While the hydrofoil drag induced portion of the shaft power remains constant independent of submergence depth, the larger waves produced at shallower submergence depths require more shaft power as the submergence is reduced. This effect is nonlinear, and the changes in shaft power become larger as the CycWEC approaches the surface.

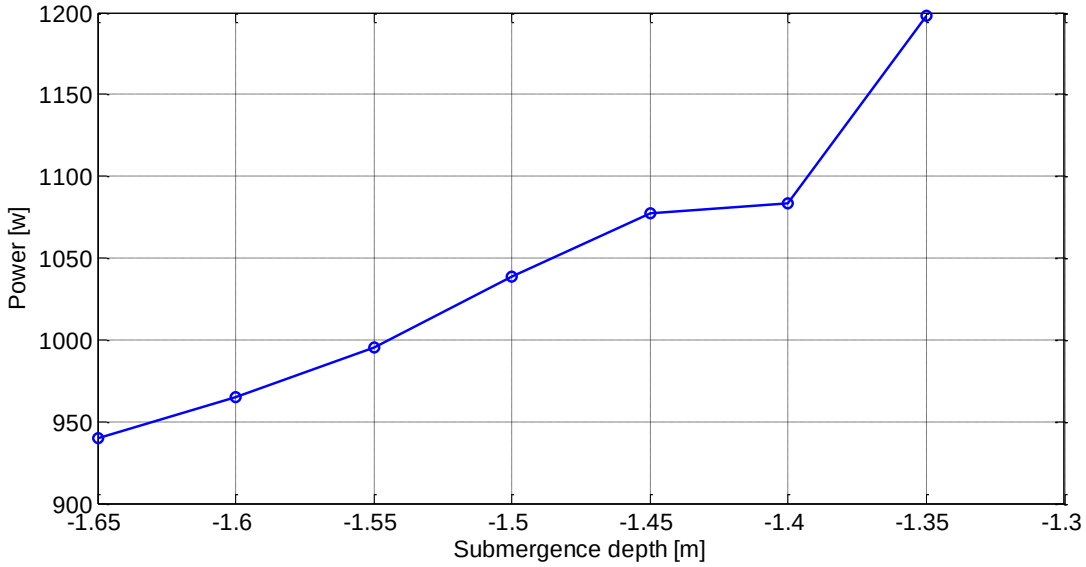

Figure 20: Power versus submergence depth for fixed angle of attack and rotational period. At larger depths less power is needed to spin the WEC due to less losses with surface interactions

Another objective of the wave generation measurements was to validate the 3D diffraction model, which is shown in Figure 21 in comparison to wave gauge measurements. The wave heights are in good agreement between experiment and numerical model, with the exception of the wave gauge located in the basin center. The deviation at that location is most likely due to transverse waves from reflections of waves at the basin side walls. Otherwise the agreement between model and measurements is excellent for all submergence depths investigated.

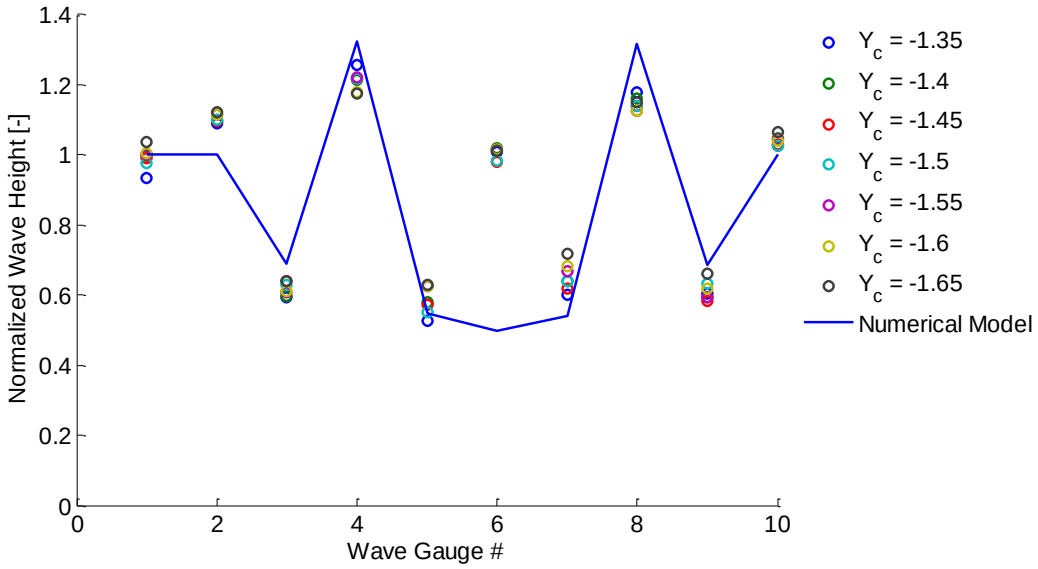

Figure 21: Comparison of measured wave heights at different submergence depths and numerical diffraction model for wave cancellation case

In summary, the two testing campaigns at OTRC allowed us to achieve successful power extraction using a CycWEC for the first time. They also yielded new insight into the wave diffraction flow physics, where the CycWEC in the present experiments showed an almost circular single sided wave generation pattern. Observations and measurements from these experiments were subsequently used to develop a numerical diffraction model, and to predict the performance of the CycWEC at full ocean scale. The results from these developments are presented in the following sections.

Simulations

Code Development and Results

Single Vortex Code

During the project period, an existing code to simulate a simplified model of the CycWEC has been extensively extended and validated to provide the simulation environment necessary to achieve the project goals.

The main goal of extending the code was to allow for feedback control simulations with a controller 'in the loop'. In order to achieve this, the whole code had to be modified since the underlying data structure had to be extended. During the modification, the code was also changed to solve the non-dimensionalized equations. For the CycWEC simulations, this change has a number of advantages, including i) a single resolution study is sufficient for all simulations, regardless of the CycWEC or wave

parameters used, ii) the results of a single simulation can be scaled to match many different scenarios as long as the CycWEC scaling (with respect to the wave climate) is not changed.

The code was verified and validated extensively, first with a thorough resolution study (described in detail in this report) and second against small scale experiments in a two-dimensional wave flume (1:300 scale).

As mentioned above, the re-structuring of the code was necessary mainly to allow for feedback control simulations. This required a complete redesign of the data structures as well as the layout of the function since numerous quantities that were contained in function in the previous version of the code needed to be accessible from the main routine. Once this task was accomplished and thoroughly tested, the control model was implemented in a straightforward manner: one additional function call in the main time stepping loop.

Since the verification and validation of the code also exposed some bottlenecks regarding code performance, extra steps were taken to ensure optimal computer utilization. Toward that end, various numerical routines were re-written to make use of all the time saving functionality offered in Matlab®. Due to these improvements, typical code execution times were reduced by almost one order of magnitude (a simulation of 10 revolutions of the CycWEC can now be modeled in less than one minute on a typical desktop PC). With this speedup, numerous simulations were performed in a short time so that an accurate model of the flow field could be developed using advanced system identification methods. In turn, this model was crucial for the development of a state-of-the-art controller. With this controller, it was possible, within physically reasonable limits, to adjust the hydrofoil angle of attack as well as the rotation phase (or shaft angle) in order to successfully extract the vast majority of incoming waves, including in irregular wave climates. This truly novel technique is described in more detail elsewhere in this report.

In addition to enabling the development of feedback control strategies for CycWECs, this simulation code also allows for wide-ranging parameters studies. Typical design parameters include the CycWEC radius and the hydrofoil circulation (which is related to the hydrofoil lift). In addition, the performance of a given CycWEC design in various waves (defined by their wave length and height) can be studied quickly and efficiently.

An example of this type of study was presented at the European Wave and Tidal Energy Conference in 2011. This study investigated the performance of a CycWEC to extract energy from irregular deep ocean waves. The wave climate under consideration is defined as the Bretschneider wave spectrum for sea-state 5 (H_s=3.25m, T_p=9.7s). For the numerical simulations, the spectrum was decomposed into 21 wave components (Figure 22).

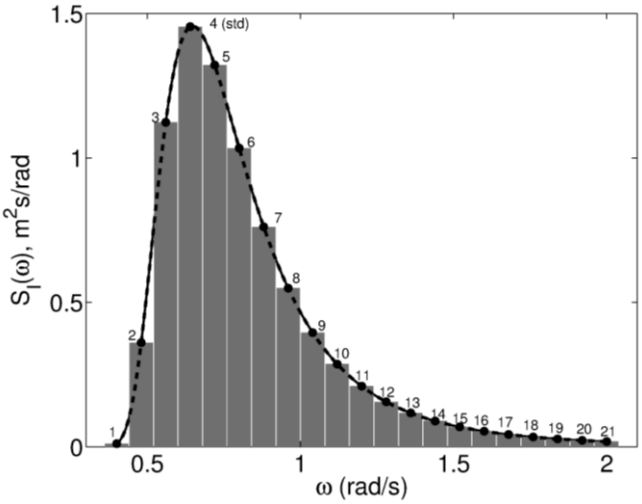

Figure 22: Bretschneider spectrum, H_s=3.25m, T_p=9.7s (sea-state 5).

Performing numerous simulations for controller development, it was possible to achieve hydrodynamic efficiencies up to 98%, and most simulations showed efficiencies greater than 80%. An example of the simulations results for seven wave components (see Figure 22) is shown in Figure 23. Comparing the upstream wave heights (blue and green) with the downstream wave height (red), the results show that a significant portion of the wave spectrum is canceled using a properly sized and feedback controlled CycWEC. In this case, the overall efficiency was 85%.

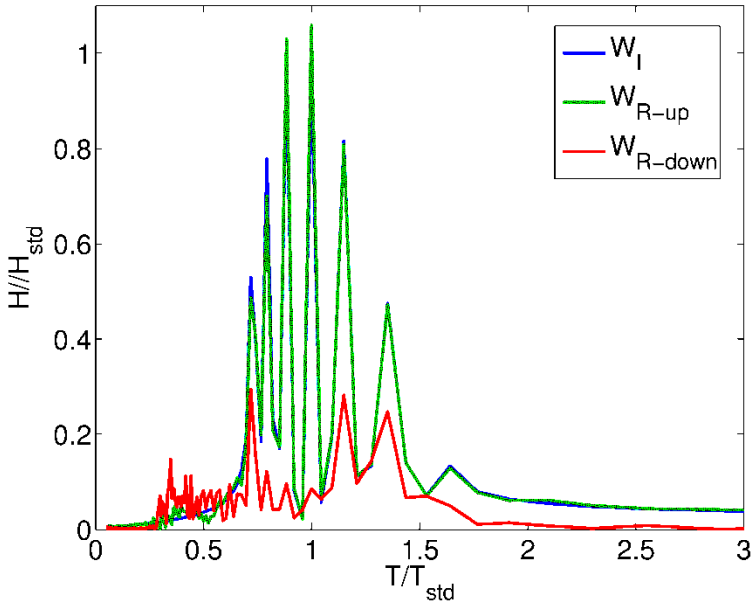

Figure 23: Fourier analysis of upstream (green and blue) and downstream (red) wave fields one wavelength from the CycWEC.

However, because of the modeling assumptions, it is not possible to compute lift and drag forces on the hydrofoils or the whole CycWEC using this code. Therefore, it is also not possible to compute the shaft torque, which ultimately is the measure of power extraction from the incoming waves. This limitation is inherent in the assumptions that needed to be made to develop this code.

During the course of this program, however, it became obvious that it is well worth the effort to develop this code for the design studies and controller development mentioned above. Furthermore, a method to add a viscous force estimate was established based on the results of this code. The methodology for this estimation is described elsewhere in this report.

To overcome the obvious shortcoming of the single vortex code, a panel code was developed. The details of that code are described in the following section.

Panel Code

In addition to the single vortex code described above, a panel code that models the hydrofoils of the CycWEC has been developed. The details of the equations and the methods for solving them are given elsewhere in this report; here only a short summary and the pertinent results obtained with the code are presented.

The newly developed panel code uses a standard panel method. The basic premise is that the hydrofoil is comprised of a number of panels, each of which carries an a priori unknown circulation. In the

method, an algebraic system of equations is developed based on the surface boundary condition on the hydrofoil that the flow has to be tangential to the panel (since potential flow is assumed, only the no-penetration boundary condition can be enforced). The right-hand-side vector of the system of equations contains all the known velocities, here in particular the velocities due to the radiated waves.

Solving this system results in the determination of the unknown vortex strengths of each panel. Once the vortex strengths are known, the velocity at each panel can be computed by summing up the induced velocity from all vortices at a given point. While the code contains the logic to check that the flow is in fact tangential to the panel, this is implicit in the method and has never raised a flag.

Since the submerged hydrofoil creates lift, it is paramount to also enforce the Kutta condition, which postulates that the flow has to leave the trailing edge of the hydrofoil tangentially. In the context of a panel method, this can be enforced by requiring that the strength of the wake vortex is the sum of the strength of the vortices on the panels at the top and bottom of the trailing edge. While not exactly correct, in the code it is assumed that the wake vortices decay rapidly and therefore they are not tracked (an option to do so is implemented, but validation simulations have shown minimal effect of the wake on the velocity—and therefore pressure—distribution on the hydrofoil). This results in the additional requirement that the strengths of the vortices at the top and bottom panel at the trailing edge have to have equal magnitude but opposite sign. To enforce this condition, the algebraic system of equations has to be appended by this condition, which yields the system to be over-specified. A simple and well known solution is to discard one equation for a panel vortex—usually where the pressure distribution is fairly uniform—and substitute the Kutta condition in its place. The missing vortex strength is then interpolated from the upstream and downstream panel after the solution to the algebraic system is obtained.

Once the hydrofoil surface velocities are known, the Bernoulli equation $p_0 + q_0 = p + q$ is used to obtain the local velocities and pressure coefficient, $c_p = 1 - \left(\frac{U}{U_0}\right)^2$. Here U_0 is the velocity due to the CycWEC rotation and U is the local velocity on the panel surface. The details of the derivation are given elsewhere in this report.

Geometry modeling

In order to mathematically describe the hydrofoil cross section, a code was developed and integrated in the main panel code that automatically generates the necessary coordinates. To date, hydrofoil cross sections are based on the 4 digit Naca series, e.g. the Naca0015. (see Figure 24).

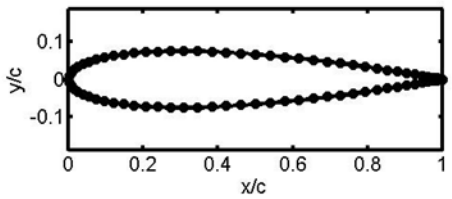

Figure 24: Naca0015 hydrofoil.

Since the hydrofoil that was tested at the OTRC facility is based on the Naca0015, a code was written to replicate the design steps of the *curved* hydrofoil (Figure 25). The tested CycWEC has a radius R=1m To compensate for the circular motion of the CycWEC, the hydrofoil chord is curved such that at $\alpha=0^o$ angle of attack, the chord is aligned with the circle along which the blade travels. The design chord length is c=0.75m.

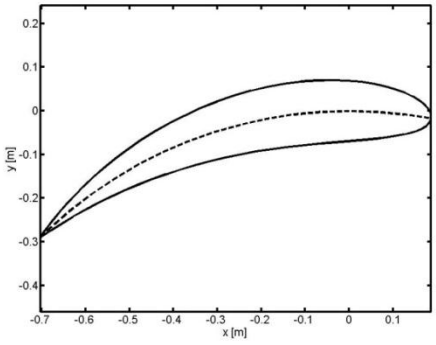

Figure 25: Curved Naca0015 hydrofoil. The dashed line indicates the chord and the path or travel ($a=0^o$).

For simplicity, data for only one hydrofoil are computed here. The waves generated (or cancelled) by a CycWEC with two blades can be computed from this data using the method of superposition since the underlying model is linear. In a typical setup, one blade of the CycWEC is pitched at a positive angle of attack (nose outward) while the other blade is pitched at the same angle inward, i.e. in the negative direction. Earlier simulations and experiments have shown that this configuration results in the best one-sided wave generation and therefore also the best wave cancellation [1].

The first simulation with a curved hydrofoil traveling along a circular path (using the experimental CycWEC dimensions, R=1m, c=0.75m) was performed at a deep submergence, y_c=1,500m. This eliminates the wave interaction, but provides some insight into the effect of the curvature of the hydrofoil and its motion in a circular path when compared to results obtained for a straight hydrofoil in a uniform stream. The comparison data was obtained using Javafoil [4]. The pressure distribution for an angle of attack of $\alpha=6^o$ is shown in Figure 26. The results show that the CycWEC hydrofoil traveling in a

circle obtains a drastically different pressure distribution than the standard Naca0015 hydrofoil in straight motion. The suction side pressure (upper curve) is lower than for the straight hydrofoil (note that the vertical axis shows $-c_p$), and the pressure side shows a higher pressure. The suction peak pressure, interestingly, remains the same. Since the overall lift is effectively the area between the two curves, the curved hydrofoil traveling in a circle can create higher lift than the straight hydrofoil. This is a favorable result in terms of projected CycWEC performance, since the shaft torque is generated by the lift force and a larger lift force means greater shaft torque and better wave energy extraction.

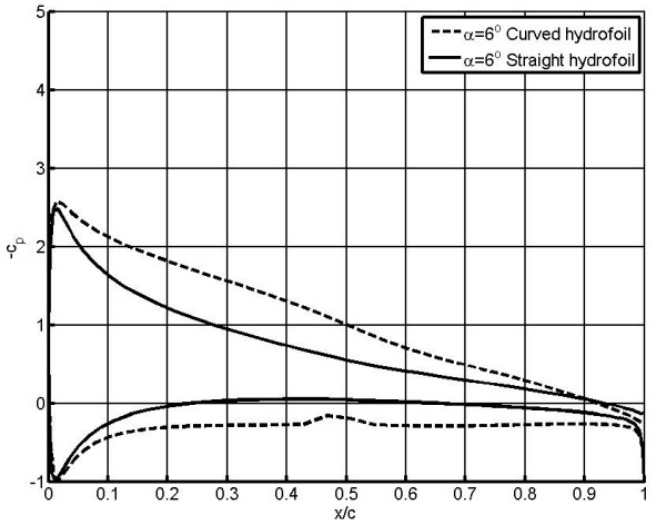

Figure 26: Comparison of pressure distribution of curved and straight hydrofoil at α=6°.

With this positive result, simulations of the CycWEC matching the operating conditions at the OTRC test facility were performed. The submergence depth was y_c=1.5m. A sample picture of the modeled CycWEC is shown in Figure 27, where the blade at the top of the figure has an angle of attack of α=+6°.

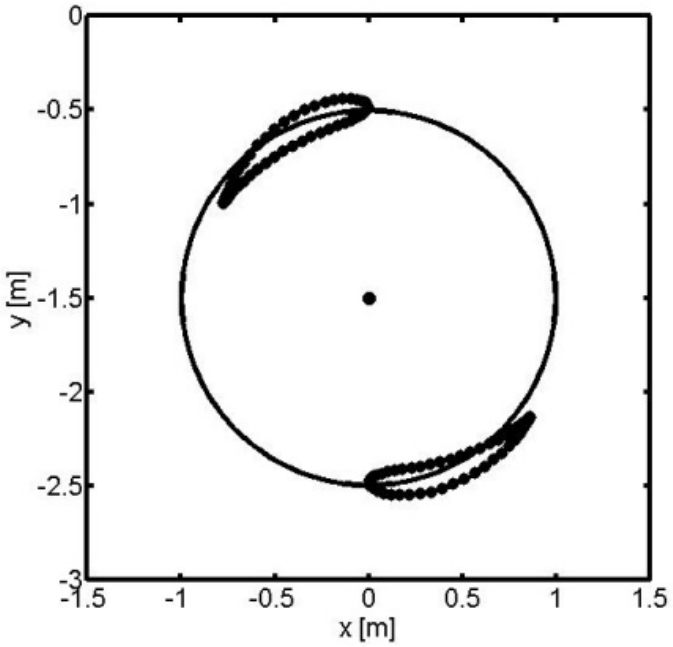

Figure 27: CycWEC with two blades. Top hydrofoil angle of attack α=6°, bottom hydrofoil angle of attack α=-6°.

The pressure distributions obtained for the positively and negatively pitched hydrofoils are shown in Figure 28 and Figure 29. A number of observations can be made from these plots. First, the data show that the pressure distribution around the hydrofoil is not constant as the hydrofoil rotates around the main shaft when the CycWEC is close to the free surface.

Second, even in the best case where the hydrofoil is in the 'left' position, the suction side pressure coefficient is well below the straight hydrofoil and the deeply submerged rotating hydrofoil. From this data, it is clear that the proximity of the free surface has a significant effect on the hydrofoil pressure distribution; if the hydrofoil is close to the surface, the capacity to create lift—and therefore shaft torque—is greatly limited.

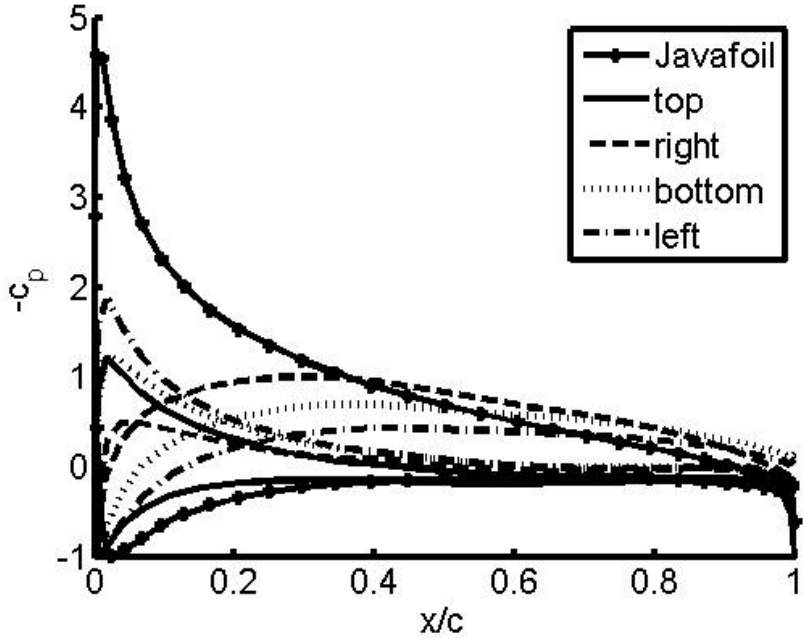

Figure 28: Pressure distribution on curved NACA0015 hydrofoil. α=+6°. Included for comparison data for a straight hydrofoil from Javefoil.

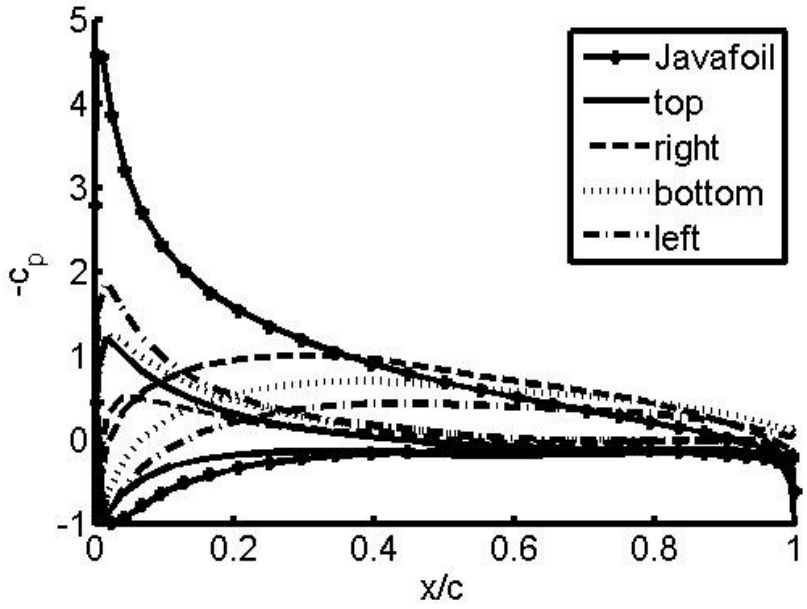

Figure 29 Pressure distribution on curved NACA0015 hydrofoil. α=-6°. Included for comparison data for a straight hydrofoil from Javefoil.

Irregular Wave Cancellation

For the deployment of the CycWEC in the real world scenario, the efficiency of the CycWEC must be shown and understood for uni-directional, non-harmonic, irregular Airy waves. In previous work the efficiency of the CycWEC in a 2 dimensional, inviscid simulation is shown to be greater than 99% for a large frequency bandwidth for periodic incoming Airy waves. The problem is that real life deep water ocean waves are not limited to a monotonic frequency. For the successful cancellation of irregular sea states, feedback control is essential to measure the incoming wave and predict the wave state as defined below. The CycWEC is then synchronized to realtime measurements and estimates of the incoming wave phase and height. It is shown below that once a proper estimation and controller are developed that the CycWEC achieves the same efficiency envelope for the harmonic cancellation results.

The irregular incident wave field is modeled using a linear superposition of a finite number of linear Airy wave components. The fidelity of the irregular wave field will increase as the number of wave components is increased. According to [2], a minimum of 20 wave components are required for modeling a unidirectional irregular seaway. The amplitude for component i is based on a specified wave spectrum according to,

$$a_i = \frac{H_i}{2} = \sqrt{2 S_I \omega_i \, \Delta\omega_i},$$

where $S_I$is the spectral density and $\Delta\omega_i$ is the wave frequency interval for component i. For the current study the incident wave field is modeled using the Bretschneider wave spectrum, which is a commonly used two parameter model for wave spectra in the open ocean. The Bretschneider spectrum is defined as [3]:

$$S_I(\omega) = \frac{486 H_s^2}{T_s^4} \omega^5 e^{-1948.2 \omega^4 T^4},$$

where H_s is the significant wave height and T_s is the wave period associated with the peak energy. The Bretschneider wave spectrum is non-dimensionalized by the standard wavelength λ_s and the standard period T_s as shown in Figure 30. Also shown are the resulting wave components when the spectrum is divided into 40 wave components with $0.7\omega_s \leq \omega \leq 1.3\omega_s$. With the period and amplitude of each component wave defined, the associated wave length and power can be determined from Airy wave theory. The wave length is determined from the dispersion relationship as follows,

$$\lambda_i = \frac{T_i^2 g}{2\pi},$$

where λ_i and T_i are the wavelength and period of component i. The wave power per unit length, P_i, associated with each component is related to the wave height and period by,

$$P_i = \frac{1}{32\pi}\rho\, g^2 H_i^2 T_i.$$

Since the wave power scales linearly with the wave period, higher harmonic waves of the same wave height will contain less energy in proportion to their period. Also note the quadratic relationship between wave energy and wave height.

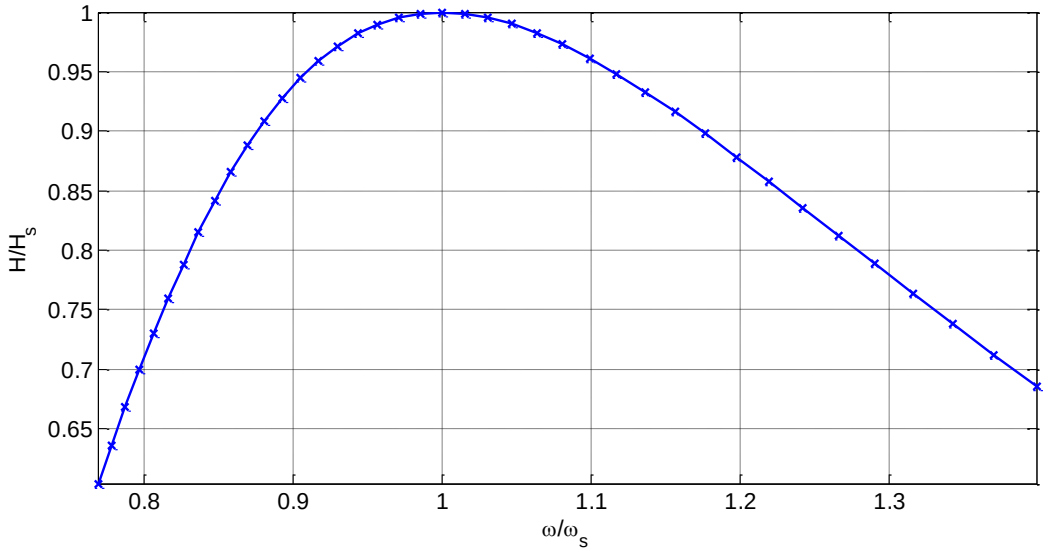

Figure 30 Bretschneider spectrum discretized into 40 components over the range of $\frac{2}{3}T_s \leq T \leq \frac{4}{3}T_s$

A typical time history of the resulting wave surface is shown in Figure 31.This is formulated by the linear combination of each component with random phase between $\theta = 0$ and $\theta = 2\pi$.

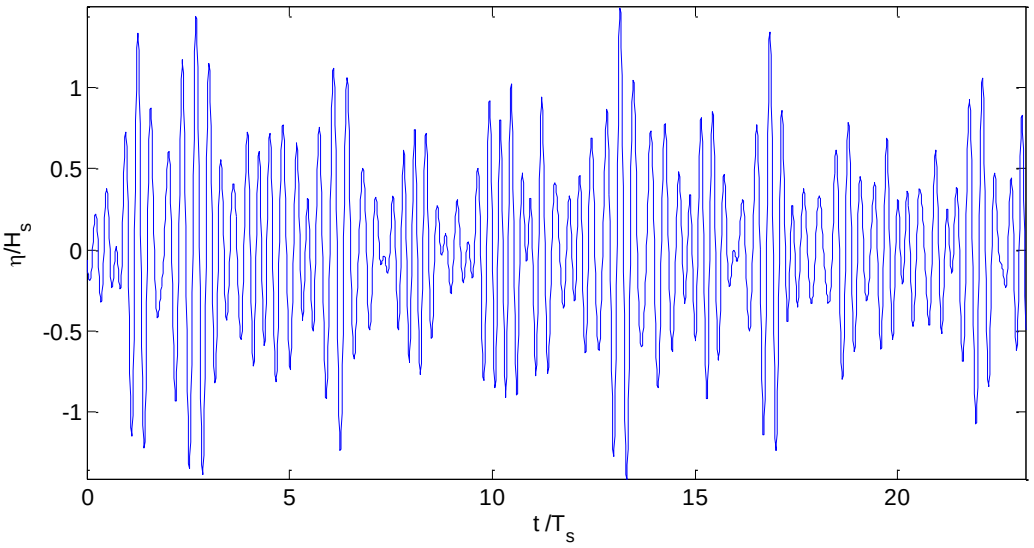

Figure 31 Time history of 40 component Bretschneider wave linearly superimposed with randomized phase

For the successful cancelation of an unknown, incoming airy wave, feedback control and wave state estimation are necessary for operation of the CycWEC. Algorithms to interpret and estimate the wave state in real time fashion are needed to adequately control and efficiently extract energy. The wave state for a single Airy wave is defined as its phase θ, frequency ω, and wave height H. A sensor which measures the surface elevation over time is placed upstream of the CycWEC. This measurement is defined as $\eta(t)$ and for a single Airy wave displays a purely periodic signal with unknown frequency and amplitude. The implemented feedback control scheme is shown in Figure 32. The sensor relays a signal to the estimator which estimates the wave height, phase and period. The controller then computes the rotational position and blade angle to generate an opposing wave that effectively cancel the incident wave field.

Given a time history of the upstream measurement, a relation is sought such that $\left[\hat{\omega}(t)\ \hat{\phi}(t)\ \hat{H}(t)\right]^T = f([\,\eta(t), \eta(t-1), \ldots, \eta(t-n)]) + e(t)$ with minimal estimation error, $e(t)$. A typical Fourier analysis falls short because instantaneous phase information is lost in the decomposition. Therefore, other digital signal processing methods need to be implemented. Because the up-wave wave height measurement contains no negative frequency components, the signal can be expressed as an analytic signal such that,

$$\eta(t) = \frac{1}{2\pi} \int_0^\infty \eta(\omega) e^{i\omega t}\, d\omega.$$

A complex representation of a periodic signal is $e^{i\omega t} = \eta(t) + i\,\hat{\eta}(t)$. The complex component of the analytic signal, which is unknown at this point, is analogous to the Hilbert transformation, $\mathcal{H}[\cdot]$, of the real component; that is $\hat{\eta}(t) = \mathcal{H}[\eta(t)]$. The Hilbert transformation is a linear filter which produces a phase shift of $\pm\pi/2$ over all frequencies present in the signal, $\eta(t)$. In the time domain the transformation for this linear filter is identical to the convolution with $1/\pi t$ which is shown as,

$$\mathcal{H}[\eta(t)] = \frac{1}{\pi t} * \eta(t) = \frac{1}{\pi}\int_{-\infty}^{\infty} \frac{\eta(t-\tau)}{\tau}\, d\tau.$$

In the frequency domain the transform of the signal $f = 1/\pi t$ is

$$-i\,sgn(f) = \begin{cases} -i & f > 0 \\ 0 & f = 0. \\ i & f = 0 \end{cases}$$

The transfer function of this ideal filter will have a magnitude of one and phase of $\pm\pi/2$ for $\pm\omega$, respectively. Because the Fourier transform is a non-causal transformation (dependent on previous, current and future measurements), an approximation to this transformation is necessary. Typical filters such as finite impulse response (FIR) and infinite impulse response (IIR) filters can be designed to simulate the response of $1/\pi t$. As for the purposes of this paper a 3 stage cascading IIR filter is used to estimate the complex component of the Hilbert transformation with minimal phase (although non-linear) delays at the designed frequency.

Now that the real and complex components of the analytic signal are known to some degree of error, the instantaneous amplitude is estimated from the L_2 norm of the signals, (i.e. $\widehat{H}(t) = ||\eta(t) - \hat{\eta}(t)||_2$). The instantaneous phase is then computed as the angle between the real and complex estimate as, $\hat{\phi}(t) = \tan^{-1}(\hat{\eta}(t)/\eta(t))$. The instantaneous frequency is the time derivative of the phase estimate.

As seen in Figure 32, the wave state is now fully estimated. The control scheme is very basic for the purposes of this paper. Proportional control is used for the blade pitch (i.e., bound circulation), such that $\alpha_i(t) = P_{gain}\widehat{H}(t)$. This is a reasonable assumption as open loop wave generation results shown in [1] display a very linear relationship between the bound circulation and resulting wave height. As for rotary control of the WEC, the group velocity is estimated and compensated for as a phase delay. The time delays are then superimposed to control the rotational velocity of the main shaft in a stepwise fashion, such that $\theta(t) = \hat{\phi}(t) + \eta_{\lambda_s} C_g + \theta_f$, where C_g is the group velocity of the wave, θ_f is the phase compensation of the Hilbert transformation filter, η_{λ_s} is the measured surface elevation at a distance of λ_s in the up-wave direction, and $\hat{\phi}(t)$ is the estimate of the real time phase.

To analyze the performance of the CycWEC over a range of varying wave irregular states, sea state probability data tabulated in the Northern Atlantic was taken from [3]. The data gave the statistical probability of the occurrence of a particular sea state in terms of standard period and significant wave height. The data is presented in number of hours in which that sea state occurred throughout the year. Because the power varies linearly with wave period and quadratically with significant wave height, the data was modified by a weighting matrix to estimate the power at each sea state. The resulting power scatter plot is presented in Figure 33. The scatter diagram is normalized ($T/T_s = 1$) to the peak power location which is the design point for the CycWEC; that is as further described in [8] the optimum radius of the CycWEC is

$$R = \frac{\lambda}{2\pi} = g\frac{T_s^2}{(2\pi)^2}.$$

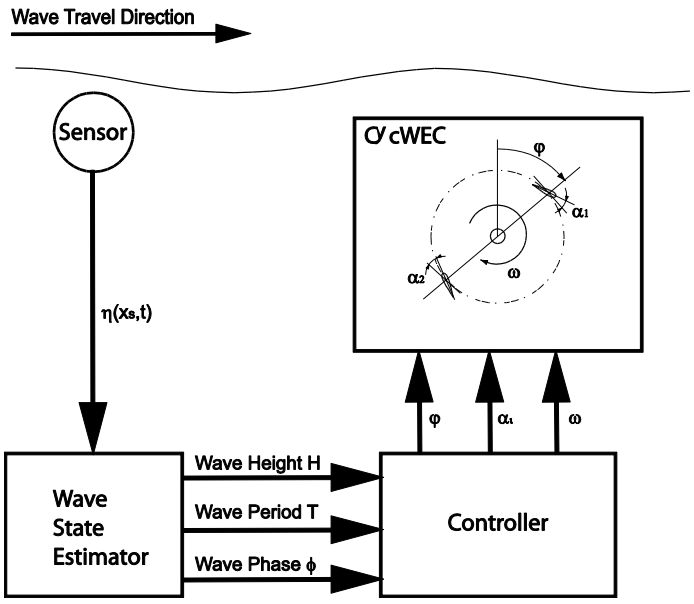

Figure 32 Block diagram of the implemented feedback flow control scheme for the CycWEC

The simulation parameter space was designed to span the range of the scatter plot shown in Figure 33. The parameter varied was the radius of the CycWEC. The radius ranged from $2R/\lambda = 0.1 \rightarrow 1$ with a total of 17 simulations performed over that range. Each simulation used discretization parameters (temporal and wave number) as presented in previous publications [8]. Each simulation was performed such that feedback control was started at $t = 2s$ and continued throughout the remainder of the simulation. Typical resulting wave patterns are shown in Figure 34 at the up-wave ($x = -1\lambda$) and down-wave ($x = +1\lambda$) directions. The case presented in Figure 34 is the optimal design case at which $2\pi R = \lambda$. As shown, the down-wave wave height is significantly reduced by the CycWEC indicating that the majority of the energy has been extracted.

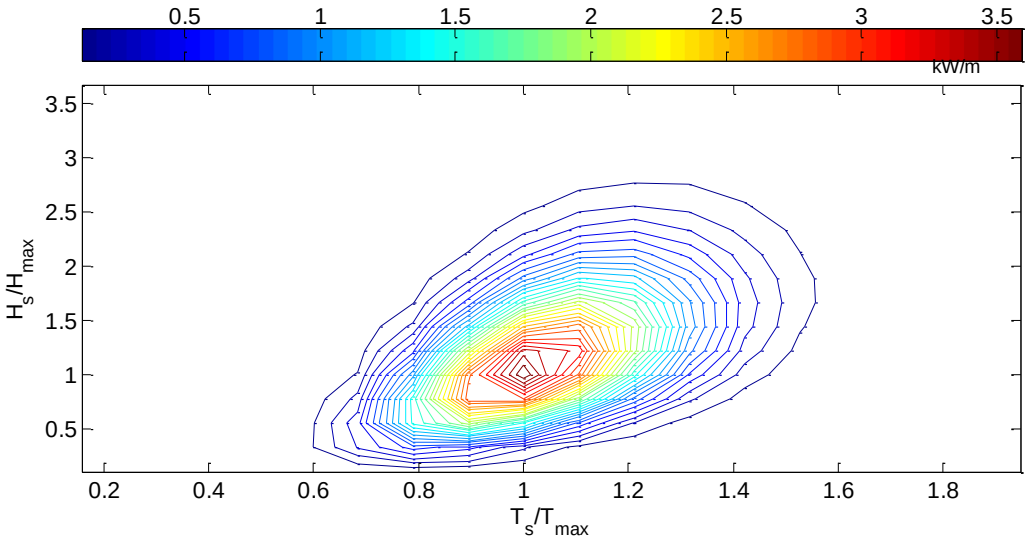

Figure 33 North Atlantic scatter diagram normalized to CycWEC design period of $T_S = 1$. Data is represented in *Watt−hr/mwavecrest*.

The entire surface was computed for the simulation of the design case for the spatial range of $-1 \leq x/\lambda \leq 1$. The space-time plot is shown in Figure 35 for only a time segment of the simulation. It can be seen that the wave height is reduced spatially as well as temporally.

The primary figure of merit for the CycWEC design is the percentage of the wave energy extracted from the incident wave field, defined as the device hydrodynamic efficiency, ϵ. The efficiency is determined from a control volume analysis based on energy conservation which is implicit in the unsteady Bernoulli equation. The analysis assumes that all energy leaving or entering at the up--wave and down--wave boundaries is contained in traveling Airy type waves. Thus, the power difference at both boundaries is to be provided or absorbed by the CycWEC hydrofoils. The domain boundaries are located at $\pm\lambda$. The hydrodynamic efficiency is defined as,

$$\epsilon = 1 - \frac{P_{-\lambda}}{P_{+\lambda}},$$

where the power is computed from power equation in above section The hydrodynamic efficiency will reach a value of one when the incident wave field at the upwave boundary is undisturbed by the CycWEC and the wave field at the down-wave boundary approaches zero.

The resulting wave fields at the up- and down-wave boundaries (i.e., $x = \pm\lambda$) are analyzed using a fast Fourier transform. To ensure that initial transients did not affect the analysis transformation, data prior to $t = 5\ s$ was discarded. To determine the total power in the wave fields P_{Rup} and P_{Rdown}, each wave component identified in the FFT was assumed to be an Airy type and its associated power was determined from the power equation above. The resulting hydrodynamic efficiency was then determined using efficiency equation above.

The resulting spectra of wave height and wave power after an FFT analysis are shown in Figure 36 a) and b), respectively. The computed efficiency for this optimal case was $\epsilon = 99.45\%$.

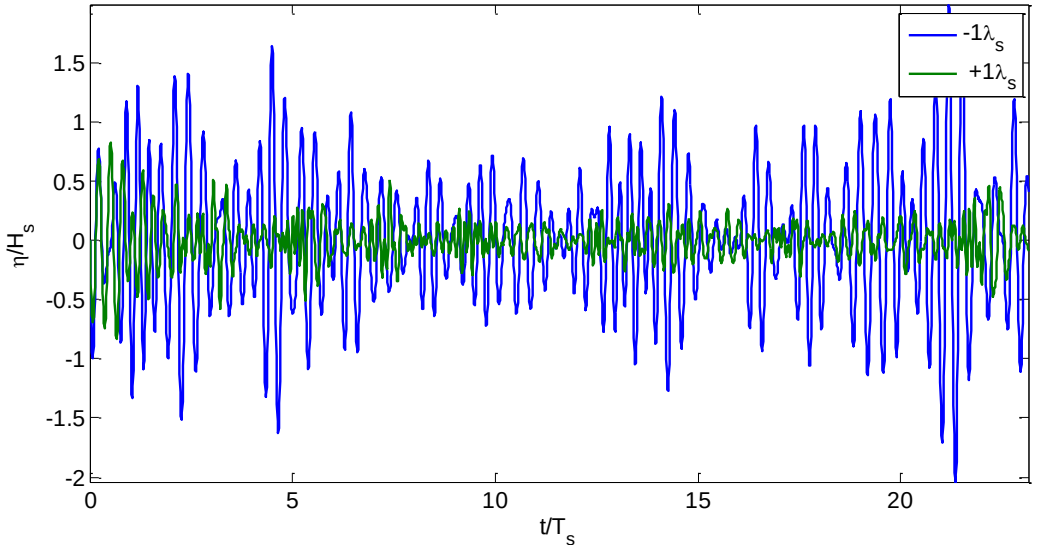

Figure 34 Surface elevation at up-wave (−1λ) and down-wave (+1λ) locations for case $R = \lambda/2\pi$

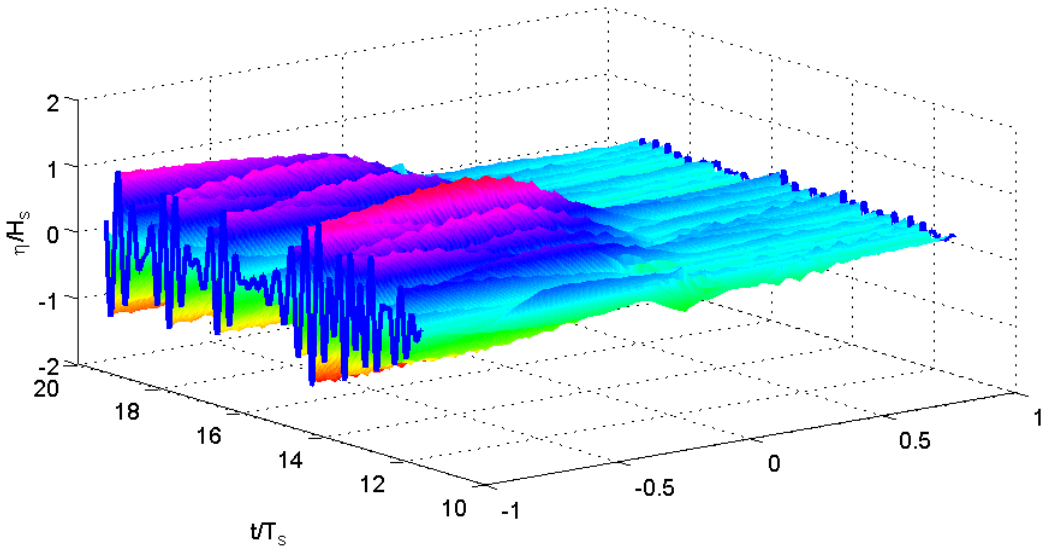

Figure 35: Surface elevation as a function of time and space. Unidirectional airy waves travel in the $+x$ direction. The CycWEC is located at the $x = 0$ position and terminates all waves in the $+x$ direction.

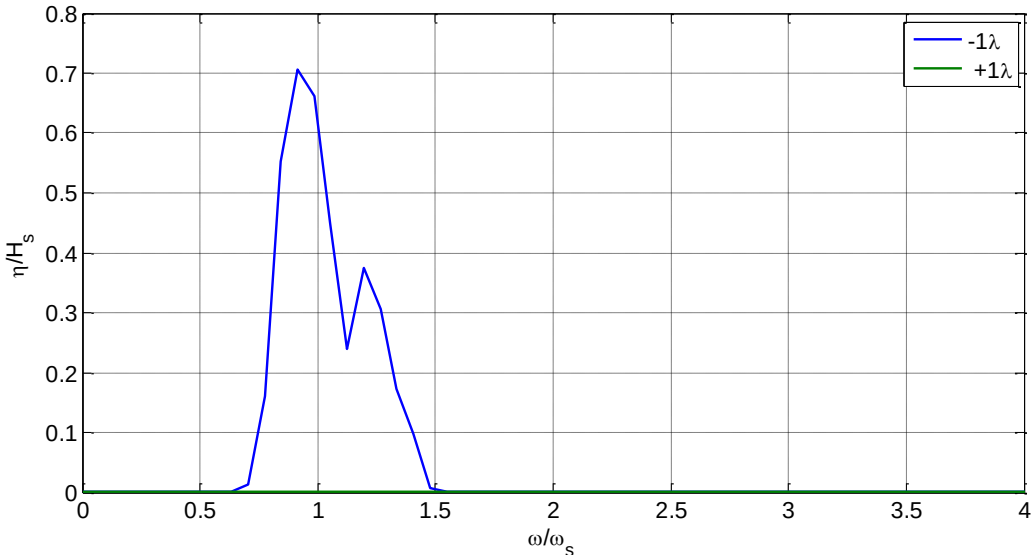

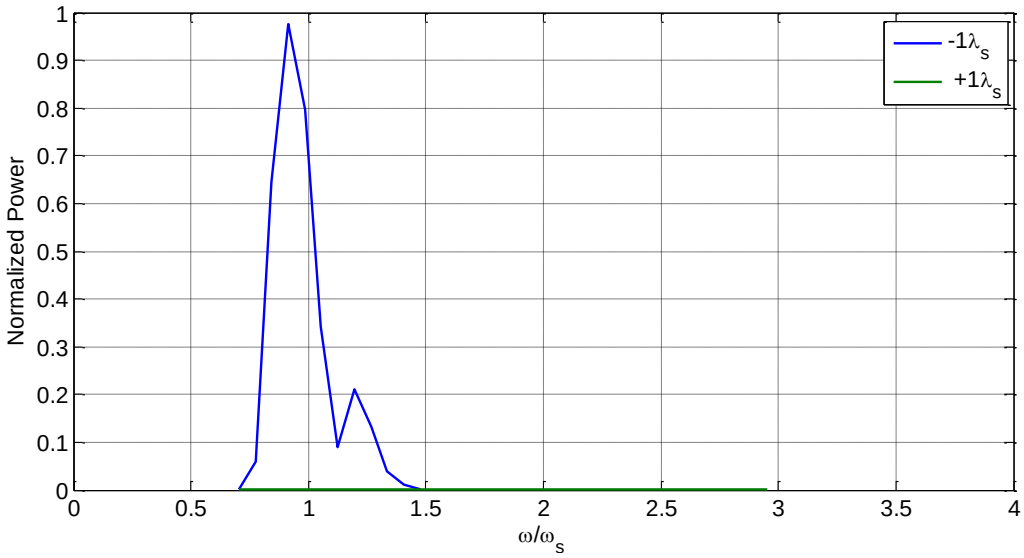

Figure 36 Fourier analysis of resulting wave surface a) height b) power for the design case. Efficiency for this simulation is $\varepsilon = 99.45\%$

This same approach was carried out for the entire parameter range and is summarized by the efficiency of energy extraction based on the approach presented above. The summary of the overall irregular efficiencies is plotted in Figure 38 in blue. As shown the efficiency remains near 100% for a large portion of the off design operating ranges. This compares very nicely with harmonic wave cancelation efficiencies also plotted in Figure 38 in green which was published in [8]. As expected the reduction in efficiency does occur sooner within an irregular wave environment as the device becomes further off design when compared to the harmonic results. It is important to note that as the WEC becomes small in comparison to the standard wave length ($2R/\lambda_s < 1/\pi$) the efficiency begins to trail off at a quicker rate than in the opposite situation ($2R/\lambda_s > 1/\pi$).

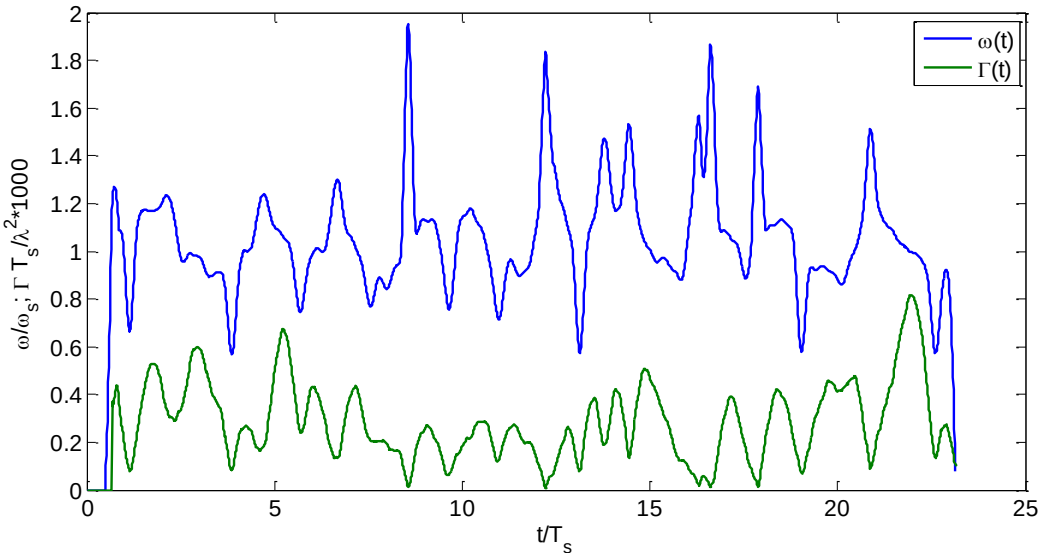

Figure 37 Controller output for near optimal design case, $R = \lambda/2\pi$

To evaluate the yearly efficiency the performance of the CycWEC is analyzed over a yearly likelihood of wave period variations. The North Atlantic scatter data which is plotted in Figure 33 (data from [4]) provides a means to compute the annual wave energy for this North Atlantic location. This is plotted in Figure 38 as the red curve. The radius of the WEC is then designed for this sea location to maximize the yearly output efficiency. For this situation the radius of the WEC is designed similar to the previous optimal relationship, $2R/\lambda = 1/\pi$, to fully encompass the range of variation in the wave periods recorded at that location. Next, an estimate of the yearly efficiency is computed from the approach above, where the energy lost (i.e., energy not converted to electricity) is also plotted in Figure 38 in cyan. Finally, those two curves are integrated and an estimate of the yearly efficiency is computed as $\epsilon_{annual} = 98.3\%$.

.

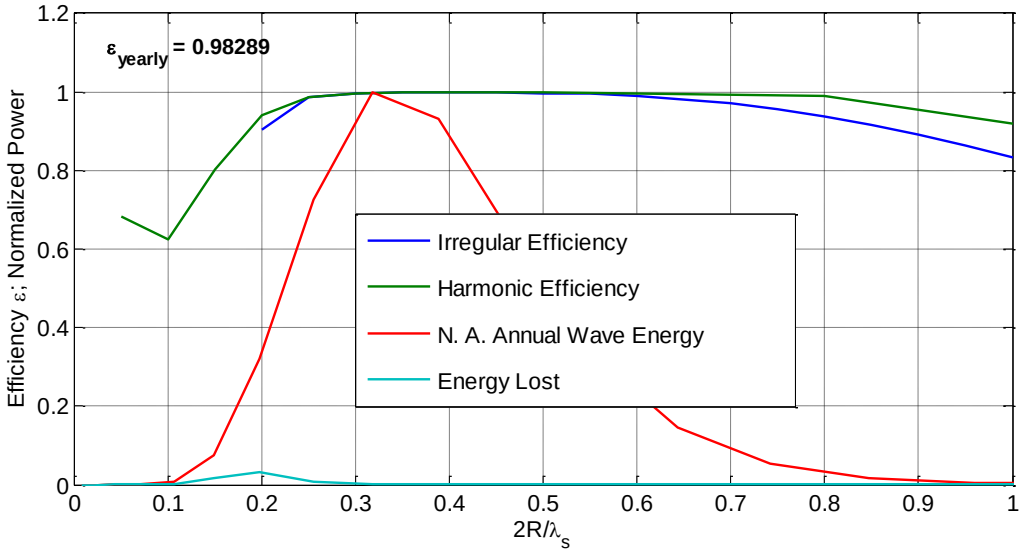

Figure 38: Overall efficiency performance vs. WEC size to wavelength ratio for harmonic and irregular airy waves. An optimally designed WEC in which 2pR = ls as in [3] shows yearly efficiency of 98.3% in a North Atlantic sea state probability.

In summary, simulation results of wave cancelation in irregular, unidirectional deep ocean waves using a Cycloidal wave energy converter (CycWEC) are presented. The simulation which has been experimentally validated at the 1:300 scale is a time integrated, inviscid potential flow solution subject to a linearized free surface boundary condition. Wave irregularity is modeled by the commonly accepted Bretschneider spectrum discretized by 40 components. The irregular spectrum is varied over a range of standard periods (T_s) to represent corresponding sea state variations in a North Atlantic environment. A non-causal Hilbert transformation of the up-wave surface elevation is used to accurately and efficiently estimate the instantaneous frequency, phase and amplitude of the irregular wave surface. A proportional control scheme is adopted to control blade pitch of the CycWEC. Phase compensation is also necessary to model the group velocity of the irregular wave packets between the up-wave sensor location and the CycWEC. Efficiencies are computed from a control volume analysis by up and down-wave surface elevations.

The efficiency of the CycWEC is shown to be above 85% for the entire range of standard wave periods and above 99% for the optimal design case. The CycWEC efficiency in irregular wave climates aligns very nicely with previously published harmonic efficiency analysis. Annual estimates of efficiency were computed from North Atlantic sea likelihood data and showed that 98.85% of the energy was extracted over the course of a year. These results show that the CycWEC is truly a wave termination device over a large band of irregular waves. In a companion paper, OMAE 2012-83388, the irregular wave cancelation results are verified experimentally.

Viscous Estimate

Since the potential flow solver used to perform CFD simulations of the CycWEC does not consider any losses due to viscous effects by design, first order estimation means were used to understand the impact of these losses on CycWEC performance. The detailed approach and validation of the approach to perform these estimates are shown in the respective subsection of the Computer Modeling section. Here, the viscous estimate code is used to investigate the performance of the CycWEC in a typical North Atlantic wave climate. A good characterization of a wave climate can be found in a scatter diagram like the one shown in Figure 39. The number of hours per year during which a sea state identified by the wave period and wave height is encountered are shown as color contours. It can be seen that the most common sea state is characterized by a wave period of about 8-9s and a significant wave height of 1.5-3.0m. Thus, a design goal for a wave energy converter would be to achieve its best performance at this sea state, while still being able to capture the waves at the less common sea states surrounding the design point.

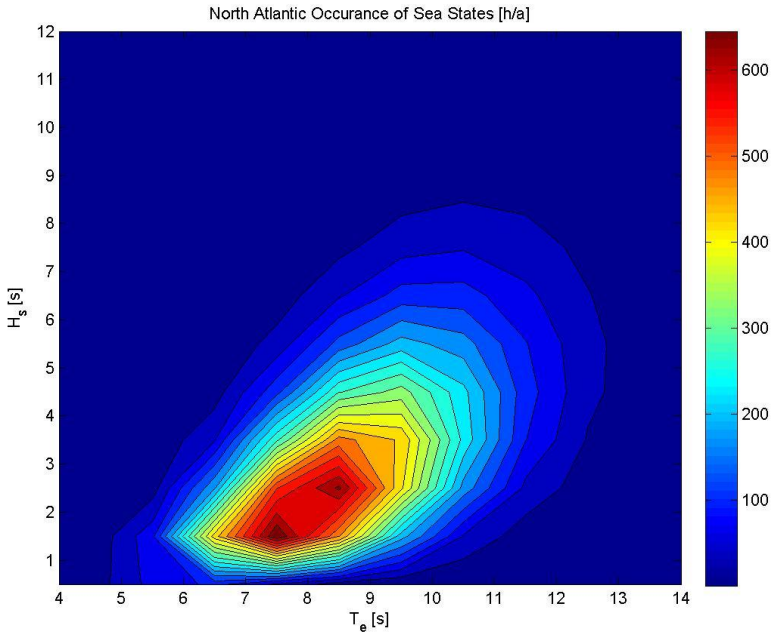

Figure 39: North Atlantic Scatter Diagram from open literature

The performance of the CycWEC, on the other hand, does vary with wave period (which causes a change in wave length), as well as with wave height. Figure 40 shows two typical efficiency plots for CycWECs where the plot on the left is for a CycWEC with a radius of R=15m and a foil chord length of C=4m, where the plot on the right shows the efficiency for R=10m and C=10m. All simulations were based on the assumption of a NACA 0015 hydrofoil. These efficiency plots include viscous losses based on two dimensional flow assumptions, and efficiency is defined as the ratio between power available at the

CycWEC shaft compared to incoming wave power. It can be seen that the maximum efficiency achieved is slightly higher for the R=10m CycWEC than for the R=15m CycWEC. More importantly, though, the range of wave periods and wave heights for which efficient wave energy conversion can be achieved is increased significantly for the R=10m CycWEC. In addition, the peak efficiency can be found at smaller wave heights, which provides a better match between the efficiency of the WEC and the likelihood of sea states shown in Figure 39. This will improve the annual energy yield for the R=10m CycWEC. As no power is produced outside the color contour filled area of the efficiency plot, the R=10m CycWEC will also produce power for a larger portion of the overall time.

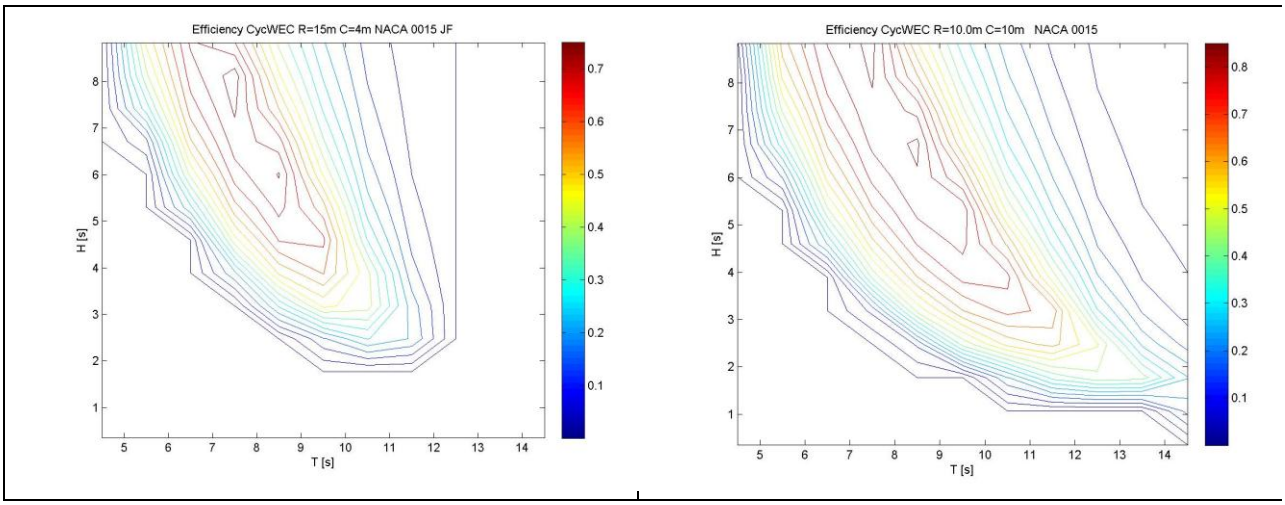

Figure 40: Efficiency of two different CycWEC designs

The scatter data plot shown in Figure 39 can be combined with the efficiency plot in Figure 40 to estimate the overall annual energy yield. The resulting plots in Figure 41 show the annual power production in kWh for the R=10m C=10m CycWEC design. While the CycWEC geometry is the same for both plots, the maximum generator power has been limited to 75kW/m for the left plot. The annual power production without generator limitation is shown on the right for comparison; in this particular case the maximum power produced was 550kW/m or more than seven times larger than the chosen generator power for the right plot. Despite the more than 700% larger (and thus more costly) generator, the overall annual power yield did not increase in proportion but by only 20%. It is thus fair to assume that sizing the generator by the maximum encountered wave power is not a good design choice in terms of economy. The maximum power output as a function of sea state is shown in Figure 42 and confirms that the unlimited size generator (shown on the right side) will only produce its maximum output for very few sea states with large wave heights and a wave period of 7.5s-9s. The 75kW/m limited generator will however produce design power for a wide range of sea states as indicated by the red area in the plot.

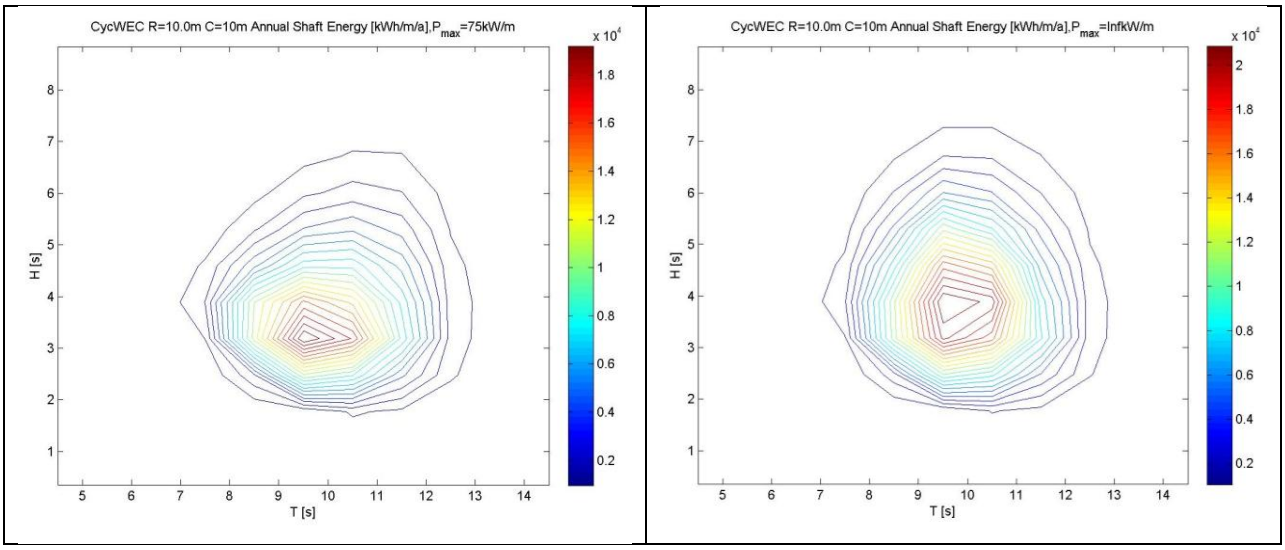

Figure 41: Annual wave energy yield for two different size generators

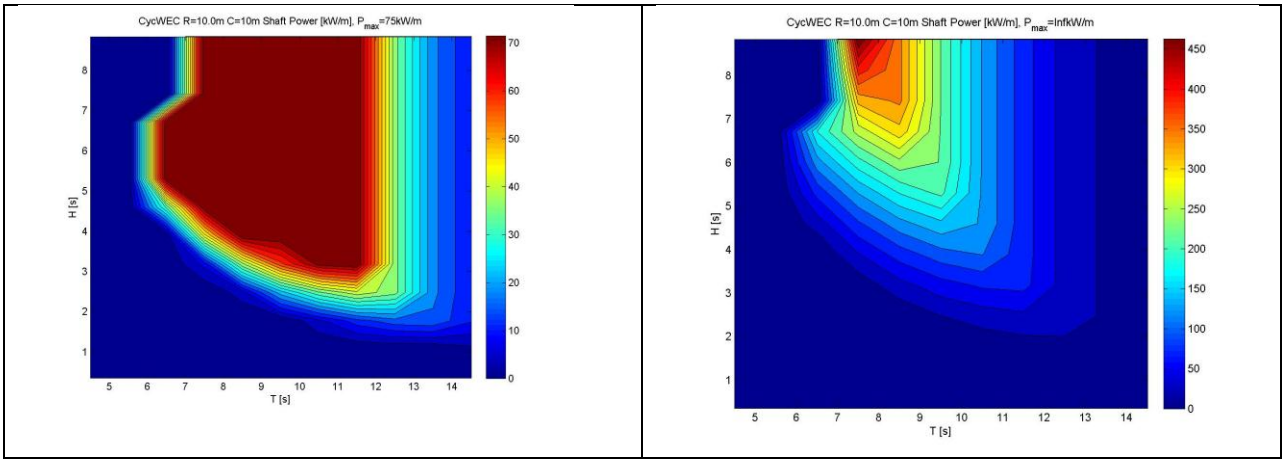

Figure 42: Maximum shaft power for two different size generators

The tradeoff between annual energy yield vs. generator size is shown in Figure 43. While there is a steep increase in Annual Efficiency which is commensurate with annual energy yield for smaller generator sizes, this increase asymptotes beyond a generator size of 200kW/m. At the same time, the capacity factor which indicates at what fraction of the name plate power output the generator is operating on average continuously declines. This tradeoff between annual energy yield and capacity factor is very typical of any energy conversion device that encounters a varying power input due to climate, and the CycWEC performance is comparable to that of wind turbines where similar tradeoffs are encountered.

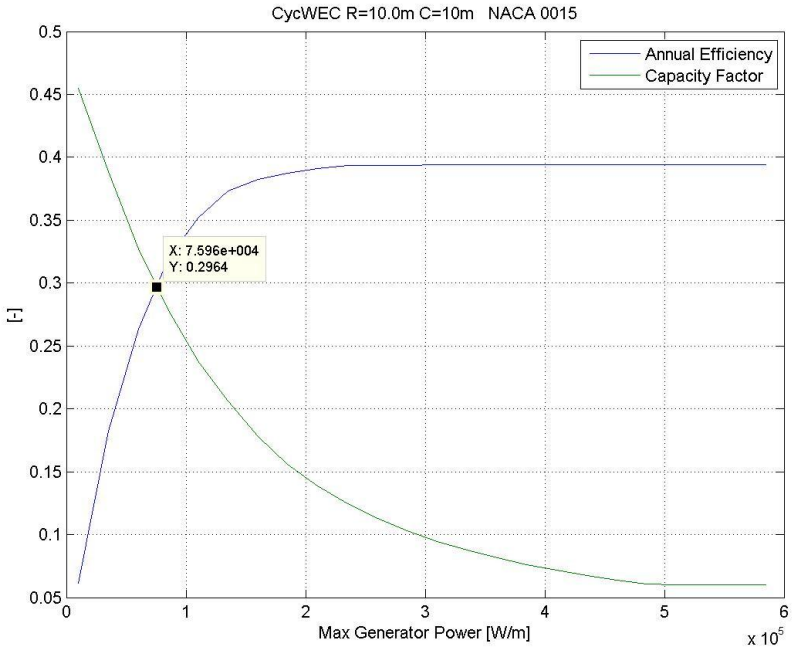

Figure 43: Capacity factor and annual efficiency

A probable design choice would be the 75kW/m generator which according to the data shown in Figure 43 will achieve an annual average efficiency of 30% along with a capacity factor of 30%. This performance is on par or above the state of the art wind turbines, which achieve 20%-40% capacity factor depending on location and wind turbine make and model.

It should be noted once more that these results do not include the effects of 3D diffraction wave focusing, which were discovered during the OTRC-2 testing campaign. We plan to update these estimates in the future with the newly discovered efficiency gains due to diffraction, but present the 2D viscous estimate results shown in this section as a conservative estimate that will be improved upon once diffraction is accounted for.

3D Diffraction

One of the new flow physics discoveries of this project is the wave diffraction behavior of the CycWEC in a three dimensional environment. Prior to this program, all numerical and experimental investigations had been conducted in a two dimensional setup. The simulations were two dimensional by design and derivation, while the experiments were conducted in a narrow wave flume where the CycWEC spanned the width of the flume. This precluded and three dimensional wave propagation due to the effect of the side walls, and the resulting wave patterns were consequently straight crested two dimensional waves.

In the OTRC wave basin, however, the CycWEC model span was a small fraction (about 15%) of the wave basin with, allowing all waves to propagate freely in all directions. The surface wave patterns observed already during the OTRC-1 measurement campaign consequently showed an almost circular wave generation pattern (see OTRC-1 results subsection). This observation raised two questions:

- What is the impact of the 3D wave propagation on the overall CycWEC efficiency?
- How do design choices like blade span impact the wave pattern?

To investigate these questions, a 3D wave diffraction code was developed. While the detailed numerical derivation of this code is shown in the Computer Modeling section, the results achieved using this code are shown here. Figure 44 shows a scale top view of the OTRC wave basin geometry along with the size of the CycWEC shown as a rectangular box in the center of the basin. Also shown is a snapshot in time of the wave generation pattern for the same span CycWEC (4.5m) as was used in the OTRC experiments. The blue color contours indicate wave troughs; while the green contours show wave crests for all diffraction plots. The waves can be seen to radiate in the positive direction with almost circular wave crests, which however decrease in height towards the sides of the basin. This wave pattern is qualitatively consistent with OTRC-1 surface pictures, and matches quantitatively with the wave gauge data which was acquired at the locations indicated. The wave period for all simulations shown was kept constant at T=2.5s resulting in a wave length of L=9.75m.

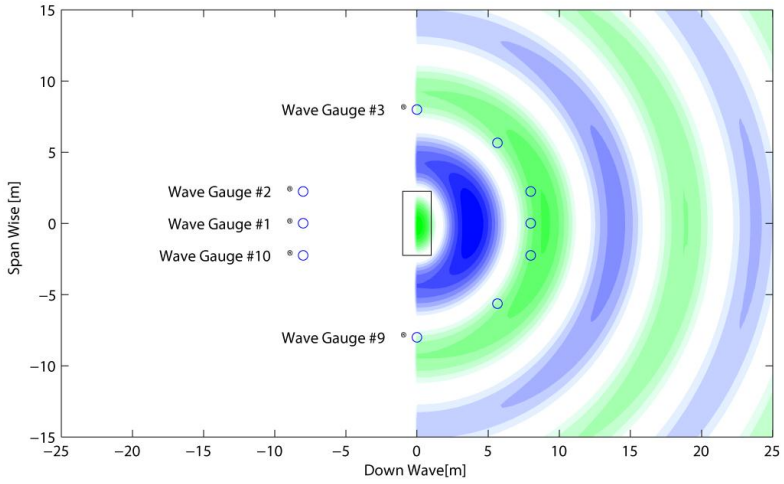

Figure 44: Instantaneous surface elevation for a wave generation simulation. WEC model is shown to scale as a rectangle, and the wave gauge locations are shown

In Figure 45 a wave cancellation simulation snapshot is shown, where the incoming wave is just out of phase with the wave generated by the CycWEC. As a result, a wake down-wave (in positive X direction) of the CycWEC can be seen which spreads out in the span wise direction as it propagates, and at the same time shows an increase in wave height with increasing distance from the CycWEC. This situation is identical to the design wave encountered during the OTRC-2 experiments.

To understand the impact of the CycWEC span on the radiated wave pattern, a CycWEC with a four times larger span is shown in Figure 46. In comparison to the short span wave radiation pattern shown in Figure 45, the wave remains narrower and shows a larger reduction in wave height. This wave radiation pattern is much closer to the two-dimensional wave flume results and shows that for large spans the radiation pattern approaches that of two-dimensional wave flume as well as two-dimensional simulation results.

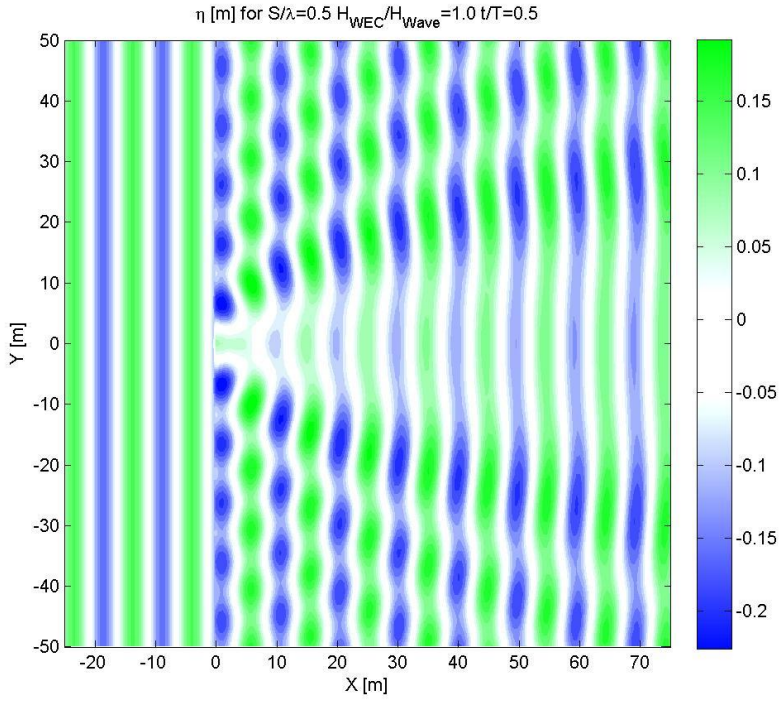

Figure 45: Instantaneous surface elevation for a wave cancellation simulation at the model span ratio of S/λ= 0.5 and an incoming wave height of H=0.3m and T=2.5s

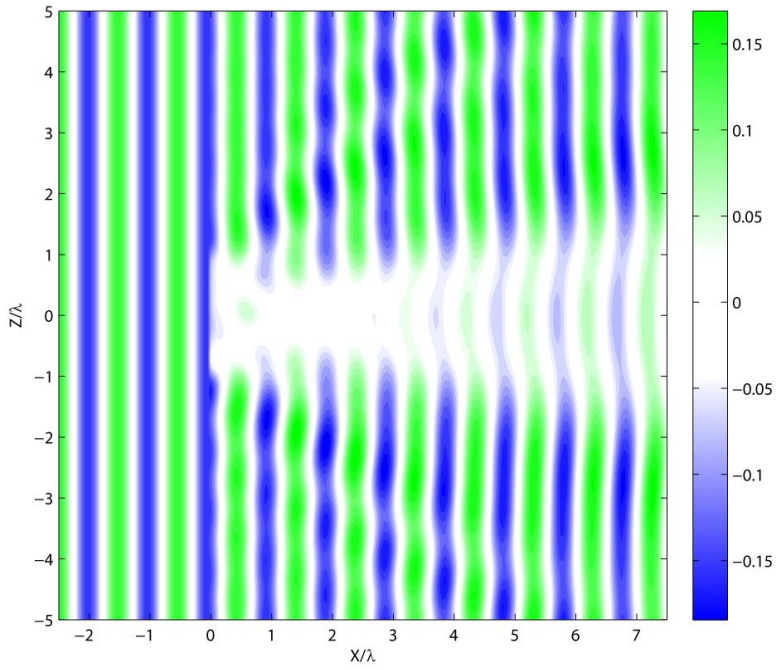

Figure 46: Instantaneous surface elevation for a wave cancellation simulation at the model span ratio of S/λ= 2.0 and an incoming wave height of H=0.3m and T=2.5s

With the wave diffraction patterns matching experimental observations, a control volume analysis was employed to investigate the effects of wave diffraction on CycWEC wave energy conversion efficiency. In addition, a parameter study was conducted where the ratio between CycWEC span and incoming wave length was varied systematically. To determine the optimal CycWEC wave generation center height, the ratio between WEC wave height and incoming wave height was also systematically varied. Figure 47 shows that there is a distinct height ratio that optimizes CycWEC conversion efficiency. While this ratio asymptotically approaches the theoretical optimum height ratio of 4/pi for large span to wave length ratios, at smaller span to wavelength ratios much larger height ratios achieve optimal efficiency. At the same time, this efficiency far exceeds the maximum possible value of 100% for a 2D wave energy conversion system with no wave diffraction effects. The results in Figure 47 thus provide evidence that the CycWEC system can achieve wave focusing using diffraction effects, which has been shown in literature to apply to other WEC devices like buoys. Unlike buoys, however, this diffraction based focusing is achieved without the losses encountered by symmetric point absorbers due to radiation of waves in the up-wave direction.

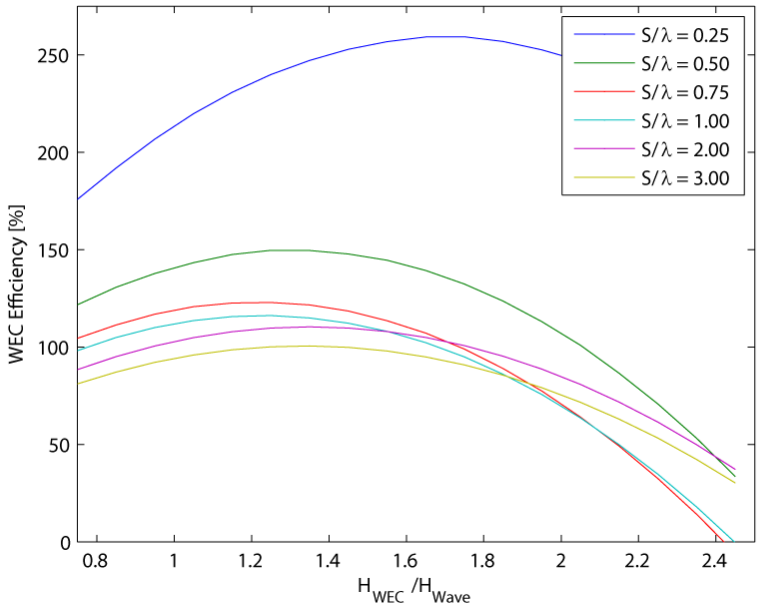

Figure 47: WEC Efficiency as a function of WEC center wave height to incoming wave height ratio

The overall efficiency as a function of the span to wave length ratio is summarized in Figure 48. It can be seen that at the smallest size ratio of 0.25, the CycWEC can extract more than 2.5 times more wave energy than what a two dimensional large span CycWEC could achieve. This efficiency gain is expected to have its greatest impacts in situations where the CycWEC is interacting with waves of much longer wave length than its design wave, where 2D losses due to a mismatch between CycWEC radius and wave length will be offset by the 3D diffraction gains.

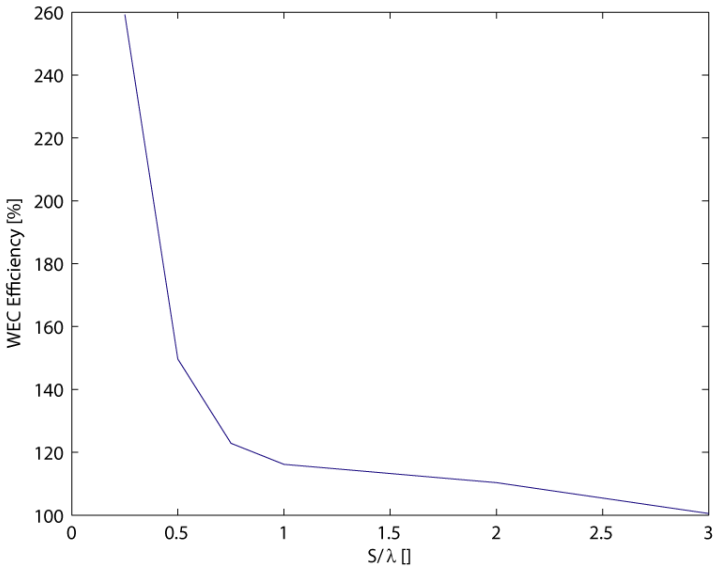

Figure 48: WEC 3D Diffraction efficiency as a function of span to wavelength ratio. The optimal WEC center wave height is used for each span ratio.

In summary, the results from the initial 3D diffraction simulations presented here indicate that 3D diffraction will improve overall CycWEC performance. While the previous section outlining the estimated performance of the CycWEC at full scale does not include the diffraction effects shown here, the full scale CycWEC performance estimates will improve throughout the entire wave climate range due to diffraction. Future work will combine these effects in an overall performance estimate. In answering the initial questions of this section, the impact of diffraction on the observed wave pattern can be quite dramatically different from the two dimensional observations, in particular for CycWECs of short span to wave length ratio. The impact on efficiency is however an improvement for all size CycWECs, again with larger improvements for shorter wavelength CycWECs.

Conceptual Design of Full Ocean Prototype

As part of the proposed work in advancing the TRL level of the CycWEC, conceptual studies were conducted to evaluate possible deployment methods, as well as to estimate the device cost and LCOE of a full scale CycWEC. The following subsections detail results from both of these investigations.

Deployment Choices

Atargis Energy performed detailed studies within this project to investigate different means on how to physically install and deploy a CycWEC in the open ocean. Based on initial patent filings, there are two fundamentally different installation methods that can be pursued: Either the CycWEC is connected to the ocean floor in a rigid or semi-rigid manner, or it is deployed in a free floating fashion. Correlating with these two implementation methods, we have filed two new patent applications in August of 2012

with the USPTO which file claim to newly conceived deployment ideas for either of these implementation methods [12] [13]. They further develop and detail the original patented ideas filed in 2006 and awarded in 2010 in the US.

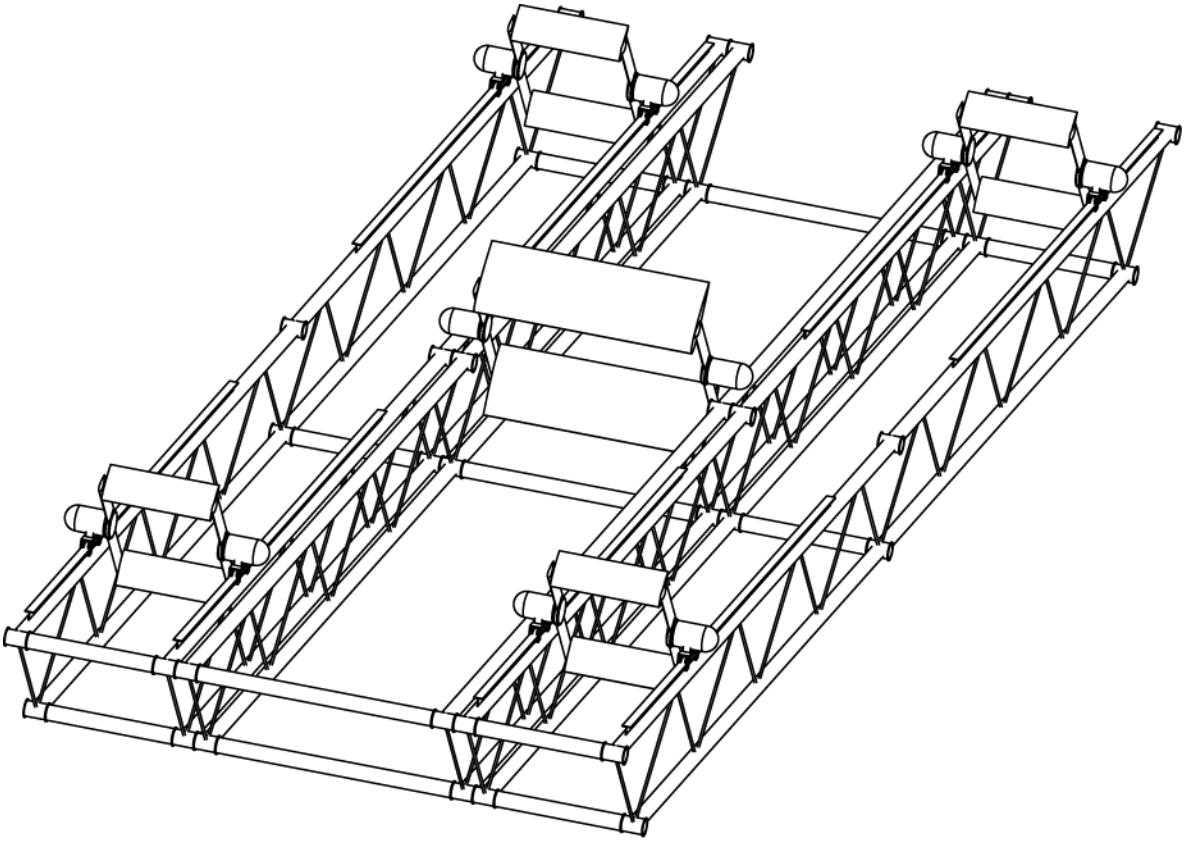

Figure 49: A free floating cluster of 5 CycWECs using a modular mounting frame. Sketch from Patent Application [13]

Studies comparing the cost for deploying free floating vs. ocean floor attached CycWECs showed that the most cost efficient deployment method depends on water depth. As any free floating structure like the example shown in Figure 49 will consist of several CycWECs connected by a common mounting frame, the cost of this frame needs to be compared to the cost of an ocean floor attachment. The required spacing of WECs causes a free floating mounting frame to be at least one wave length in length. Therefore, if the water depth at the deployment location is significantly less than one wave length, ocean floor attachment becomes more cost efficient than free floating implementation due to the smaller size and thus cost of the structure. On the other hand, the technology development required and thus risk incurred for a free floating implementation is significantly higher for a free floating implementation. For these reasons, Atargis Energy shifted its near term focus on development of an ocean floor attached CycWEC installation since it will reduce the time to market as well as the capital required for the development. Among ocean floor foundations that have been developed by the

offshore industry, the monopile foundation is one of the simplest means to attach offshore structures to the ocean floor. It also has been used extensively for deploying offshore wind turbines in the recent past, and is thus a well-developed and understood technology. At the same time, design requirements like the ability to orient the CycWEC to be aligned with the incoming waves can easily be achieved with a monopile design. Figure 50 shows one of the possibilities to achieve all of the design requirements with a monopile foundation. We have applied for patent protection of this CycWEC foundation and are planning to pursue further development of the CycWEC implementations using a monopile foundation in future work.

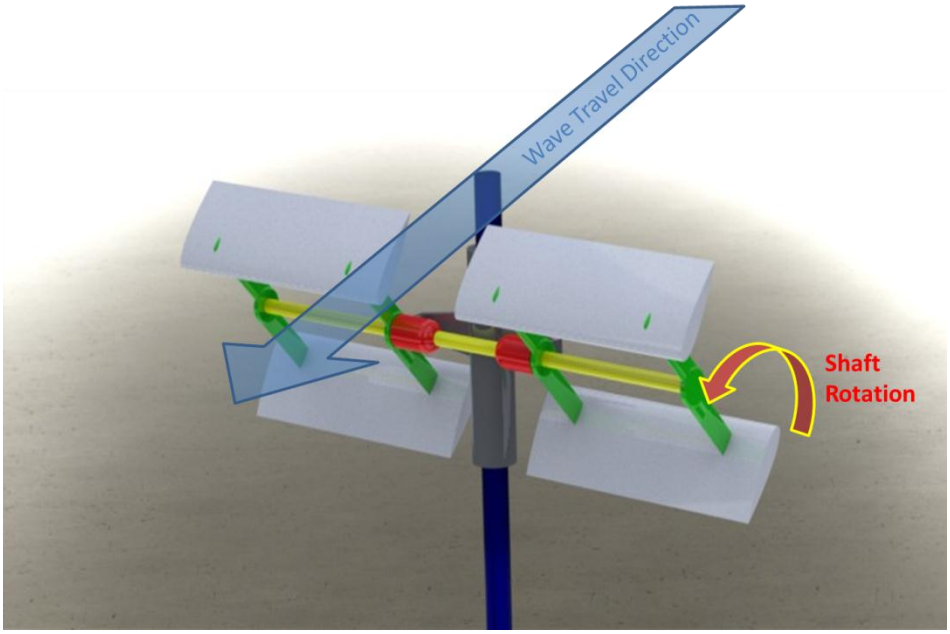

Figure 50: A set of two CycWECs mounted on a monopile. The hydrofoils (white) are the only component extracting energy from the waves, and are attached by means of struts (green) to a main shaft (yellow). The main shaft drives one or more generators (red) that are attached to the monopile in a fashion where the depth of the WEC can be adjusted to avoid storm damage (low position) or maintenance (above water level, high position). The hydrofoils remain fully submerged in normal operation.

Performance Estimate

While this document has so far outlined the technical advantages in qualitative terms, this section quantitatively investigates the impact of these advantages on the overall Levelized Cost of Energy (LCoE) for a full scale CycWEC, as well as a wave farm consisting of 40 CycWECs. We calculated LCoE based on equation 1, which is available from NREL Report NREL/TP-462-5173, page 48, equation 4.7.

$$LCOE = (TLCC/Q)\ (UCRF) \qquad (1)$$

Where TLCC is the Total Life Cycle Capital Cost in [$], Q the annual energy production in [kWh], and UCRF the Uniform Capital Recovery Factor:

$$UCRF = \alpha(1+\alpha)^{\beta}/[(1+\alpha)^{\beta} - 1] \qquad (2)$$

With α the discount rate (α =0.1) and β the number of years (β=20) were assumed. The TLCC is split into Capital Expenditures (CapEx) and Operating Expenditures (OpEx), by modifying equation 1 as follows which yields equation 3 for LCoE:

$$LCoE = (CapEx/Q)(UCRF) + OpEx \qquad (3)$$

Where both CapEx/Q and OpEx have units of [Cents/kWh]. The annual power production Q in [kWh/a] is estimated for the CycWEC based on published North Atlantic scatter data along with the efficiency estimate based on numerical simulations including viscous loss estimates performed by Atargis. It is discounted for the availability estimate detailed below to arrive at an average annual power production.

All of our estimates are based on an **installed array of 40 (forty) CycWECs**, each with a peak power output of 5MW, resulting in a **total peak output of 200MW**. The following table shows the results of the Construction Cost with itemized positions. Both a high cost (conservative) estimate as well as a low cost estimate is given for all items. As can be seen in the table, the specific cost of the **Capital Expenditures** for constructing the cluster is **between 2058 $/kW and 3206 $/kW**. It is worthwhile comparing these numbers to traditional renewables like land-based wind energy, where the CycWEC can be seen to be competitive in terms of LCoE.

CAPEx	Single WEC		Array of WECs		
	Low Estimate	High Estimate	Low Estimate	High Estimate	
# of WECs	1	1	40	40	
Design Power Output [MW]	**5**	**5**	**200**	**200**	Design point of WECs
	Cost per WEC		Cost for Array of WECs		Notes/Assumptions
WEC Devices					
Generator Cost	$ 1,500,000	$ 2,000,000	$ 60,000,000	$ 80,000,000	$300-400/kW with brake and gear or direct drive
Fiberglass Blades	$ 800,000	$ 1,200,000	$ 32,000,000	$ 48,000,000	$10-$15/kg of fabricated composites
Steel Structure (50-75 tons), bearings, seals	$ 250,000	$ 375,000	$ 10,000,000	$ 15,000,000	assume $5/kg primary steel
Steel Structure finishing	$ 250,000	$ 375,000	$ 10,000,000	$ 15,000,000	same cost as steel
Electronics and Controls and pitch/yaw/ lift	$ 500,000	$ 750,000	$ 20,000,000	$ 30,000,000	
Support structures					
Monopile Steel Construction	$ 750,000	$ 1,250,000	$ 30,000,000	$ 50,000,000	assume 30m water depth
Installation and Foundation	$ 1,000,000	$ 2,000,000	$ 40,000,000	$ 80,000,000	assume 30m water depth
Sub-sea electrical					
Sub-Sea Connecting Point			$ 1,000,000	$ 2,000,000	
Lines WECs to Conn Point (2.5km avg)	$ 1,250,000	$ 1,875,000	$ 50,000,000	$ 75,000,000	assume $500-750k / km
Line Conn Point to Shore (6km)			$ 3,000,000	$ 4,500,000	assume $500-750k / km
Installation					
Vessel hire 1 week per WEC	$ 140,000	$ 210,000	$ 5,600,000	$ 8,400,000	assume $20k-$30k per day
Fuel for 4 days of full power operation	$ 60,000	$ 60,000	$ 2,400,000	$ 2,400,000	assume $15k per day
Crew of 5-10 people	$ 50,000	$ 150,000	$ 2,000,000	$ 6,000,000	assume avg annual salary of $50-$75k
Commissioning					
Site leasing			$ 4,000,000	$ 5,000,000	
Environmental studies			$ 5,000,000	$ 10,000,000	
Certification			$ 5,000,000	$ 5,000,000	
Construction Cost US [$]	$ 6,550,000	$ 10,245,000	$ 280,000,000	$ 436,300,000	
SG&A (Sales, Management, Admin) [12%]	$ 786,000	$ 1,229,400	$ 33,600,000	$ 52,356,000	
Profit [35%]	$ 2,292,500	$ 3,585,750	$ 98,000,000	$ 152,705,000	
Total US CapEx [$]	**$ 9,628,500**	**$ 15,060,150**	**$ 411,600,000**	**$ 641,361,000**	
Specific CapEx ($ per kW of Design Power)	$ 1,925,700	$ 3,012,030	$ 2,058,000	$ 3,206,805	

The analysis results for Power Production, UCRF, and ultimately LCoE are shown in the following table. The estimate for the LCoE falls into the range of 10 to 17 cents per kWh. Between 15-20% of that cost is the OpEx estimate. Based on the simplicity of the mechanical setup, we consider this a conservative operation cost estimate. It is therefore expected to be reduced with greater operational experience over time.

	Cost Estimate	
Finance Assumptions:	**Low Estimate**	**High Estimate**
Discount Rate	0.10	0.10
Project Duration [years]	20	20
Uniform Capital Recovery Factor	0.1175	0.1175
From CapEx estimate:		
Total CapEx [$]	$ 411,600,000.00	$ 641,361,000.00
Availability:		
1 week per year for inspection [weeks]	20	20
1 month every 5 years for maint. [weeks]	12	12
Total Down time in 20 years [weeks]	32	32
Fractional Availability	0.968	0.968
Power production:		
WEC Blade Length each WEC [m]	150	150
Annual Efficiency	0.4	0.35
Incoming Wave Power Avg [kW/m]	30	30
All WECs Blade Length Total [m]	6000	6000
Annual Wave Energy to Grid [kWh/a]	610,536,960	534,219,840
CapEx [$ per kWh]	0.079	0.141
OpEx [$ per kWh] -Estimate	0.020	0.030
LCOE ($ per kWh)	**$ 0.10**	**$ 0.17**

Other noteworthy results of this analysis are a total installed length of just 6 km along the shore line for the array, which is relatively short, due to the very high efficiency of the CycWEC compared to other technologies. This length will, however, increase proportionally if the cluster is installed in a wave climate with lower annual average power. However, the impact on the total cost of energy will be minor in this case, as it primarily affects the hydrofoil blade length and the subsea electrical costs, which together represent less than 13% of total capital expenditure

In summary, the combination of high conversion efficiency, as well as small device size due to lift based operation lead to a low overall cost of energy. It also enables construction of large power output devices at an economical construction cost. For a full scale production CycWEC in a favorable wave climate, we expect an initial design power output of 5MW per WEC, which is on par with the largest wind turbines presently in commercial operation and exceeds that of any other wave energy converter in

development. Due to the higher efficiency and energy density, the size of the WEC will be much smaller than that of a comparable wind turbine, leading to low construction costs. Construction costs are projected to fall into the range 2058 $/kW and 3206 $/kW of installed power. These values will be depending on wave climate and ocean bathymetry. The low construction cost also leads to a low cost of energy. The LCoE is expected to be in the range of $0.10 - $0.17 per kWh, which is a fraction of the price estimated for any other competing WEC technology.

Based on the transformation and rapid growth encountered by the wind energy industry as it matured about 20 years ago to modern lift-based power conversion, we expect the Atargis CycWEC to transform and enable economic growth in the wave energy field in the same way. The ability to produce cost-efficient power at utility scale may prove to be even more transformative, given the attractiveness of the global wave energy resource.

Technology Transfer Activities

Atargis Energy has made active efforts to publish all relevant findings in open literature, either in the form of peer-reviewed scientific publications or as patent applications. Within this DOE funded program, three scientific papers and two patents have been published/filed respectively.

Publications

2011:

[1] Siegel, S. G.; Jeans, T. & McLaughlin, T. Deep Ocean Wave Energy Conversion using a Cycloidal Turbine. Applied Ocean Research, April 2011, Volume 33 Issue 2, pg. 110-119.

[2] Siegel, S.; Roemer, M.; Imamura, J.; Fagley, C. & Mclaughlin, T. Experimental Wave Generation And Cancellation With A Cycloidal Wave Energy Converter. 30th International Conference on Ocean, Offshore and Arctic Engineering (OMAE), 2011

[3] Imamura, J.; Siegel, S.; Fagley, C. & Mclaughlin, T. Cancellation Of Non-harmonic Waves Using A Cycloidal Turbine. 30th International Conference on Ocean, Offshore and Arctic Engineering (OMAE), 2011

[4] Tiger Jeans, Casey Fagley, Stefan Siegel and Jurgen Seidel, Irregular Deep Ocean Wave Energy Conversion Using a Cycloidal Wave Energy Converter. Proceedings of the 9th European Wave and Tidal Energy Conference, Southampton, UK, 5th-9th September 2011

[5] Stefan Siegel, Casey Fagley, Marcus Roemer and Thomas McLaughlin, Experimental Wave Cancellation using a Cycloidal Wave Energy Converter. Proceedings of the 9th European Wave and Tidal Energy Conference, Southampton, UK, 5th-9th September 2011

2012:

[6] Siegel, S.; Fagley, C.; Roemer, M. & Mclaughlin, T. Experimental Investigation of Irregular Wave Cancellation using a Cycloidal Wave Energy Converter. 31st International Conference on Ocean, Offshore and Arctic Engineering (OMAE), 2012

[7] Fagley, C.; Seidel, J. & Siegel, S. Computational Investigation of Irregular Wave Cancellation using a Cycloidal Wave Energy Converter. 31st International Conference on Ocean, Offshore and Arctic Engineering (OMAE), 2012

[8] Siegel, S. G.; Fagley, C. & Nowlin, S.
Experimental wave termination in a 2D wave tunnel using a cycloidal wave energy converter. *Applied Ocean Research*, **2012**, *38*, 92-99

[9] Seidel, J.; Fagley, C. & Siegel, S.
Numerical Simulations of a Cycloidal Wave Energy Converter
1st Asian Wave and Tidal Energy Conference (AWTEC)
Jeju Island, Korea, November 27-30, **2012**

[10] Fagley, C.; Siegel, S. & Seidel, J.
Wave Cancellation Experiments using a 1:10 Scale Cycloidal Wave Energy Converter
1st Asian Wave and Tidal Energy Conference (AWTEC)
Jeju Island, Korea, November 27-30, **2012**

While all of these publications have appeared during the course of this program, only publications [7] [9] and [10] are based on work performed within this program. All other publications are based on work performed under funding from the National Science Foundation at the US Air Force Academy.

Web site or other Internet sites that reflect the results of this project

The Atargis Energy Corporation web page (http://www.atargis.com) is being kept up to date with the latest results and developments. Also, all publications that are publicly releasable with respect to copyright issues are available for download there.

Networks or collaborations fostered

None.

Technologies/Techniques

There are proprietary findings from the present investigation that are considered company confidential and thus have not been included in this report which does not contain proprietary data. All publicly available results can be found in this report and/or the referenced publications

Inventions/Patent Applications, licensing agreements

Atargis Energy Corporation has filed a total of three new patent applications during the course of this program, two of which ([12] and [13]) are outcomes of the work performed under DOE funding, while the first one ([11]) was based on findings of work performed prior to this agreement under funding from the National Science Foundation.

[11] Siegel, S. G. Efficient Wave Energy Conversion Using Cycloidal Turbines, U. S. Patent application filed with priority date Feburary 25th, 2012

[12] Siegel, S. G. Ocean Floor Mounting of Wave Energy Converters, U. S. Patent application filed with priority date August 8th, 2012

[13] Siegel, S. G. Clustering of Cycloidal Wave Energy Converters, U. S. Patent application filed with priority date August 8th, 2012

Other products

None.

Computer Modeling

Computer modeling has been a major component of the work performed, since it allows for investigations unlimited by scale models and testing facility constraints. This section details the underlying technical details of the Atargis proprietary simulation codes. Results of all of these codes have been published in open literature and have been peer reviewed. While the numerical approaches and methodologies are detailed here, the results achieved using these codes have been presented throughout this document in subsections of the “Project Activities and Results” section. This section has three main subsections detailing the numerical details of the 2D Panel code, the Viscous Estimate code and the 3D Diffraction code, respectively.

2D Panel Code

In order to model the CycWEC and its interaction with waves, two codes have been developed. They are both based on the same fundamental equation, but differ significantly in their capabilities and concomitantly in their computational requirements. The following sections describe the models used, the fundamental equations for the codes, the key assumptions, and the intended use for each code.

All codes are developed using Matlab®.

Basic physical description, equations, and assumptions

The fundamental equations to be solved to computationally investigate a CycWEC close to a free surface are

- Continuity equation (liquid phase), i.e. conservation of mass
- Navier-Stokes equations (liquid phase), i.e. conservation of momentum
- Free surface boundary conditions
    - Kinematic boundary condition
    - Dynamic boundary condition

Assuming inviscid, irrotational, and incompressible flow, the continuity equation and the Navier-Stokes equations can be simplified and combined into the Laplace equation for the velocity potential Φ,

$$\nabla^2\Phi = 0.$$

A further assumption made in the derivation of the basic equations is two-dimensionality. In seeking two-dimensional solutions, it is convenient to define the complex stream function in terms of the complex variable $z = x + iy$, such that

$$F(z,t) = \Phi + i\Psi$$

where Ψ is the complex stream function. The complex velocity is defined by $dF/dz = u - iv$.

The free surface boundary conditions are linearized in the context of potential flow. Neglecting higher order terms, the kinematic boundary condition, which ensures that the vertical velocity of the free surface and the velocity of the fluid particles at the surface are equal, is written as

$$\frac{\partial\eta}{\partial t} = \frac{\partial\phi}{\partial y},$$

where η is the instantaneous surface elevation.

The dynamic boundary condition, which ensures that the pressure on the free surface is the atmospheric pressure, is determined from the Bernoulli equation. Again neglecting higher order terms, the final equation is

$$\eta = -\frac{1}{g}\frac{\partial\Phi}{\partial t},$$

where *g* is the gravitational constant. Note that due to the linearization of the problem, the dynamic boundary condition is imposed at $\eta = 0$, i.e. the undeformed surface.

Using the assumptions and the linearized boundary conditions stated above, the complex potential of a vortex at location $c(t) = x(t) + iy(t)$ with strength Γ moving under a free surface can be expressed in closed form as described in reference [5]

$$F(z,t) = \frac{\Gamma(t)}{2\pi i}\ln\left[\frac{z - c(t)}{z - \bar{c}(t)}\right] \quad (1)$$

$$+\frac{g}{\pi i}\int_0^t\int_0^\infty \frac{\Gamma(\tau)}{\sqrt{gk}}e^{-ik(z-\bar{c}(\tau))}\sin\left[\sqrt{gk}(t-\tau)\right]dk\,d\tau$$

The first term is the complex potential due to the vortex and its mirror image above the surface, which is necessary to satisfy the kinematic free surface condition. The second term describes the radiated waves related to the dynamic free surface condition. Note that the fluid is assumed to be infinitely deep.

Numerical integration of this equation using the trapezoidal rule provides the complex velocity potential at a point *z* for a given time *t*. Note that the result depends on the complete time history of the vortex motion because of the radiated wave field.

A resolution study for Δt, Δk, and k_{max} was conducted to ensure numerical convergence of the results (see below).

Note that since the problem statement is linear, the method of superposition can be utilized to compute the cumulative effect of multiple vortices moving under the free surface.

Finally, the CycWEC motion is defined by

$$x(t) = Rcos(\theta(t)+\varphi)$$
$$y(t) = y_c - Rsin(\theta(t)+\varphi)$$

where y_c is the submergence depth of the CycWEC shaft.

This derivation and the assumptions and reasoning were peer reviewed and accepted without corrections. They are published in the scientific literature, see [7]-[10]

Single vortex model

Purpose: Rapid design iterations, feedback control simulations (CycWEC-wave interaction)

Hardware requirements: CPU times approx. 20sec for 10 revolutions of the CycWEC (constant circulation)

Documentation: open literature (see references)

Validation and sensitivity analysis: Convergence study

Since the procedure and results obtained with the single vortex model are extensively documented in the open literature, only a short summary is given here.

In the single vortex model, each CycWEC hydrofoil is modeled as a single vortex using the equations given above. Since the current CycWEC design consists of two hydrofoils, the resulting surface waves

generated by the rotating CycWEC are obtained from the superposition of two vortices rotating under the free surface.

Based on the theoretical foundations of potential flow theory, modeling the CycWEC hydrofoils using a single vortex should result in a good approximation of the far field, i.e. the flow far away from the CycWEC. In this case, 'far away' is based on the size of the CycWEC, e.g. its radius. Observing the free surface three wavelengths up-wave and down-wave of the CycWEC satisfied this requirement.

Using the same analysis, it can also be concluded that the flow field near the CycWEC, especially around the blades themselves, is not well represented by the single vortex model. Therefore, it would be unrealistic to expect to be able to compute forces and moments, and in particular the shaft torque, which is ultimately the most important quantity since it is directly connected to the extracted power (or needed to generate waves).

However, it is possible to estimate at least the magnitude of the lift and drag force using the following relations. In potential flow around airfoils, it is well known that the lift per unit span is

$$L_s = \rho U \Gamma.$$

Furthermore, the lift of a wing can also be expressed as

$$L = \frac{1}{2}\rho U^2 S c_L,$$

where ρ is the fluid density, U is the velocity due to CycWEC rotation, Γ is the prescribed circulation, $S=bc$ is the wing area (b is the span and c is the chord length), and c_L is the lift coefficient. Since $bL_s=L$,

$$c_L = \frac{2\Gamma}{Uc}.$$

Using this relation, an estimate of the hydrofoil forces can be obtained in the following way:

- Pick a hydrofoil section, e.g. NACA0015
- Compute the Reynolds number $Re = \frac{Uc}{\upsilon}$
- Using $c_L=2\pi\alpha$, determine the angle of attack α
- Determine the drag coefficient based on published lookup tables
- Compute the drag force

Using this procedure, an estimate of the magnitude of the lift and drag forces can be obtained. However, the direction of the resulting force vector is unknown, and therefore estimating the shaft torque is not possible using this model.

Details of the results of the viscous force estimates are given elsewhere in this report.

Convergence study

The convergence of the numerical solution has been studied in detail. As parameters (see Equation 1), the time step Δt, the wave number step Δk, and the maximum wave number k_{max} have been considered. A summary of the wave heights produced in wave generation mode of the CycWEC is shown in Figure 51.

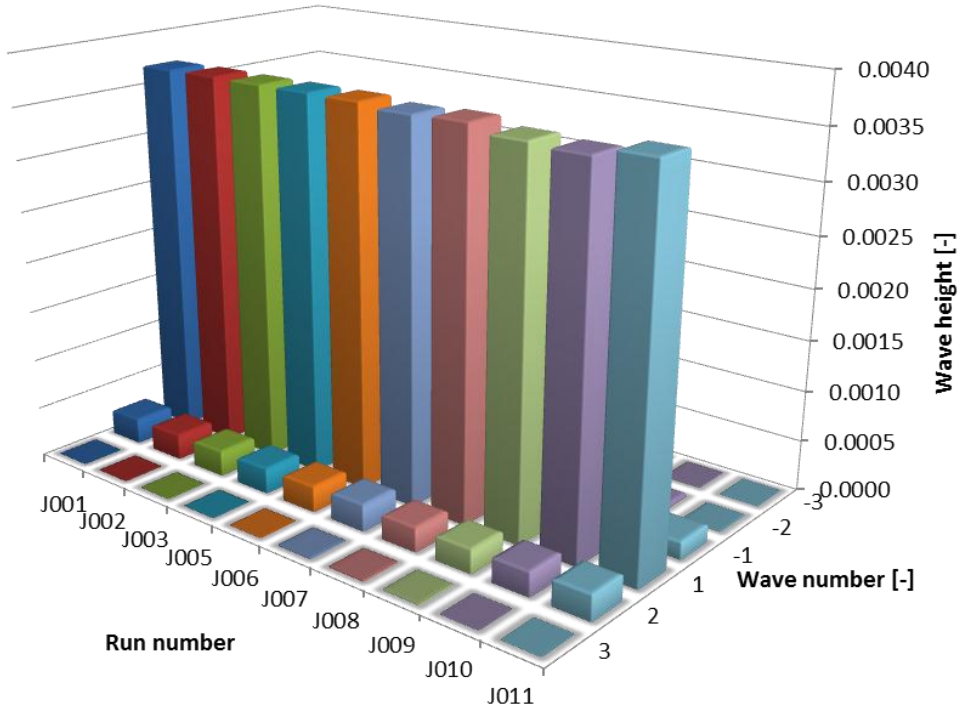

Figure 51: Wave height of 6 wave components of validation runs.

A summary of the parameters is given in Table 1. As shown in the table, the time step was varied by a factor of five and the wave number step by a factor of two. It should be noted that a similar resolution study was conducted earlier and therefore a good estimate for the values was available [1]. Also, due to the optimization of the simulation parameters, the simulation time was reduced by approximately an order of magnitude. In the end, run J011 provided the best compromise between numerical accuracy and computational time. This was necessary to allow for the use of this code for feedback controlled simulations, as explained elsewhere in this report.

As shown in Figure 51, the wave heights were not affected by this significant improvement in computational efficiency.

Table 1: Normalized simulation parameters for convergence study.

Run	**T**				**k**			
	min	max	dt	Nt	min	max	dk	Nk
J001	0	33.333	0.0278	1201	0.0316	75.8797	0.0316	2400
J002	0	33	0.02	1651	0.0316	75.8797	0.0316	2400
J003	0	33	0.025	1321	0.0316	75.8797	0.0316	2400
J005	0	33	0.02	1651	0.03	150	0.03	5000
J006	0	33	0.02	1651	0.03	150	0.015	10000
J007	0	33	0.05	661	0.03	75	0.05	1500
J008	0	33	0.05	661	0.05	50	0.05	1000
J009	0	33	0.1	331	0.05	50	0.05	1000
J010	0	20	0.1	201	0.05	50	0.05	1000
J011	0	20	0.05	401	0.05	50	0.05	1000

Hydrofoil model

Purpose: force computations, detailed design

Hardware requirements: CPU times approx. 180h for 10 revolutions of the CycWEC (constant angle of attack)

Documentation: provided here

Validation and sensitivity analysis: Convergence study and comparison to public domain potential flow codes for airfoils (JavaFoil)

Although the single vortex code described above has proven to be a great asset for the design of feedback control methods, the inability to determine the forces (magnitude and direction), moments, and shaft torque necessitated the development of a second code. This code is based on the panel method as described e.g. in Katz and Plotkin [6]. The code structure is very different than that of the single vortex code, and is therefore described here in some detail.

The basic flowchart for the panel code is given in Figure 52. In the following, the pertinent details of the various steps will be discussed in detail.

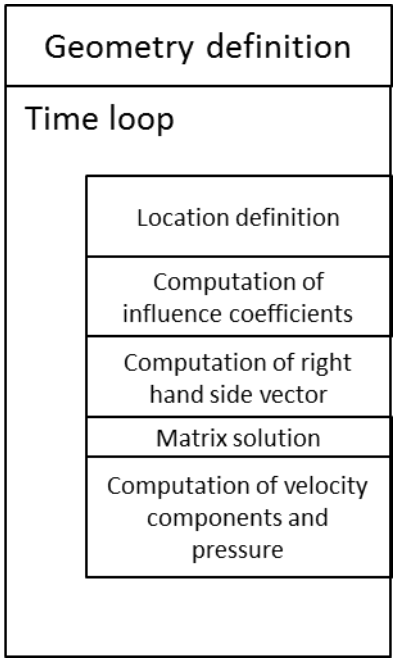

Figure 52: Flowchart for panel code.

Geometry definition

As shown in Figure 53, the hydrofoils of the CycWEC are curved such that the chord of the hydrofoil is bent along the circular path of motion. The hydrofoil shape is obtained from the basic hydrofoil, in this case the NACA0015, by bending the chord line and ensuring that the local thickness distribution remains normal to the chord line. The hydrofoil in Figure 53 is shown at an angle of attack $\alpha=0^{o}$. The code allows for defining different angles of attack as well as the pivot point about which the hydrofoil will be rotated.

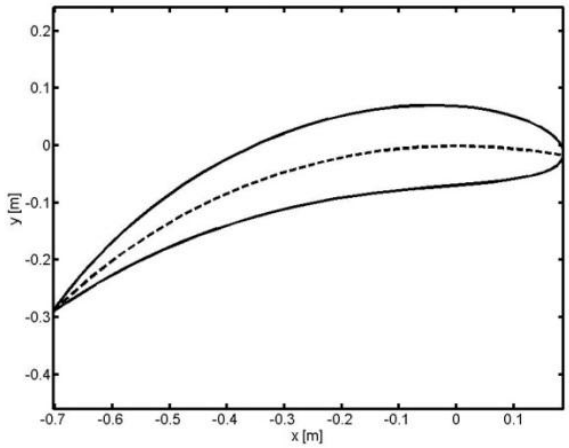

Figure 53: Curved NACA0015 hydrofoil geometry. Dashed line indicates blade chord and path of travel (α=0°).

Location definition

For this project, the angle of attack was fixed in each simulation. Therefore, once the pivot point and the local coordinates where defined, the equations describing the circular motion of the hydrofoils around the main shaft of the CycWEC were used to compute the instantaneous locations of each point on the hydrofoil surface. An example is shown in Figure 54, where a complete CycWEC configuration is shown with two hydrofoils. In addition, the figure shows the collocation points used in the panel method.

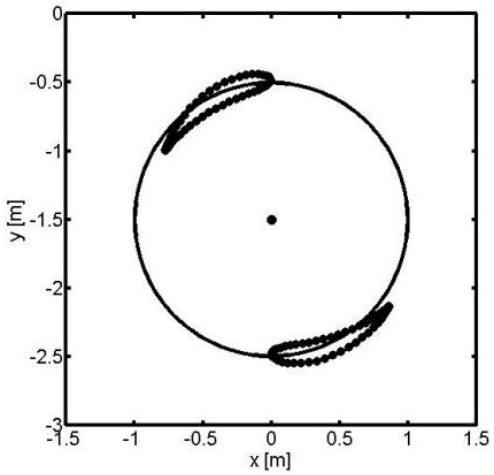

Figure 54: CycWEC with two blades, angle of attack α=±6°. Dots are the collocation points used in the panel method.

Computation of influence coefficients

The core of any panel method is the algebraic system of equations, $A\Gamma=RHS$, where $A=a_{ij}$ is the influence matrix. Its size is NxN, where N is the number of panels in the problem. In the code developed for this

project, panels with constant circulation Γ have been used. The influence coefficients a_{ij} determine what influence a unit vortex at location *j* has on the collocation point *i*. In contrast to standard panel methods, in which airfoils are computed in a uniform freestream, in the current code the influence matrix has to be computed at every time step, since the locations of the vortices are constantly changing. In particular, it is the influence of the mirror images of the vortices comprising the hydrofoil whose influence is strongly dependent on the proximity of the hydrofoil to the free surface.

Computation of the right hand side vector

Once the influence matrix is known, the boundary condition on the hydrofoil surface, which is that no flow crosses the contour line, is satisfied using the right hand side vector. For each collocation point *i*, the corresponding row of the algebraic system can be written as

$$\sum_{j=1}^{N} a_{ij}\Gamma_j = -[U(t), V(t)] \cdot \boldsymbol{n}_i,$$

where $[U(t), V(t)]$ is the local velocity vector at collocation point *i* and $\boldsymbol{n}_i$ is the local normal vector. The computation of the local velocity vector requires the solution of complex velocity potential given above.

The final step in assembling the algebraic system of equations to obtain the strengths of the vortices on the hydrofoil is ensuring that the Kutta condition is met, i.e. that the flow around the hydrofoil leaves the trailing edge tangentially. It is crucial to obtain the net circulation around the hydrofoil and the hydrofoil lift. The most common method to implement the Kutta condition is to remove one equation of the algebraic system and replacing it with the Kutta condition, which can be formulated as Γ_1=-Γ_N, i.e. the circulation at the top panel at the trailing edge is equal and opposite the circulation of the bottom panel at the trailing edge. Typically, the panel removed for this correction is near mid chord on the bottom of the hydrofoil since the pressure distribution is fairly constant there, and therefore the circulation can be computed as the average of the panel upstream and downstream.

Matrix solution

The matrix solution is obtained by standard methods for algebraic systems of equations.

Computation of velocity components and pressure

Once the system of equations is solved, the vortex strengths are known for each panel. With this information, the velocity magnitude can be computed on the surface. Note that since this is an inviscid simulation, the velocity on the surface is not zero.

Invoking the Bernoulli equation, the pressure distribution on the hydrofoil can be obtained using

$$p_0 + q_0 = p + q$$

$$= p + \frac{\rho}{2} U^2 .$$

In addition, with the definition of the pressure coefficient

$$c_p = \frac{p - p_0}{q_0},$$

the pressure coefficient can be computed from the velocity ratio,

$$c_p = 1 - \left(\frac{U}{U_0}\right)^2.$$

Here U_0 is the velocity due to the rotation of the CycWEC and U is the velocity computed from the waves as well as all the vortices of the panels comprising the hydrofoil. Note that in the derivation, it has to be assumed that the Bernoulli equation holds in the whole fluid. This derivation is standard for panel codes used in airfoil design.

Finally, the resulting forces created by the hydrofoil can be computed by integrating the pressure distribution around the hydrofoil, taking the local surface normal into consideration,

$$\vec{F} = \oint p \, d\vec{n},$$

where the vector $\vec{n}$ points in the direction of the surface normal with a magnitude equal to the length of the local panel.

Validation

For validation of the newly developed panel code, a simple test case was designed.

To approximate the conditions of a standard panel code, i.e. a uniform free stream velocity, the CycWEC radius was set to R=1000m and the submergence depth to y_c=1500m. Therefore, at the bottom of the motion path, the hydrofoil is submerged at y=2500m. While no detailed study of the influence of the free surface was performed for these simulations, earlier results indicated that a depth y_c>10m is sufficient to render the free surface effects negligible. The large radius was chosen so as to approximate a linear motion, which is kinematically equivalent to a uniform free stream. Geometrical considerations show that in the motion segment considered in the validation simulations, the angle of attack changes by less than 0.01°, approximating a linear movement very well. The simulations converged in less than 20 iterations. These simulations were performed using 80 panels on the hydrofoil surface.

Symmetric hydrofoil

The first test of the newly developed simulation code was performed using a NACA0015 hydrofoil. The hydrofoil and the computational panels are shown in Figure 55. Note that panels are clustered at the leading and trailing edges to capture the expected large velocity, and therefore pre ssure, gradients.

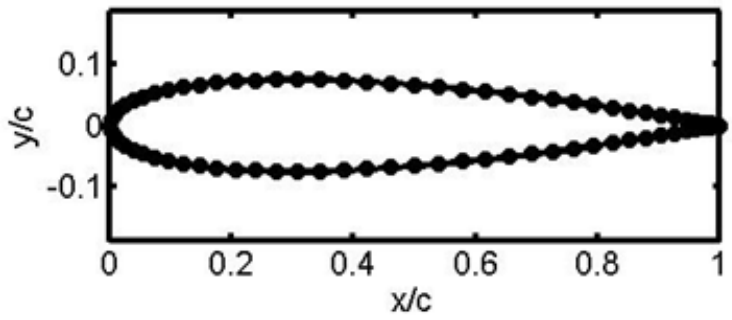

Figure 55: NACA0015 geometry and discretization.

Figure 56 shows a comparison of data obtained from Javafoil with the data from the new code [4]. Javafoil employs a linear panel method; for the comparison computations, 60 panels were used. The figure shows a comparison of the computed pressure coefficient for angles of attack of α=0°,6°,and 10°. Good agreement of the pressure distribution is achieved. The slight differences in the suction side pressure distribution are due to slightly different panel distribution and the fact that Javafoil uses a linear vorticity distribution on the panels while the current code uses a constant vorticity value for each panel. Due to the symmetry of the hydrofoil, only positive angles of attack have been computed.

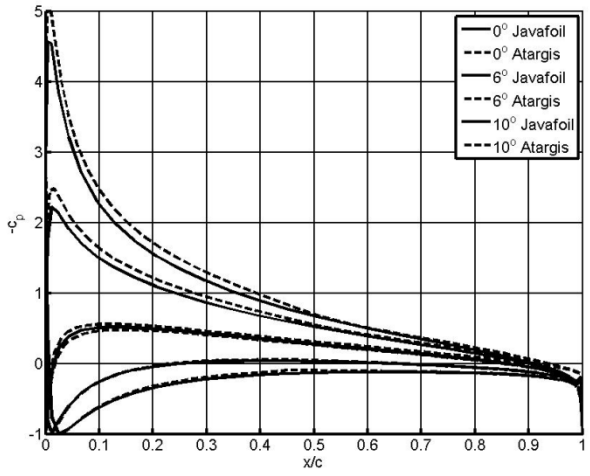

Figure 56: NACA0015 pressure distribution. Comparison of pressure coefficient on the hydrofoil surface between Javafoil and Atargis Panel Code.

Asymmetric hydrofoil

In order to test the simulation code for a hydrofoil that creates lift at α=0° angle of attack, simulations have been performed using a NACA4412 hydrofoil. The hydrofoil contour is plotted in Figure 57.

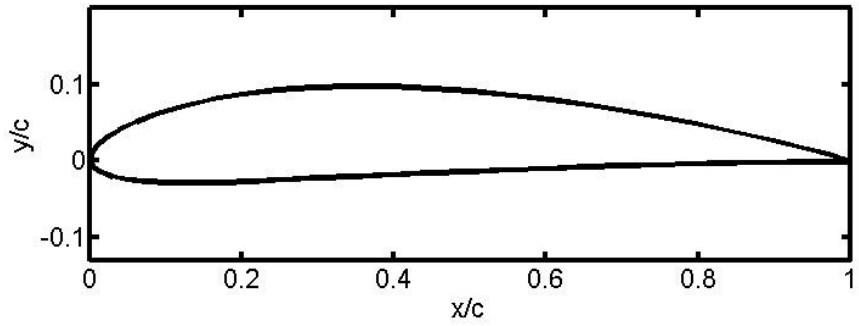

Figure 57: NACA4412 hydrofoil.

A comparison of the pressure distribution at angles of attack α=0°,6°,and 10° with the results obtained using Javafoil is shown in

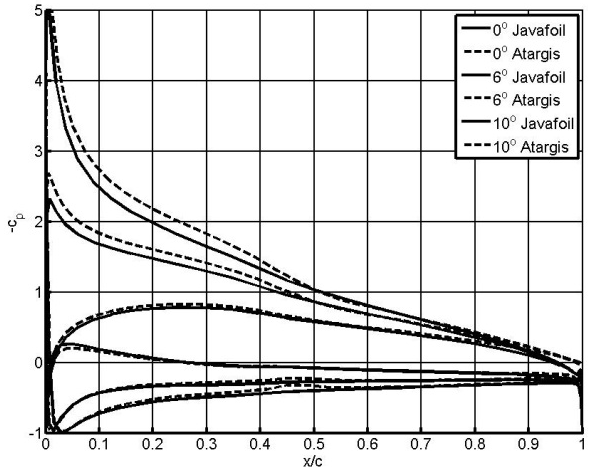

Figure 58: NACA4412 hydrofoil. Comparison of pressure coefficient on the hydrofoil surface between Javafoil and Atargis Panel Code.

Overall, good agreement is achieved. At $\alpha=0^{o}$, both the suction and pressure side c_p distribution are in very good agreement with the results obtained by Javafoil. As the angle of attack is increased, the Atargis code computes a slightly lower pressure on the suction side, while the pressure side c_p distribution remains in very good agreement with the Javafoil data. This is most likely caused by the difference in the discretization schemes as mentioned above. To improve the predictions, more panels would have to be added to the suction side of the hydrofoil. However, the level of prediction accuracy using the current discretization was determined to be adequate for the intended design purposes.

Using these validation simulations, it was concluded that the code performance criteria were met. It should be noted that this code, to the authors' knowledge, is the only panel code that can model a

lifting body in motion under a free surface with minimal wave energy dissipation. This is achieved by using Equation (1) rather than discretizing the free surface using panels or other numerical methods that are inherently dissipative.

Viscous Estimate

The need to estimate effects on the performance of the CycWEC arose from the use of an inviscid potential flow solver for all of the numerical simulations performed to date. By design this code, detailed in the previous section, does not consider viscous effects at all. However, viscous effects will cause power losses in the conversion process of wave energy to shaft power. This section outlines the approach used to estimate these losses.

Model description, key assumptions, version, source and intended use

The viscous estimate code uses published data for hydrofoils in order to estimate the drag force due to viscosity of the fluid water. In particular, we use data from experiments published by Sandia National Labs for hydrodynamic performance of NACA 0015 hydrofoils. The data is provided as lift and drag coefficient as a function of Angle of Attack and Reynolds numbers. The angle of attack covers 0 to 360 degrees in 2 degree increments, while the Reynolds number ranges from 80,000 to 10 Million. These ranges cover the operating conditions of the hydrofoil employed in this research and are thus applicable to the task at hand. The viscous estimate code performs linear interpolation of these values to estimate lift and drag coefficients.

Performance criteria for the model related to the intended use

Test results to demonstrate the model performance criteria were met

The results in terms of wave energy to shaft power conversion were validated at the OTRC-2 testing campaign. For a series of wave energy extraction runs with increasing wave heights at a wave period of 2.5s, the breakeven point where the viscous losses are equal to the shaft power (indicated by the transition from the white to the blue area of the contour plot) as shown in Figure 59 was predicted to be at 0.3m of wave height. This was matched by the experimental results (see respective section OTRC-2 of this document). In addition, the wave power produced at H=0.55m also matches with the model predictions.

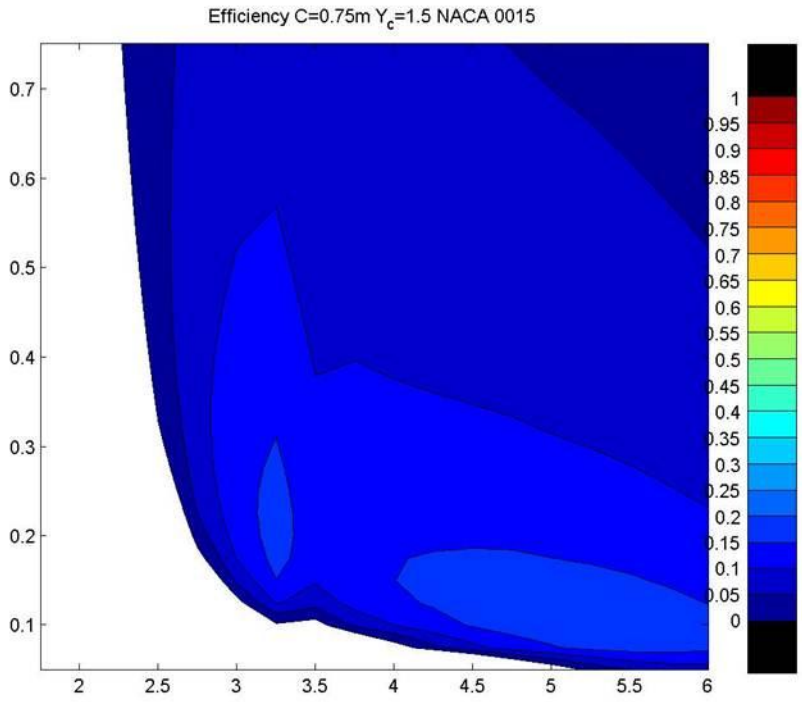

Figure 59. Viscous efficiency Prediction of OTRC-2 CycWEC 1:10 scale model with NACA 0015 hydrofoil and submergence depth of yc=1.5m. Vertical axis, wave height in [m]. Horizontal Axis, wave period in [s]. Color contours show efficiency of wave energy conversion.

It should be noted that the poor overall efficiency shown in Figure 59 was caused by a poor choice of both hydrofoil and operating condition (i.e. submergence). As such, the code provided the physical understanding of the losses and the results will be used to design the next generation CycWEC considering these effects.

Theory behind the model, expressed in non-mathematical terms

The theory behind the numerical model is based on the forces acting on the hydrofoils as shown in Figure 60. The flow velocity approaching the CycWEC blade, which is the vector sum of the wave induced velocity Uw and the rotational velocity of the WEC Urot , result in hydrofoil Lift force L as well as drag force D. The components of these forces acting in the tangential direction cause a torque at the main shaft, and subsequently shaft power. While the lift force produces a torque in the direction of rotation and thus positive shaft power, the drag force is detrimental and causes a reduction in shaft power.

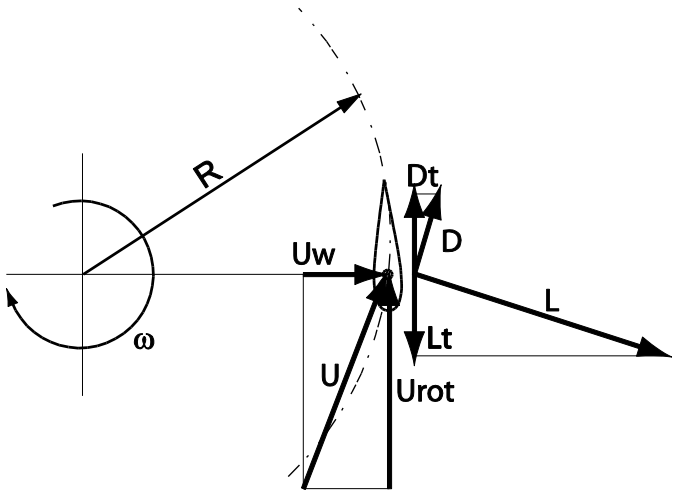

Figure 60. Sketch of Forces acting on the rotating hydrofoil of a CycWEC. (from reference [1]).

Mathematics to be used, including formulas and calculation methods

The model calculates the required hydrofoil lift based on results from the inviscid single vortex panel code, which determines the circulation G for given wave height and period. This is then used to calculate the required pitch angle α of the foil using the equation:

$$G = U_\infty c \pi \alpha$$

With U_∞ the hydrofoil velocity and c the hydrofoil chord. Once the hydrofoil pitch angle is known, the Lift and Drag force can be determined from the published hydrofoil data using a lookup table along with linear interpolation. With lift L and drag D known from published experimental hydrofoil data, the shaft power P_s can be calculated:

$$P_s = \frac{2\pi R}{T} R(L_t - D_t)$$

With T the rotational period of the WEC and all other quantities defined as shown in the sketch of Figure 60.

Whether or not the theory and mathematical algorithms were peer reviewed

The approach to viscous estimation has been peer reviewed in the context of the numerical simulation journal article [1]. No deficiencies or issues were found by the reviewers.

Hardware requirements

The entire viscous estimate code was written in Matlab, and can thus be run on any computing platform that is supported by the The Mathworks.

Documentation

The code is considered Atargis proprietary, and so is the more detailed documentation beyond what is provided here.

3D Diffraction

Based on observations during the two testing campaigns at OTRC, the need arose to establish a theoretical comparison for the three dimensional wave diffraction effects observed in these experiments. The goal was to establish as simple a diffraction model as possible to enable understanding of the flow physics, as well as to be able to perform parameter studies that cannot easily be conducted in experiments, for example variations of the span of the WEC.

Model description, key assumptions, version, source and intended use

The key assumption of the model is conservation of wave energy, which is a valid assumption for most non-breaking waves, but in particular for the harmonic waves encountered in the OTRC wave basin. The model was further limited for the present investigations to a single wave period and straight crested waves, which is what was produced by the wave makers in the tank during the testing campaigns.

Performance criteria for the model related to the intended use

The goal for the model was to provide a theoretical comparison for the experimental observations from the two testing campaigns. However, with the model validated against these experiments, it can be used to predict the performance of the CycWEC at different scales and sizes and will be used to improve the estimate of full scale CycWEC performance in the future. It also allows for investigation of interactions between multiple WECs in different geometric arrangements, which makes it a very valuable asset for the planning of wave energy converter farms in the future.

Test results to demonstrate the model performance criteria were met

Wave gauge measurements were employed to validate the model predictions with the actual wave measurements. We present two validation data sets here, one where wave generation data are compared to the model, and a second set where wave cancellation results are shown.

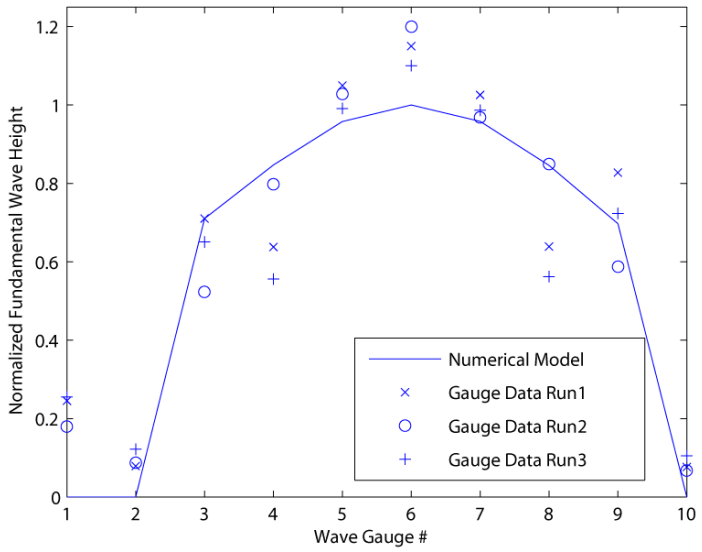

Figure 61: Comparison of wave gauge measurements to numerical diffraction model wave heights for wave generation. Wave period T=2.5s

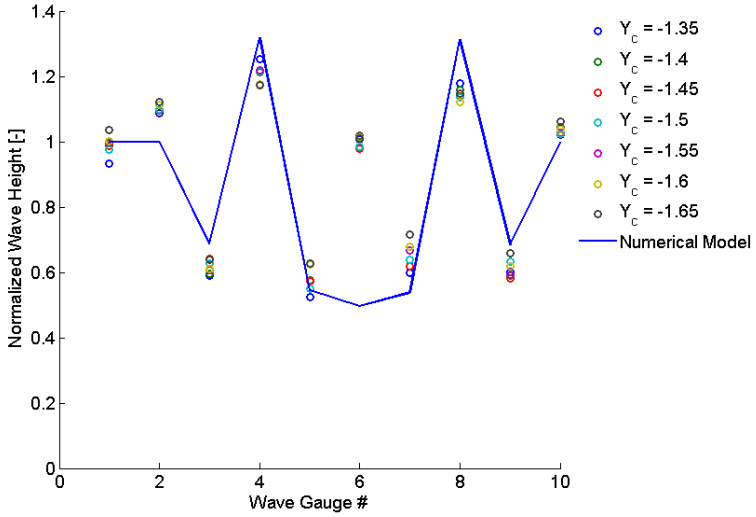

Figure 62: Wave Heights during wave cancellation as a function of wave gauge location in comparison to numerical model

It can be observed that the numerical model provided accurate predictions of the wave heights generated as shown in Figure 61. Differences between model and wave gauge measurements were

most likely attributable to wave reflections encountered in the experiments. These reflections were caused both by reflections from the basin side walls causing transverse waves, as well as longitudinal waves due to less than perfect absorption of the longitudinal waves at the screens acting as wave absorbers. Furthermore, the paddle wave makers would re-reflect any incoming waves since they had no active wave absorbing capabilities.

A comparison of the measured wave heights from the wave gauges, as well as the predictions from the numerical diffraction model for wave cancellation are shown in Figure 62. With the exception of wave gauge #6 the agreement is found to be very good, the discrepancy is most likely due to reflected waves from the basin side walls as discussed above.

Theory behind the model, expressed in non-mathematical terms

The model uses point sources of circular waves in order to synthesize the wave generated by the CycWEC. By varying the strength of the circular component waves along the span of the WEC, the effect of the span wise lift distribution on wave generation can be modeled. The wave generated by the WEC is then free to interact with an incoming straight crested wave. All waves are assumed to be linear, and linear superposition of the waves is used to investigate the interaction of the different waves. The resulting wave pattern is then analyzed using control volume analysis, which allows for calculation of the wave energy extracted by the CycWEC from the incoming wave. As the model is non-dissipative in nature, energy is conserved throughout independent of spatial discretization.

Mathematics to be used, including formulas and calculation methods

The surface elevation η_c of a circular wave can be described as, $\eta_c(x,z,t) = H(r)\sin(\omega t - kr)$ with x and z the horizontal coordinates; k the wave number, r the distance from the wave center, ω the wave period and t time. If this wave is to conserve energy as it radiates outward, the wave height H has to decrease with distance from the wave generator. If the initial wave height is specified as H_0 at a finite distance r_0 from the center,

$$H(r) = \sqrt{\frac{H_0^2\, r_0}{4r}}$$

is a height function that does conserve wave energy resulting in a reduced wave height as the wave propagates away from the wave center. It is possible to use several circular waves to approximate the wave pattern caused by more complex wave generators. For a CycWEC, the waves generated can be approximated as a sum of individual circular wave generators arranged along a line of finite length equal to the span S of the WEC blades.

$$\eta_{WEC}(x,z,t) = \sum_{n=1}^{N} \eta_{cn} \ , x > 0$$

Single sided wave generation is assumed and assured by setting the WEC wave to zero for negative x coordinates and is experimentally verified in following sections. The N circular wave generators are located between z=-S/2 and z=S/2 along x=0. A number of N=25 individual circular waves was found to produce converged results. The strength of each circular wave generator used to discretize the WEC wave generation was approximated by an elliptical distribution.

$$H_0(z) = H_c\sqrt{1-\left(\frac{z}{2S}\right)^2}$$

This modeled the lift distribution along the span of the foil which caused a wave height that was proportional to the local circulation. To assure that the maximum wave height at the center of the foil was H_c, the overall generated wave height was renormalized to the value specified. The wave field generated by the WEC was then superimposed with the wave field generated by the incoming wave. The incoming wave in this investigation was a long crested Airy wave traveling in the positive x direction modeled as, $\eta_A(x,z,t) = H\sin(\omega t - kx)$.

The final surface elevation was then calculated by superimposing the incoming airy wave with the wave generated by the WEC.

Control Volume analysis

The wave field resulting from the interaction of incoming Airy wave and the waves generated by the circular waves used to model the WEC were used to determine the overall energy absorbed by the WEC. Using a control volume that enclosed the WEC completely, the fundamental waves entering and leaving that control volume could be calculated. To ease calculations, the control volume chosen was a rectangle aligned with the coordinate system axes. The circular waves were decomposed in a x and z component. Thus, the portion of each circular wave leaving the control volume boundaries could be calculated at each location along the boundaries. For an Airy wave, wave power P per unit length can be calculated as

$$P = \frac{\rho g}{8}H^2 C_g$$

where Cg is the wave Celerity, ρ the density of water and g the gravity constant. Thus the wave power traversing a control volume boundary extending in the z direction from z_1 to z_2 could be calculated.

$$P = \int_{z_1}^{z_2}\sum_{m=1}^{M} P_{mx}(z)dz$$

$$P_x(z) = \frac{\rho g}{8}({H_x}^2 + {H_z}^2)C_{gx}$$

The subscripts indicate the vector component of the respective quantity in that direction. These equations can be modified to calculate the power traversing across a horizontal control volume boundary by swapping the subscripts x and z. The overall amount of power extracted by the WEC could then be calculated by choosing a closed rectangular control volume.

To determine the efficiency with which the WEC extracted energy from the waves, a reference quantity equal to the wave power of the Airy wave times the span of the WEC was used. Thus, if the control volume analysis showed that this amount of energy was extracted from the waves, the efficiency was unity or 100%. Any efficiency larger than this indicated that diffraction induced wave focusing was encountered.

Whether or not the theory and mathematical algorithms were peer reviewed

The model has been peer reviewed in the context of the AWTEC paper [10], and no deficiencies have been found in the approach or data presented there. The paper has passed peer review and will be presented in the present form in November 2012 at the AWTEC conference in South Korea.

Hardware requirements

The entire 3D Diffraction code was written in Matlab, and can thus be run on any computing platform that is supported by The Mathworks.

Documentation

The code is considered Atargis proprietary, and so is the documentation beyond what is provided here.

Lessons Learned

There were many valuable lessons learned throughout the development performed within this program. While some are clearly related to the learning curve of setting up a small high tech startup company and need not be discussed here, there are others that are related to developing marine hydrokinetic devices in general and performing the related testing and development. The following subsections detail lessons learned both on the administrative side as well as the technical side of this program that Atargis feels may be of value to other developers of MHK devices.

Administrative

- The availability of large scale MHK testing facilities is very limited in the US and to a lesser degree internationally. This makes scheduling of tests difficult and requires long lead times, at present more than one year.
- For large (1:10 scale) testing there is a monopoly situation in the US at present, where the Texas A&M (OTRC) wave tank is the only commercial option. This facility thus can afford to NOT provide customers with a contract or firm testing date until one week prior to the start of

testing causing major administrative problems, from short term induced increases in air fare to missed lodging bookings.

- The OTRC facility is at present overbooked and backlogged and in relatively poor maintenance, which caused half a year of unexpected delay for our second testing campaign. This caused significant delays in our overall development as well as major expenses in facility cost and staff salaries that were not planned for. It appears to be impossible at present to perform development with a predictable schedule with OTRC as a testing facility.
- While international competitors to OTRC operate on a more predictable schedule, they are also significantly more expensive. However, this cost may be less than what one might spend in waiting for OTRC availability. For a professional development program, paying a higher testing fee as well as incurring cost in international travel and shipping would have been more cost efficient in our case and would have allowed the testing schedule to be met.
- With the present shortage of testing facilities in the US, Atargis would recommend all federally funded MHK programs to relax the requirement to perform tests in the US in order to allow for predictable development schedules, even if this causes the testing to be performed abroad.
- In looking ahead to the next development levels, the present US political and administrative environment for testing of MHK technologies appears to be difficult if not outright hostile to developers. There is a lot of improvement that can be achieved on these levels (administrative and political) in order to speed up and ease permitting and reduce related costs to developers. Established testing sites in Europe have set examples on how this can be achieved without sacrificing environmental protection or other causing other ill effects.

Technical

- Perform analysis of all critical components bought off-the-shelve in house prior to testing, instead of relying on assurances of suppliers. Examples include but are not limited to:
    - The inability of the pitch actuators to perform in a wet environment despite the manufacturers rating of IP-68 (pressure wash proof) could have been discovered by doing in house verification of these claims before testing
    - The inability of the main shaft motor control system to maintain synchronous operation of the left/right side of the WEC in a dynamic environment could have been discovered by performing dry run testing under load
- With all MHK technology being novel in terms of the testing facility requirement, it is important to perform in house analysis of the suitability of the facility for the planned tests instead of relying on assurances of the facility staff:
    - The structural deficiency of the OTRC tunnel bridge could have been discovered before testing by performing in house finite element analysis, instead of relying on the assurance of structural performance made by the facility director and his staff.

- Even for model testing, it makes sense to perform a Failure Mode and Effect (FMEA) analysis. Since a lot depends on successfully performing these types of tests, the model design should be resilient against single point failures which can be achieved by improved design at reasonable expense. It also paves the path toward Open Ocean testing.
- Failure of a computer based control system should not cause any structural damage in any situation. In other words, critical electrical controls systems need a failsafe mechanical backup
- It is operationally advantageous to have a double backup system against water intrusion for all moisture sensitive components (i.e. electronics). Thus, electrical components located in submerged sealed compartments should have a secondary enclosure that is at least splash proof rated and proven.
- All moving components need a mechanical brake system to enable safe shutdown and/or ease deployment of the WEC. We did retrofit brakes to the main shaft motors and pitch actuators in preparation of our second testing campaign; and it helped in reducing installation time greatly while preventing installation related damage.
- In large scale, testing time is (a lot of) money, and one means to reduce time in the facility is to design the model such that installation and removal time is minimized. Installation of our model during the OTRC-2 testing campaign was a fraction of the time spent for the same task during OTRC-1, and was reduced by carefully planning the deployment of the model in the tank considering the available infrastructure (ceiling heights, crane capacity etc.).
- Submerged model portions that are air filled and water tight should be designed for sustaining a maximum pressure differential in BOTH directions that is at least an order of magnitude larger than the expected operational hydrostatic pressure. This allows for thorough leak testing in a dry run environment
- It is advantageous to perform dynamic dry run testing, ideally with simulated predicted loads. While this causes added expense to simulate the loads, the ability to detect potential problems related to dynamic issues justifies this effort. Dynamic testing under simulated operating conditions with all hardware and software in the loop was performed in preparation for the second testing campaign.
- While using as many off-the-shelve components as possible reduces component cost, careful examination, especially of motion control products in terms of their suitability for the task at hand, is required. We found that, in particular, the software portion of COTS motion controllers is geared towards a very different application which causes problems in the adaptation to MHK energy conversion. This can and will be addressed by only using low level software functionality of motion controllers and developing a larger portion of the higher level software from scratch to better suit the needs of the application.
- Numerical simulations and first principles estimates are invaluable to development progress in a technical development as challenging as ocean wave energy conversion. There is virtually no

point in testing without having detailed estimates of device performance prior to performing the tests.

- For numerical tests, it is important to have a range of numerical models ranging from simple and fast to run all the way to very accurate, but very slow to run. The low to mid-level potential flow simulations that can run in minutes on a desktop PC have turned out to be most valuable to the development since they allow parameter studies in short order that are too time consuming in large scale experiments. They are also very valuable in understanding flow physics since they isolate the effects most important to device performance, if set up correctly.
- An integrated software environment where the control algorithms can be tested in simulations before being used in the actual experiment is of the essence.
- Accurately performed back-of-the-envelope estimates of device performance and cost at the lower TRL levels can show the potential (or lack thereof) of a new MHK technology relatively early in the development process, before spending millions of dollars in testing. If the device economics cannot be made to work at this development level, it probably never will.

While hindsight tends to be always 20/20, we do hope that sharing these lessons learned will ease the learning curve for other developers in the future. However, all devices are significantly different in their design and thus may encounter challenges in other areas. Thorough engineering testing is the only way to achieve a successful device design; and there will always be a need to iterate, improve, redesign and test again. We have found the TRL defined development path outlined in the proposal request of this program to be very valuable and an excellent guideline in how to systematically progress along the development path. While it might appear to be slow in terms of getting to ocean scale testing, we feel that it is actually the fastest path to a *successful* ocean testing without having to back track during the development. It is our hope that future US government funding opportunities will support this structured approach to development.

References

[1] Stefan G. Siegel, Tiger Jeans, and Thomas McLaughlin. Deep ocean wave energy conversion using a cycloidal turbine. *Applied Ocean Research*, Volume 33 Issue 2:110–119, April 2011.

[2] McTaggart, K. Modelling and simulation of seaways in deep water for simulation of ship motions Defence R&D Canada - Atlantic, September 2003

[3] IACS Report No 34. Standard Wave Data International Association of Classification Societies LTD., 2000

[4] Hepperle, M. Javafoil, http://www.mh-aerotools.de/airfoils/Javafoil.htm

[5] Wehausen, J., Laitone, E., 'Surface Waves,' Handbook of Physics, Vol. 9, Springer, 1960.

[6] Katz, J., and Plotkin, A., 'Low-Speed Aerodynamics, 2nd edition, Cambridge University Press, 2010

[7] Tiger Jeans, Casey Fagley, Stefan Siegel and Jurgen Seidel, Irregular Deep Ocean Wave Energy Conversion Using a Cycloidal Wave Energy Converter. Proceedings of the 9th European Wave and Tidal Energy Conference, Southampton, UK, 5th-9th September 2011

[8] Stefan Siegel, Casey Fagley, Marcus Roemer and Thomas McLaughlin, Experimental Wave Cancellation using a Cycloidal Wave Energy Converter. Proceedings of the 9th European Wave and Tidal Energy Conference, Southampton, UK, 5th-9th September 2011

[9] Fagley, C.; Seidel, J. & Siegel, S. Computational Investigation of Irregular Wave Cancellation using a Cycloidal Wave Energy Converter. 31st International Conference on Ocean, Offshore and Arctic Engineering (OMAE), 2012

[10] Seidel, J.; Fagley, C. & Siegel, S. Numerical Simulations of a Cycloidal Wave Energy Converter 1st Asian Wave and Tidal Energy Conference (AWTEC) Jeju Island, Korea, November 27-30, 2012